THE PENNSYLVANIA
STATE UNIVERSITY

IONOSPHERIC RESEARCH

Scientific Report No. 320

AN INVESTIGATION OF MICROWAVE INTERACTION WITH A PLASMA CONFINED IN A DIPOLAR MAGNETIC FIELD

by

T. G. Twardeck

July 30, 1968

IONOSPHERE RESEARCH LABORATORY

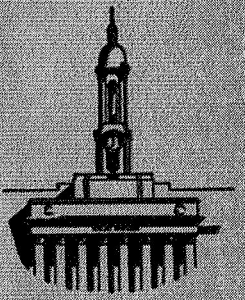

University Park, Pennsylvania NASA Grant NsG 134-61

Ionospheric Research

NASA Grant NsG 134-61

Scientific Report

on

"An Investigation of Microwave Interaction with a Plasma Confined in a Dipolar Magnetic Field"

by

T. G. Twardeck

July 30, 1968

Scientific Report No. 320

Ionospheric Research Laboratory

Submitted by: J. S. Nisbet (aw)

John S. Nisbet, Professor of Electrical Engineering
Project Supervisor

Approved by: A. H. Waynick

A. H. Waynick, Director
Ionosphere Research Laboratory

The Pennsylvania State University
College of Engineering
Department of Electrical Engineering

TABLE OF CONTENTS

ABSTRACT

An investigation of the properties of a plasma confined in the dipolar magnetic field of a uniformly magnetized sphere has been conducted. The main laboratory diagnostic tools were microwave interferometers operating at 3.0, 1.34 and 0.86 cm.

Laboratory measurements included changes in received power and phase for various plasma densities, scattering angles and frequencies, and changes in the received power for different pressures in the vacuum vessel, plasma densities and frequencies.

The assumptions used in formulating a theoretical model of the experiment are stated and examined for validity. Consistent with these assumptions an idealized model of the scattering geometry is presented and expressions for the scattering coefficients and scattered field quantities are formulated in terms of the plasma parameters. The digital computer techniques for evaluating the appropriate expressions are described and the influence of each physical parameter on the calculations is considered.

The comparison of the simple theoretical model with experimental results indicates that in forward scattering angles the plasma is accurately described as a plasma shell characterized by a constant complex refractive index for the plasma densities, collision frequencies and incident wave frequencies encountered in the laboratory investigation. The electron density profiles synthesized from the scattering data are in agreement with the density profiles determined by double Langmuir probe measurements.

1. INTRODUCTION

1.1 Review of Literature and Statement of the Problem

In principle, the physical properties of a plasma can be deduced from the changes in phase and amplitude of an electromagnetic wave brought about by introducing the plasma into an otherwise unperturbed transmission path. When dielectric or conducting bodies form part of this unperturbed transmission path or when the plasma configuration can be considered as a scattering center, the theory and practical laboratory techniques related to the diffraction and scattering of electromagnetic waves are relied upon to give the desired information.

Some recent literature describing work of this type, of both an experimental and theoretical nature, are of interest to this investigation. Given a cylindrical plasma column with a density distribution which is a decreasing function of radius, Shmoys (1960) has shown that the diffraction pattern can be calculated from a knowledge of the density distribution. Easley (1963) investigating the scattering patterns of a plasma jet has concluded that the plasma parameters are relatable to the scattering measurements although, as usggested by him, the simple model of a homogeneous plasma gave relatively poor agreement. Jones and Wooding (1966) were able to conclude that the variation of power scattered by a plasma enclosed in a glass discharge tube can be predicted theoretically by assuming that the plasma consists of two homogeneous regions. Midzuno (1961) presents the angular distribution

of a wave scattered from a cylindrically symmetric nonuniform plasma in an integral formalism. Nagelberg (1964) has studied the interaction of microwaves with gyroelectric plasmas of cylindrical and spherical geometries and has shown that one obvious effect of the anisotropy is to induce changes on the polarization of the scattered wave.

Mikulski and Murphy (1963) discuss the problem of scattering by many concentric spherical structures using the Mie series solution in each region. The regions are assumed to have complex characteristic constants which can be related to plasma properties. Baker, Bachynski and Carswell (1964) have formulated the backscattering cross section of a plasma covered conducting sphere in terms of the plasma frequency and the collision frequency and have observed the effect of varying these parameters on this cross section through numerical calculations. Erma (1965, 1967) has catalogued the radar cross sections as a function of frequency for four types of spherically symmetric plasma spheres and discusses the inverse scattering problem, i.e., whether the precise electron density distribution can be unambiguously inferred from measured radar cross sections. In more of a theoretical nature Bisbing (1966) analyzes the scattering by a plasma distribution in which the electron density decreases exponentially with radial distance; he indicates how parametric changes affect the static scattering. Wyatt (1962) studied scattering from spherically symmetric inhomogeneous absorbing particles and showed the dependence of the polarization and scattered intensities on surface diffuseness.

Thus it may be stated that there exists a considerable amount of theoretical and experimental results concerning electromagnetic

scattering from various plasma, plasma-conductor and plasma-dielectric configurations. However, no laboratory measurements of the scattering of microwaves from a configuration of a static plasma coating a conducting rod or sphere are available.

The realization of the latter plasma-conductor configuration in the laboratory has only recently been made possible through the work of Quinn. (1965, 1966) The method used to form the plasma clad spherical conductor is to make a spherical magnet the negative electrode of a glow discharge; the resulting ionized gas is trapped in the dipolar magnetic field and forms a sheath around the sphere.

The specific aim of this investigation is to deduce the properties of the plasma trapped in the dipolar magnetic field of the spherical magnet through a study of microwave interaction with this plasma-conductor configuration. The endeavor involves both laboratory and theoretical work. During the laboratory phase both microwave scattering and Langmuir probe measurements are conducted.

A suitable mathematical model is formulated to predict the experimental scattering patterns. These results are then compared with the Langmuir probe data.

1.2 Definition of Symbols

The definition of the symbols used throughout this paper are given below. The symbols are arranged alphabetically in the order of upper case Latin letters, lower case Latin letters, upper case Greek letters and lower case Greek letters.

$A = [2/n_2^3(x)\ dn_2(x)/d\rho\ X(x)/n_2^2(x)]$

A^* = conjugate of complex A

e, m_{A_i} = component i of transverse magnetic, electric wave vector

$B = A(Y)$

$\bar{B}$ = magnetic flux density vector

e, m_{B_ℓ} = scattering coefficients of electric, magnetic wave

$C = -A(x)$

$D = -B(y)$

$\bar{D}$ = electric displacement density vector

$E = [-U'(x)/k_2^{II}\ n_2(x) + U(x)\ dn_2(x)/d\rho\ (k_2^{II}\ n_2^2(x))^{-1}]$

$\bar{E}$ = electric field vector

E_o = magnitude of the incident electric field

$F = E(V(x))$

$G_\ell(\rho)$ = radial dependence of $r^{m}\Pi^{II}$

$\bar{H}$ = magnetic field vector

$H_\ell^{(1)}(x)$ = Hankel function of the first kind

I = current

$\bar{J}$ = current density vector

$J_\ell(x)$ = Bessel function of the first kind

K^i = wave number in region i = $-k_1^i\ k_2^i$

M_ℓ = arbitrary constant

N_i = particle number density of species i

$N_\ell(x)$ = Neumann function

N_ℓ = arbitrary constant

$P_\ell^m(x)$ = associated Legendre function

P = power of a given wave or pressure

R = distance from scattering center to the point of observation

S = switch on circuit diagram

$\bar{S}$ = Poynting vector

T = temperature

U = general function of position or $1+i\nu/\omega$

$U_\ell(\rho)$ = one solution of the $G_\ell(\rho)$ D. E.

V = voltage

$V_\ell(\rho)$ = one solution of the $G_\ell(\rho)$ D. E.

$W_\ell(\rho)$ = radial factor of $r^{e}\Pi^{II}$

$X_\ell(\rho)$ = one solution to the $W_\ell(\rho)$ D. E.

$Y = \omega_B/\omega$

$Y_\ell(\rho)$ = one solution to the $W_\ell(\rho)$ D. E.

Z = ratio of collision frequency to incident radian frequency

a = radius of the conducting sphere

$a_{\ell,m}$ = constants

b = radial extent of plasma

$b_{\ell,m}$ = constants

c = velocity of light

$c_{\ell,m}$ = constants

$d_{\ell,m}$ = constants

e = magnitude of the charge of an electron or the left superscript to denote the electric wave

f = frequency of the incident wave

i = $(-1)^{1/2}$ or right superscript to denote a particular region of space

$k_1^i = i\omega(\varepsilon + i\sigma/\omega)$

$k_2^i = i\omega\mu$

ℓ = summation index

m = mass of electron, summation index or left superscript or denotes the magnetic wave

n = refractive index

n_o = refractive index of the ordinary wave

n_x = refractive index of the extraordinary wave

r = radial variable in a spherical coordinate system

t = time

x,y,z = reference directions in a rectangular coordinate system

$e,m_{\Pi}i$ = transverse magnetic, electric potential in region i

Ω = solid angle

α_ℓ = constants

β_ℓ = constants

γ_ℓ = constants

δ_ℓ = constants

ε = permittivity

$\zeta_\ell^1(x)$ = spherical Hankel (Ricatti) function of the first kind

η_o = impedance of free space

θ = colatitude angle in a spherical coordinate system or the scattering angle

μ = magnetic permeability

ν = electron-neutral collision frequency

ρ = charge density or the dimensionless parameter $K^i a$ or $K^i b$

σ = conductivity or bistatic radar cross section

ϕ = azimuthal angle in a spherical coordinate system

$\chi_\ell(x)$ = spherical Bessel (Ricatti) function of the first kind

$\psi_\ell(x)$ = spherical Bessel (Ricatti) function of the second kind

ω = radian frequency of incident wave

ω_p = plasma frequency = $(Ne^2/m\varepsilon_o)^{\frac{1}{2}}$

ω_B = gyrofrequency = eB/m

2. APPARATUS AND MEASUREMENT TECHNIQUES OF THE LABORATORY INVESTIGATION

In this section the apparatus and measurement techniques of the laboratory investigation are presented. The method to establish and maintain the steady state plasma is given along with a description of the changes of the plasma geometry with pressure and discharge current. Figures displaying the electron and ion density profiles obtained from double Langmuir probe data are shown. Described with the microwave interferometers are some of the data obtained with these systems.

2.1 The Steady State Plasma

A uniformly magnetized 3.3 cm diameter Alnico V cylinder was shaped into a spherical magnet by a cathodal deterioration process. During the experiment the sphere is rigidly attached, at one magnetic pole, to a brass rod (0.635 cm diameter) and both are fitted into a device which centers them vertically over the base plate of the vacuum station. (The vacuum system used throughout the experiment was a basic Veeco pumping station consisting of roughing and diffusion pumps fitted with a stainless steel base plate 50.8 cm in diameter and a Pyrex glass bell jar 45.7 cm in diameter and 81.3 cm high. The gas pressure in the bell jar was measured with a standard thermocouple gauge.)

When the permanent spherical magnet is made the negative electrode of a glow discharge arrangement in an evacuated environment, the

resulting ionized gas becomes trapped in the magnetic field and forms a plasma sheath around the sphere. The electrical circuit used to initiate and maintain the plasma has two current paths. In one path a high voltage low current supply (1200 v, 10 ma) initiates the gaseous discharge. After the initial breakdown a low voltage high current supply (600 v, 200 ma) in the second path gives the desired high discharge current. For any following diagnostic measurements, the plasma is maintained by the second voltage supply with the first voltage set to zero. The anode of the discharge circuit is the bared tip of insulated wire lying along the support rod. A consideration of the physical configurations of anodes suitable for the plasma generation shows that the shape of the anodes does not in anyway effect the plasma formation. (Quinn et al., 1966) For example, using wire loops, cylindrical rods of arbitrary orientation, or the walls of a metallic vacuum vessel (Quinn et al., 1967) gives rise to the same spatial variation of plasma particle density at a given pressure and discharge current.

The changes in plasma configuration due to pressure variations can perhaps be best described by referring to Figure 2.1. In all these photographs the current in the discharge is 30 ma. The shutter speed of the camera and the distance separating the camera from the sphere is the same in all cases. When the residual gas pressure in the vacuum chamber is 500 microns of mercury, the plasma totally covers the sphere although the particle densities are much higher in the regions away from the magnetic poles. The farthest radial extent of the visible plasma remains within a distance of one half a sphere radius from the

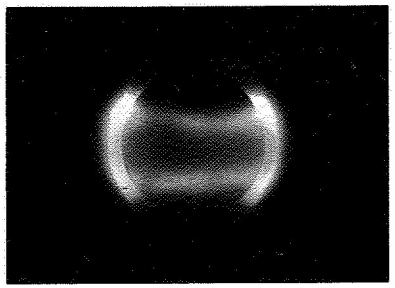

a. P = 500 microns

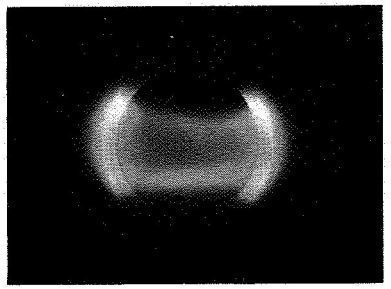

b. P = 400 microns

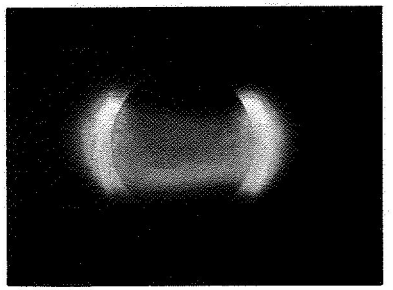

c. P = 300 microns

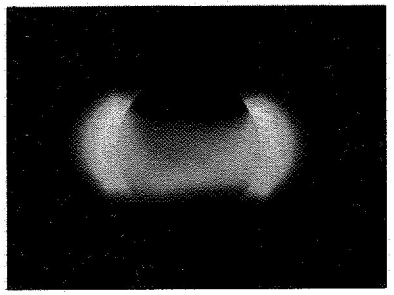

d. P = 200 microns

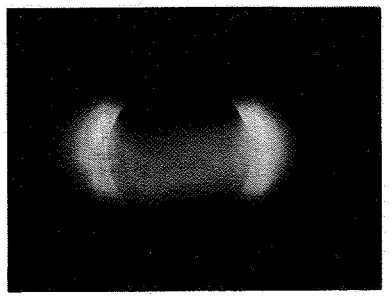

e. P = 90 microns

THE CHANGE OF PLASMA CONFIGURATION WITH PRESSURE

FIGURE 2.1

surface of the sphere. As the pressure is lowered the plasma becomes restricted to regions of lower latitude and is no longer visible above the poles of the magnet. The decrease of pressure is also accompanied by an increase in the maximum radial distance to which the visible plasma extends.

At a pressure of 200 microns, the light intensity emitted by the plasma appears to be most intense. Lowering the pressure below this point produces a more and more diffuse plasma until it is extinguished due to too small a magnitude of sustaining voltage.

If one assumes the maximum particle densities occur at points in space where the light intensity of the plasma is the greatest, then these regions of maximum particle density exist near 0.23 radii for the full range of pressures used. The "halo" glow appearing above the top magnetic pole in some of the photographs is a reflection from the far surface of the bell jar and is not a region of space occupied by the plasma.

The plasma extent can also be varied by increasing the discharge current. Figure 2.2 shows that as the discharge current is increased from 30 ma to 70 ma the extent of the plasma nearly doubles. The shutter speed was slower in these last photographs than for the photographs shown in Figure 2.1 and thus the plasma appears to be more intense. Viewing the plasma along the polar axis shows that the sphere is not totally covered at a pressure of 150 microns.

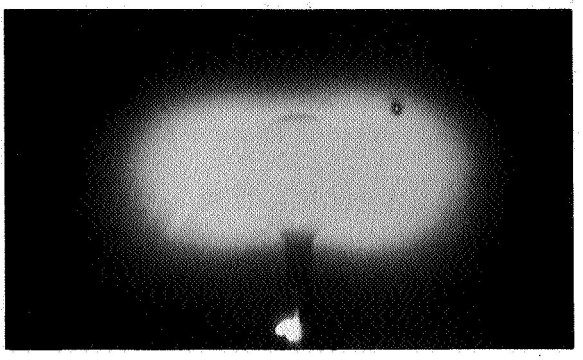

a. I = 70 ma; P = 150 microns

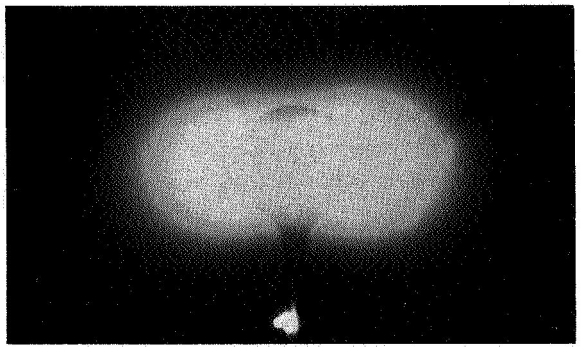

b. I = 50 ma; P = 150 microns

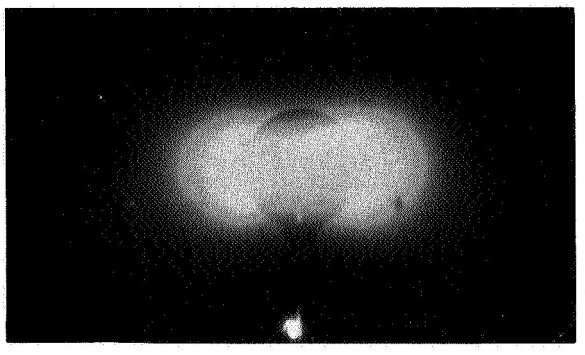

c. I = 30 ma; P = 150 microns

CHANGE OF PLASMA CONFIGURATION WITH CURRENT

FIGURE 2.2

2.2 Langmuir Probe Measurements

Langmuir probe measurements were made to determine the plasma density profiles in the equatorial plane for various combinations of pressure and discharge voltage. A double probe is used since the resulting data is more reliable than that obtainable from single probes when magnetic fields are present. Two experimental advantages of the double probe technique are that the electrical circuit of the double probe is not connected to the high voltage discharge circuit as in the case of the single probe and the double probe draws a very small portion of the total discharge current (usually less than 0.50 percent) and thus has a smaller disturbing effect on the plasma.

Two similar single probes comprise the double probe. The single probes are made of glass encased 10 mil tungsten wire having particle collecting lengths of 0.55 cm. To form the double probe the single probes are attached with a Sauereisen cement which has excellent heat resistive and insulative properties. The probe circuit is shown in Figure 2.3.

A typical set of probe data is plotted in Figure 2.4. The pressure in the vacuum vessel is 150 microns while the current in the discharge is 30 ma. The parameter of this family of curves is radial distance from the surface of the sphere. For an ideal double probe (one with two physically identical single probes) a zero current reading should result with zero applied voltage. However, the electric field existing in the plasma region (Quinn et al., 1967) is apparently of sufficient magnitude to make the saturation curves asymmetric with respect to the origin. Further for an ideal probe the portion of the

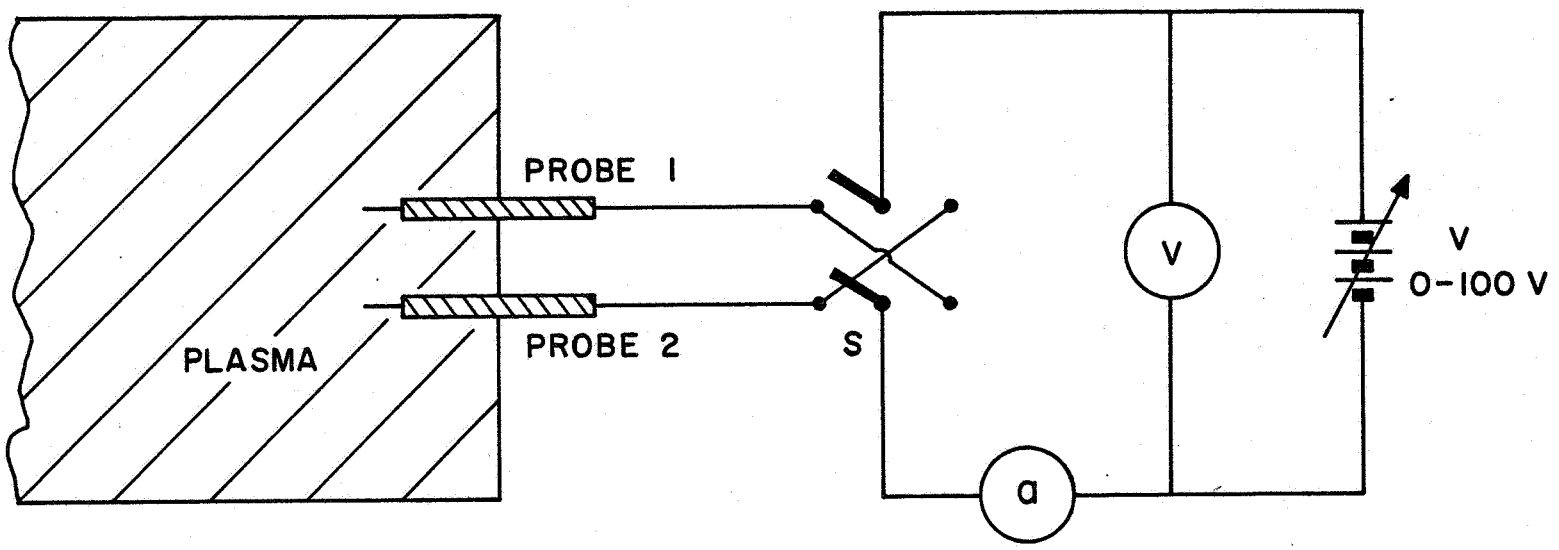

ELECTRICAL CIRCUIT OF DOUBLE LANGMUIR PROBE

FIGURE 2.3

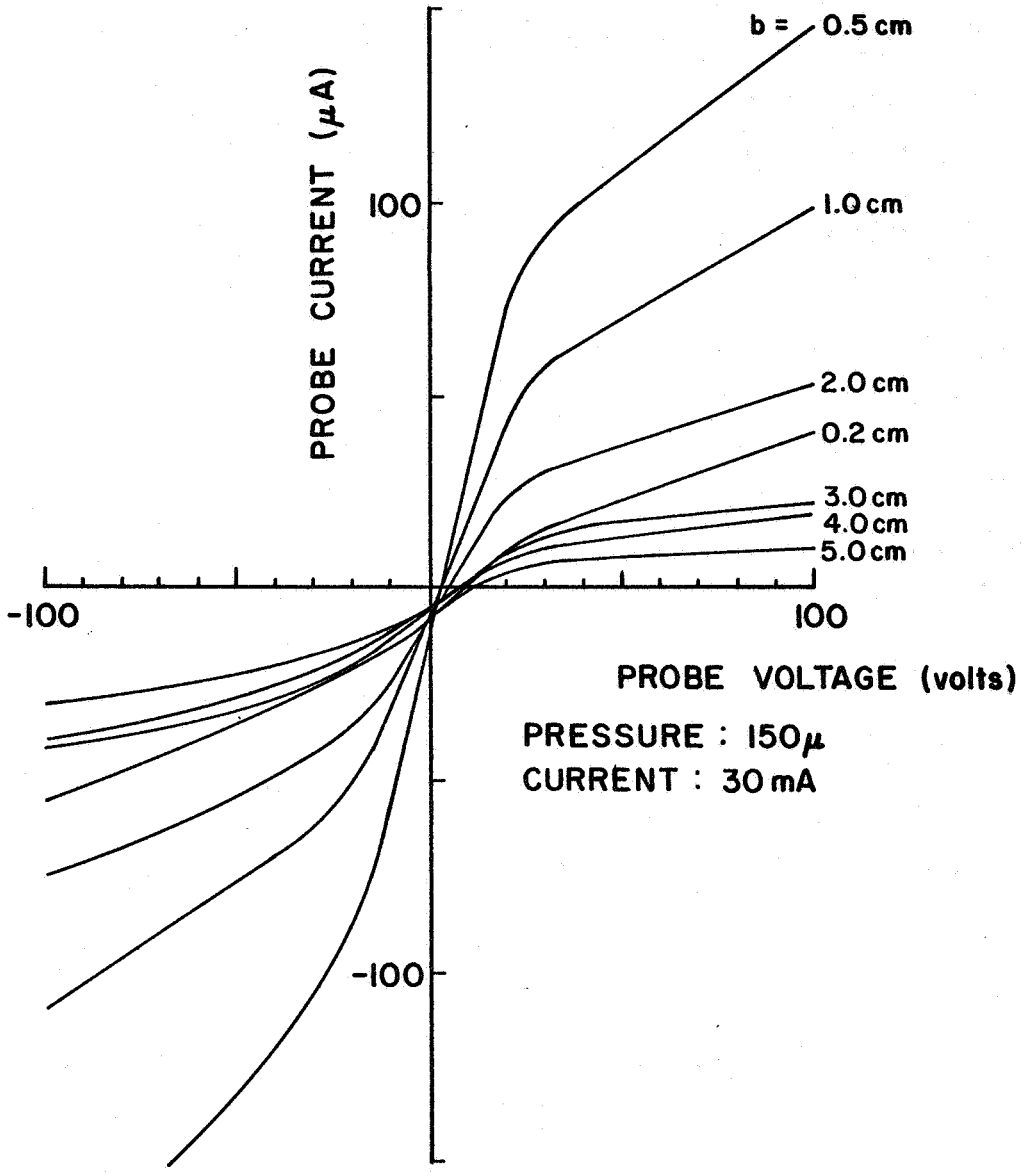

DOUBLE PROBE CHARACTERISTICS

FIGURE 2.4

curves beyond the "knee" should have zero slope. This increase of current is due to an expansion of the sheath thickness as the one tip of the probe goes increasingly negative with respect to the plasma. (Chen, 1965) Similar sets of curves were obtained for other pressures and discharge currents.

Assuming the ideal probe theory proposed by Johnson and Malter (1950) to hold in this case one can calculate the density of the ions at the points in space where probe data has been recorded (see Appendix A for sample calculations). Figures 2.5 and 2.6 display the results of these calculations. The greatest ion density occurs near 0.4 cm, 0.24 radii, form the surface of the sphere and is independent of pressure. The shape of these curves is identical to those published by Quinn and Fiorito. (1967)

To obtain electron densities from this data we can assume $N_e = N_+$ (assumption of charge neutrality) as does Johnson and Malter. But Quinn and Fiorito (1967) show that in a similar plasma configuration the maximum electron number density is a factor of 0.245 less than the maximum ion density. Thus as a closer approximation to the values of electron densities than can be obtained by assuming charge neutrality, N_e at each radial position is determined from the corresponding values of N_+ through the relation $N_e(r) = 0.245N_+(r)$, i.e., by reducing $N_+(r)$ by the factor $0.245 = N_e(\text{peak value})/N_+(\text{peak value})$ as deduced form the curves of Quinn and Fiorito. (1967) Figures 2.7 and 2.8 show the resultant electron density profiles.

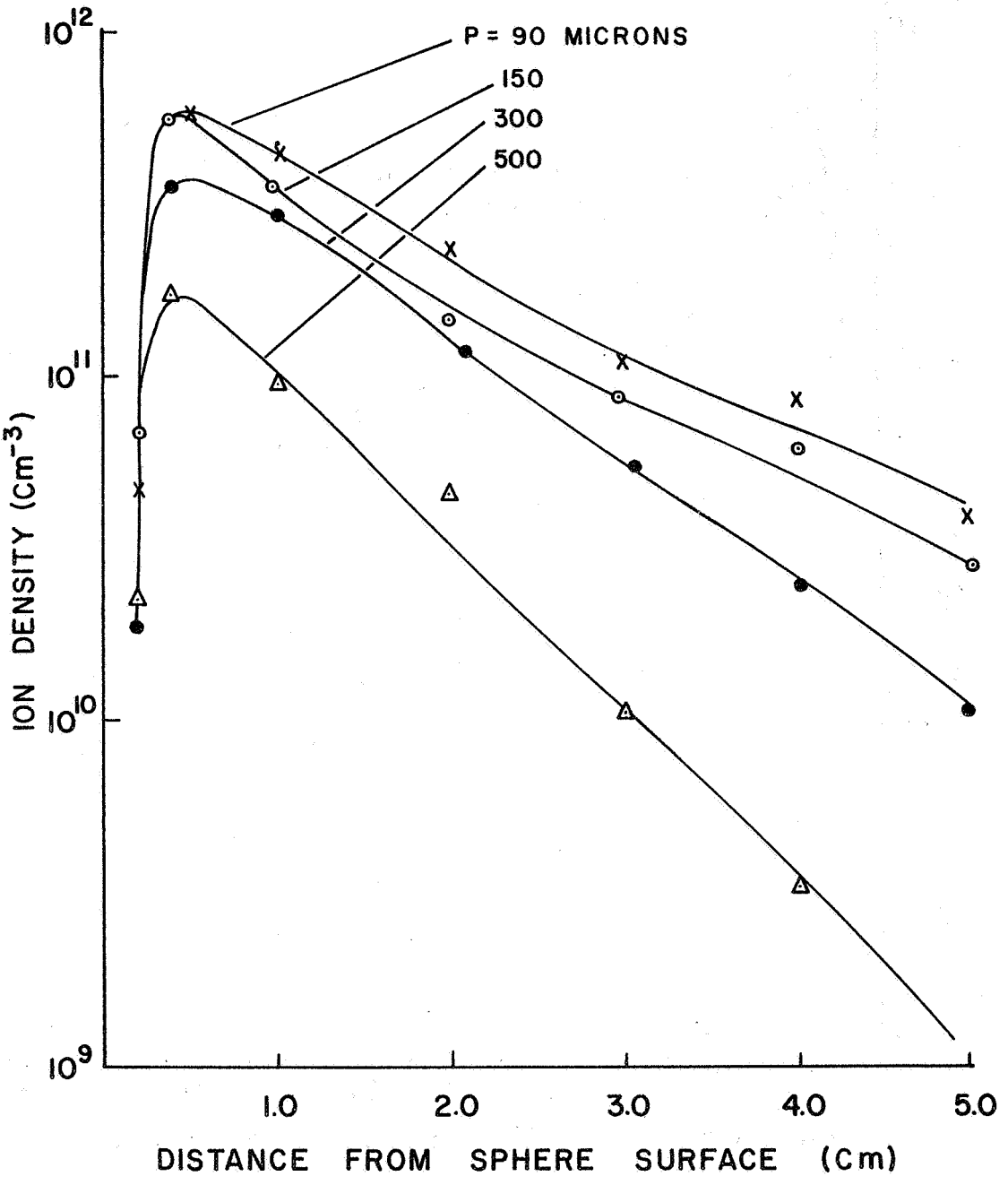

ION DENSITY PROFILES: 30mA

FIGURE 2.5

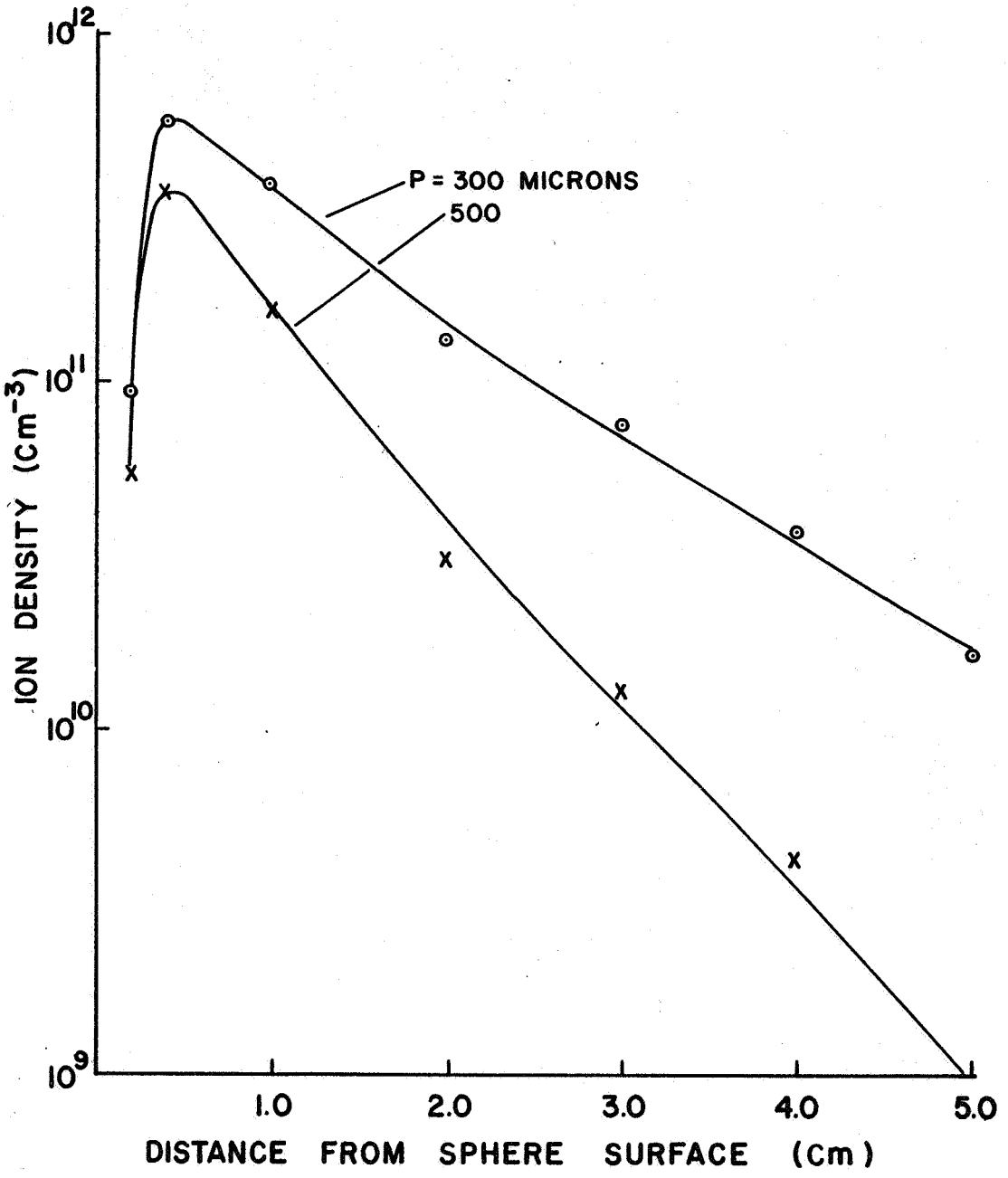

ION DENSITY PROFILES: 50mA

FIGURE 2.6

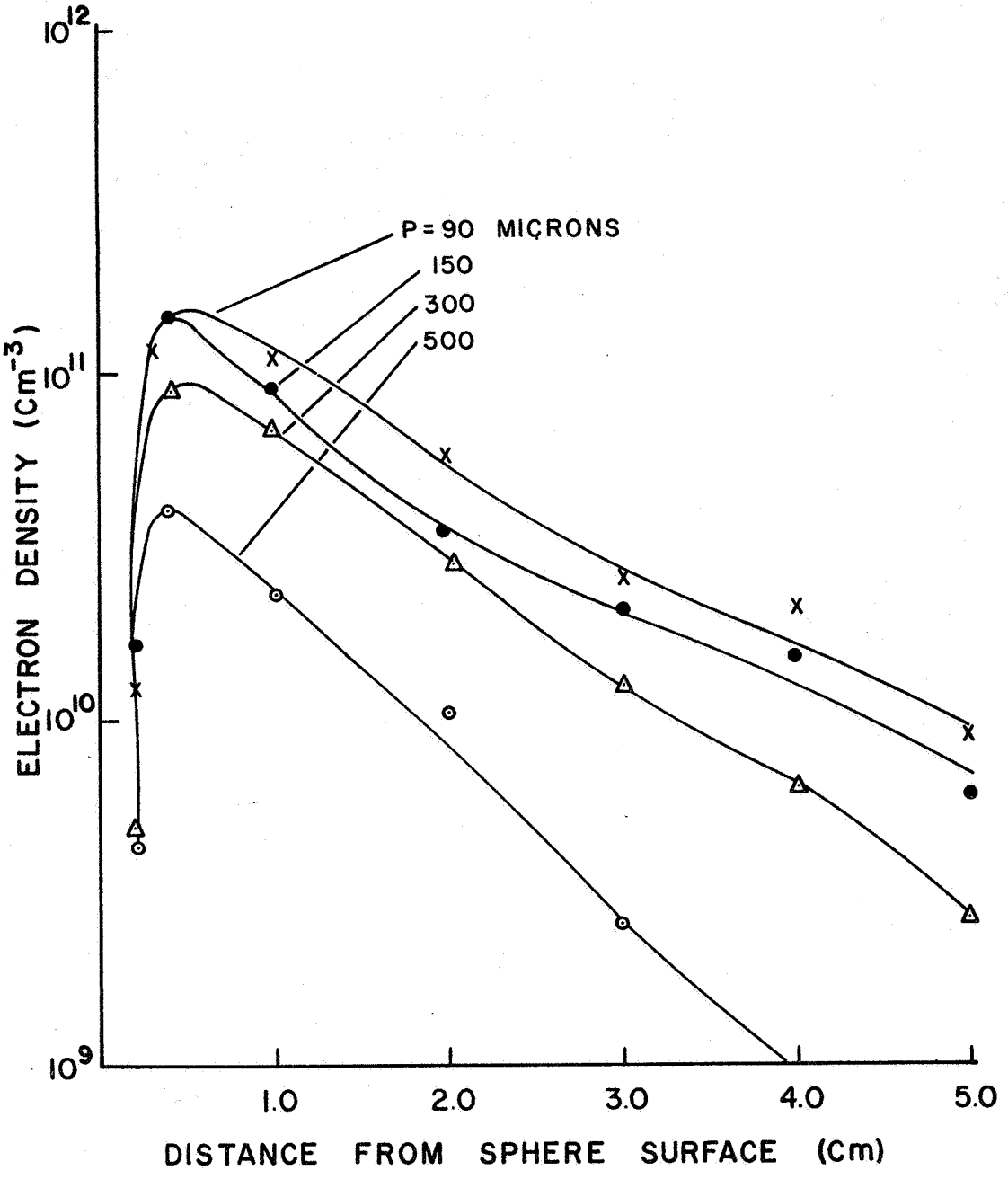

ELECTRON DENSITY PROFILES : 30mA

FIGURE 2.7

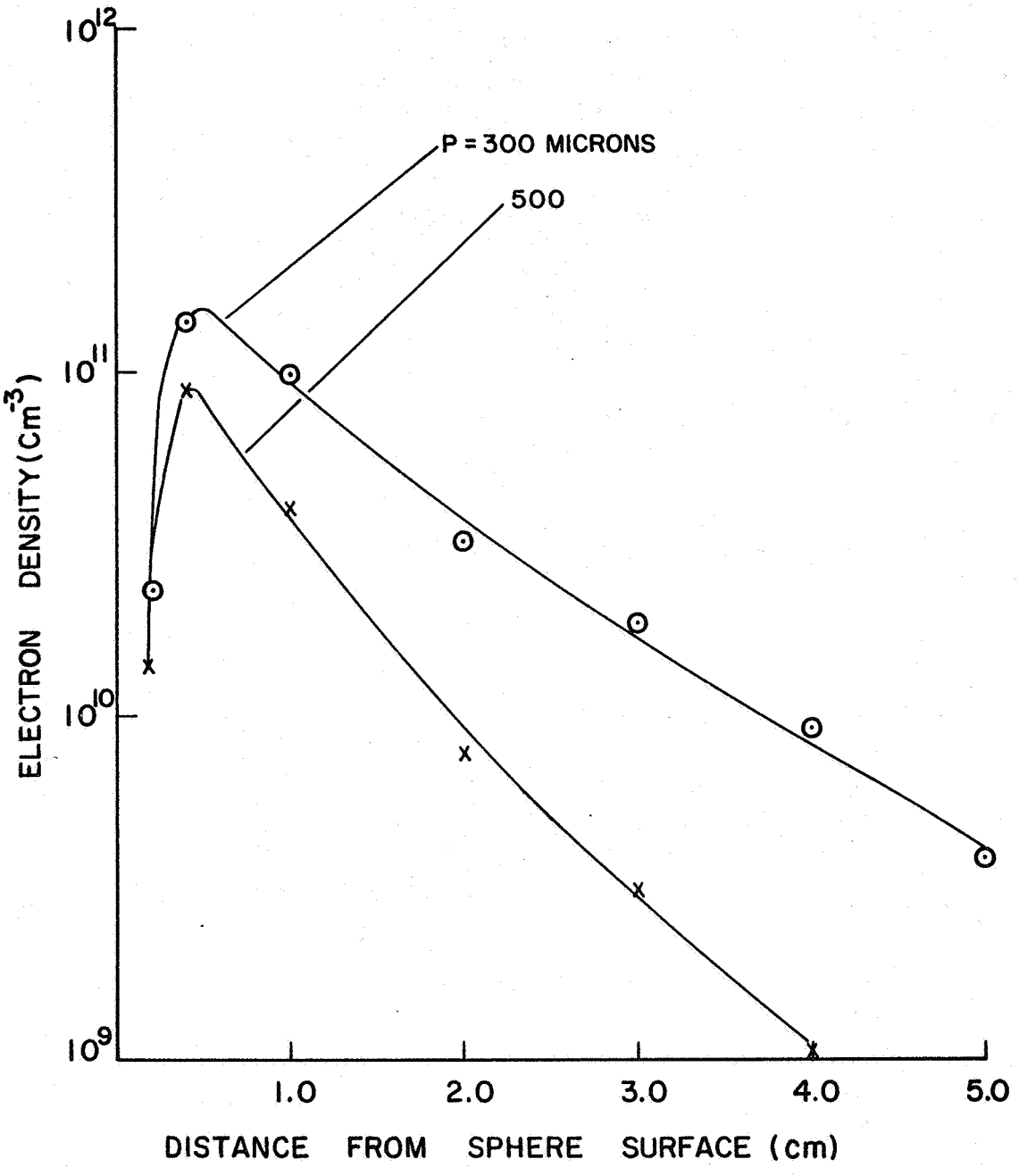

ELECTRON DENSITY PROFILES : 50 mA

FIGURE 2.8

2.3 Microwave Interferometer Measurements

The purpose of the microwave interferometer or microwave bridge used in plasma diagnostic applications is to measure very small changes in the electrical properties of the transmission path. These changes of the transmission properties can then be related to the properties of the plasma.

Although these devices can be designed to varying degrees of sophistication, the operation of all interferometers is usually based on the transmission of a microwave signal through a volume of ionized gas to be analyzed. Figure 2.9 is a schematic diagram of the interferometers, except the K-Band interferometer which utilized flexible wave guide instead of a rotary joint, used in this experiment. The signal sources, reflex klystron oscillators, are operated with 1000 Hz square wave modulation. The isolator permits unattenuated propagation in the direction of the arrow and serves as a protective device against possible large reflections which would tend to detune the oscillator. The directional coupler to the right of the isolator, lets a small amount of the signal to be channeled into the bridge arm. The remainder of the original signal is transmitted. The received signal combines with the portion of the transmitted signal in the hybrid junction. The tuners are used as matching devices.

The orientation of the magnetic field of the sphere with respect to the interferometer can be determined by considering a rectangular coordinate system with its origin at the center of the sphere. Using this coordinate system, the x-axis (pointing out of the paper) passes through a magnetic pole of the sphere while the transmitting and

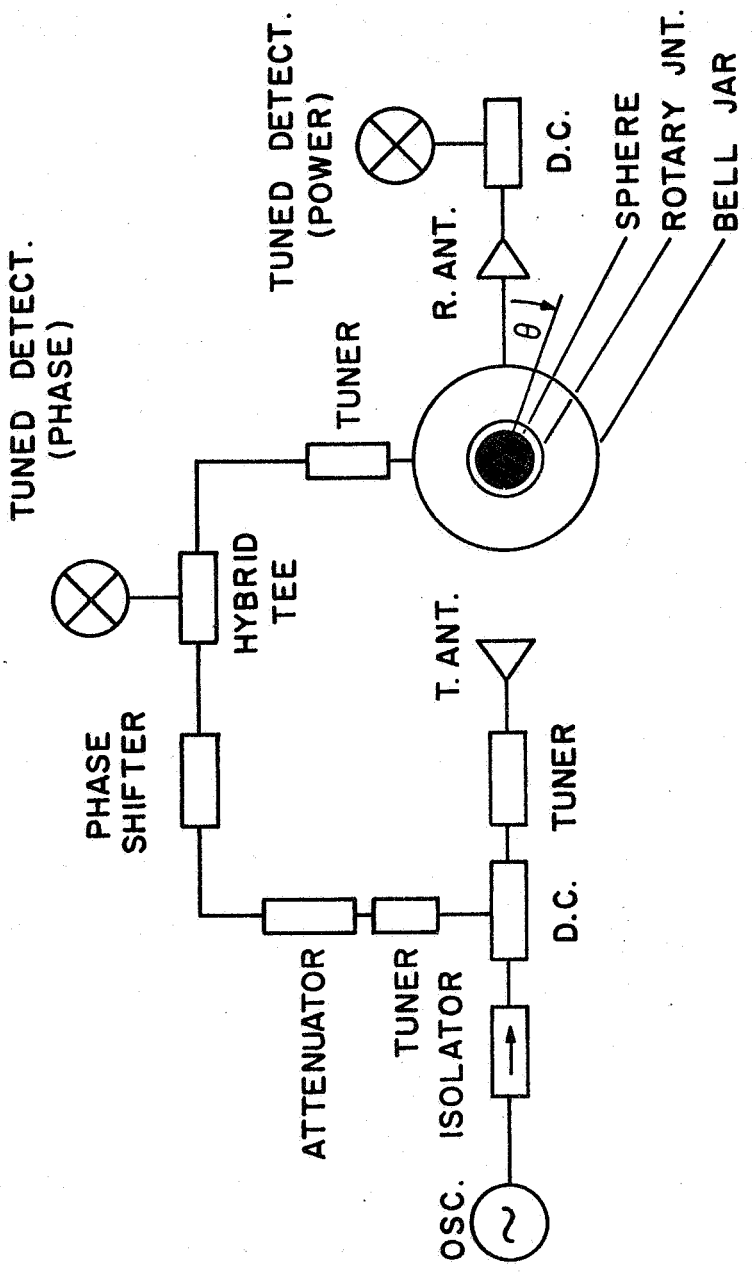

MICROWAVE INTERFEROMETER

FIGURE 2.9

receiving antennae are positioned along the -z and z-axis respectively. The center of the receiving antenna moves in the y-z plane of this coordinate system at a fixed distance from the origin. Any position of this antenna off the z-axis can be defined in terms of the angle θ. A rotary joint, located directly below the sphere, makes this angular variation possible.

The use of the bridge is described below. In Figure 2.10.a, when the plasma does not surround the sphere, the reference signal is $A_o \sin(\omega t + \phi_o)$ while the received signal is $A_1 \sin(\omega t + \phi_1)$. The phase and amplitude of the reference signal are varied until the signal in the difference arm of the hybrid junction is zero. This condition gives a null reading on the "phase detector." The setting of the phase shifter and the "received power detector" are recorded. In Figure 2.10.b, the plasma is formed around the scattering center. The received signal now changes to $A_2 \sin(\omega t + \phi_2)$. Again the phase and amplitude of the reference signal are varied to give a null reading on the phase detector. The change in settings of the phase shifter and received power indicator because of the conditions of plasma on and off are a measure of the phase shift and attenuation introduced into the transmission path by the plasma. The receiving antenna is then moved to a new position and the recording procedure repeated.

The frequencies of operation of the three interferometers used in this experiment at 10Ghz, 22.4GHz and 35GHz; they will be referred to as X-, K- and A-Band respectively. Figures 2.11 to 2.12 are photographs of these systems.

The X- and K-Band antennae are pyramidal horns while the antennae in the A-Band system are conical horns fitted with lenses. The

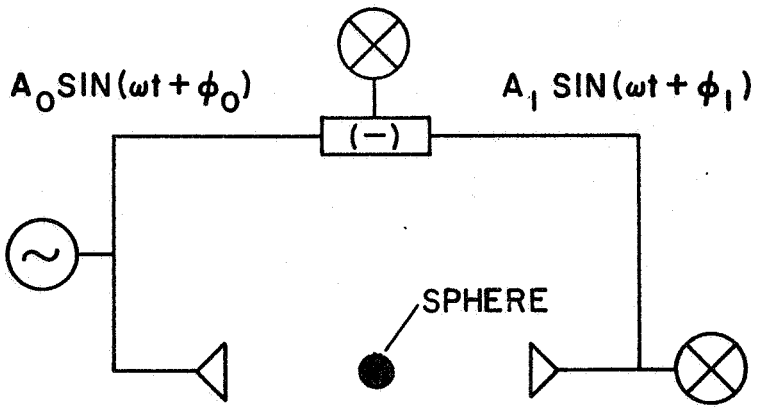

(a) SCATTERING FROM SPHERE

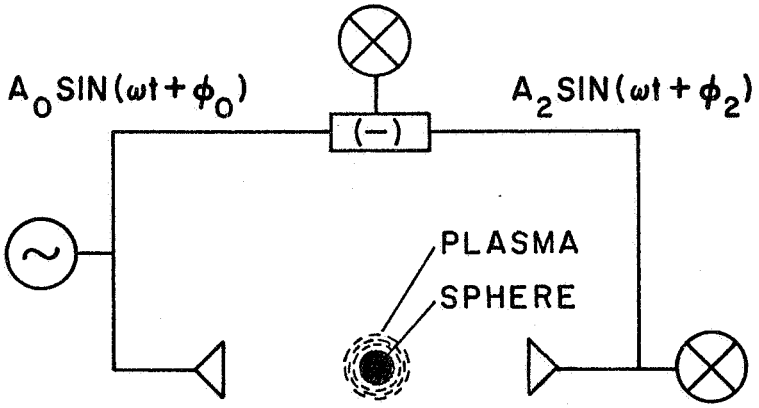

(b) SCATTERING FROM SPHERE AND PLASMA

SIGNALS IN A MICROWAVE BRIDGE

FIGURE 2.10

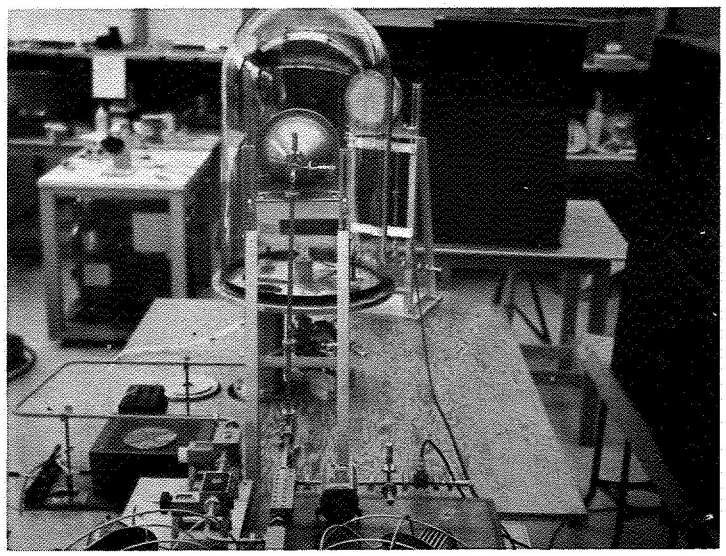

a. A-Band

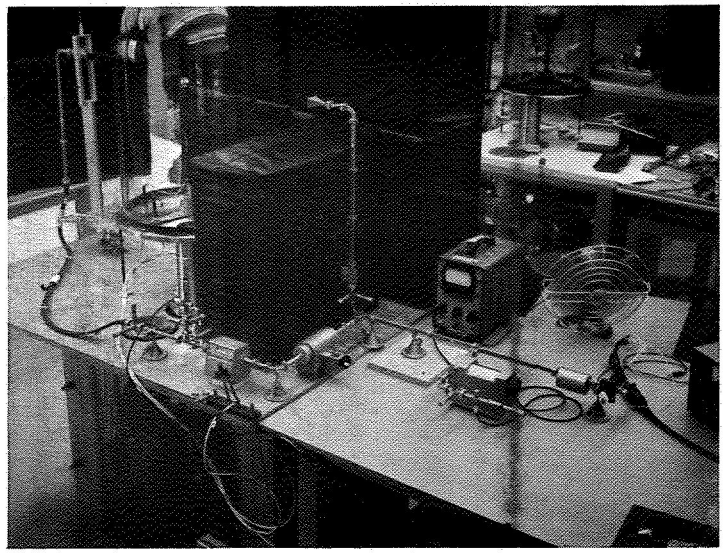

b. K-Band

A-BAND AND K-BAND INTERFEROMETERS

FIGURE 2.11

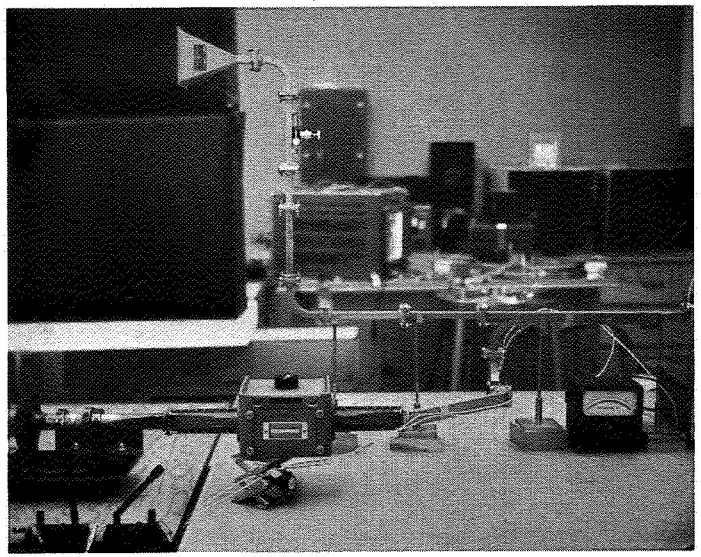

a. Transmitting End

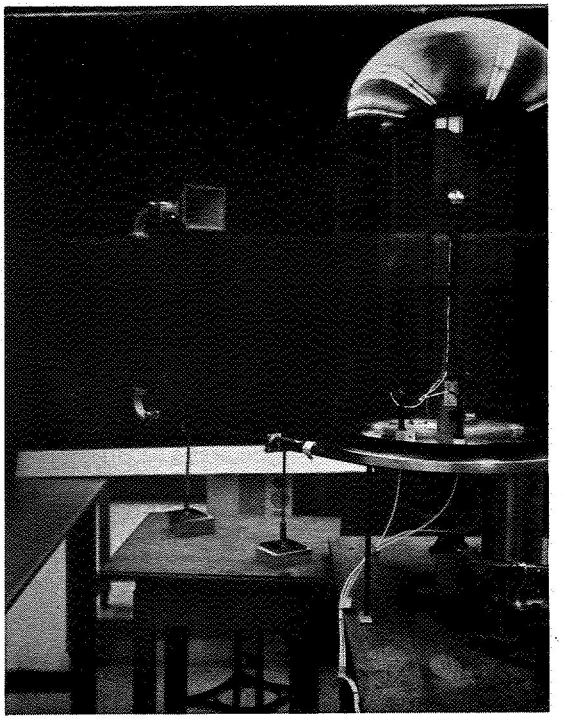

b. Receiving End

X-BAND INTERFEROMETER

FIGURE 2.12

distances from the scattering center to the antennae are 73.7 cm, 53.3 cm and 37 cm for the X-, K-, and A-Band interferometers respectively. The smallest value of attenuation that can be measured is 0.025 ± 0.05 dB while the smallest phase change is 1 ± 1.5 degrees.

The data of this section can be displayed graphically according to three groups, power change as a function of scattering angle, phase change versus scattering angle and power change as a function of pressure for various scattering angles. These results are presented and compared with the theoretical results in Section 4. However, some additional information which has direct bearing on the interpretation of these results is given now.

To obtain an approximation to the angular dependence of the magnitude of the incident electric field the horn patterns were taken with the bell jar in place. These patterns are shown in Figure 2.13. As an example of the corrections applied to the incident field it is straight forward to show from these curves that for the X-Band interferometer the angular dependence for $|E^i|$ is approximately $0.5(-1/40\theta + 1)$ where the 0.5 accounts for the decrease in field strength due to the 1/r dependence of the transmitted fields.

Of chief concern to the investigator is the interaction between the bell jar and the electromagnetic fields and the limitations that the bell jar imposes on the range in θ over which the microwave scattering measurements are valid. In trying to resolve this question a number of laboratory tests, to be described, were conducted.

In all the figures to be discussed in connection with this problem the circular dots are to be taken as reference and represent power

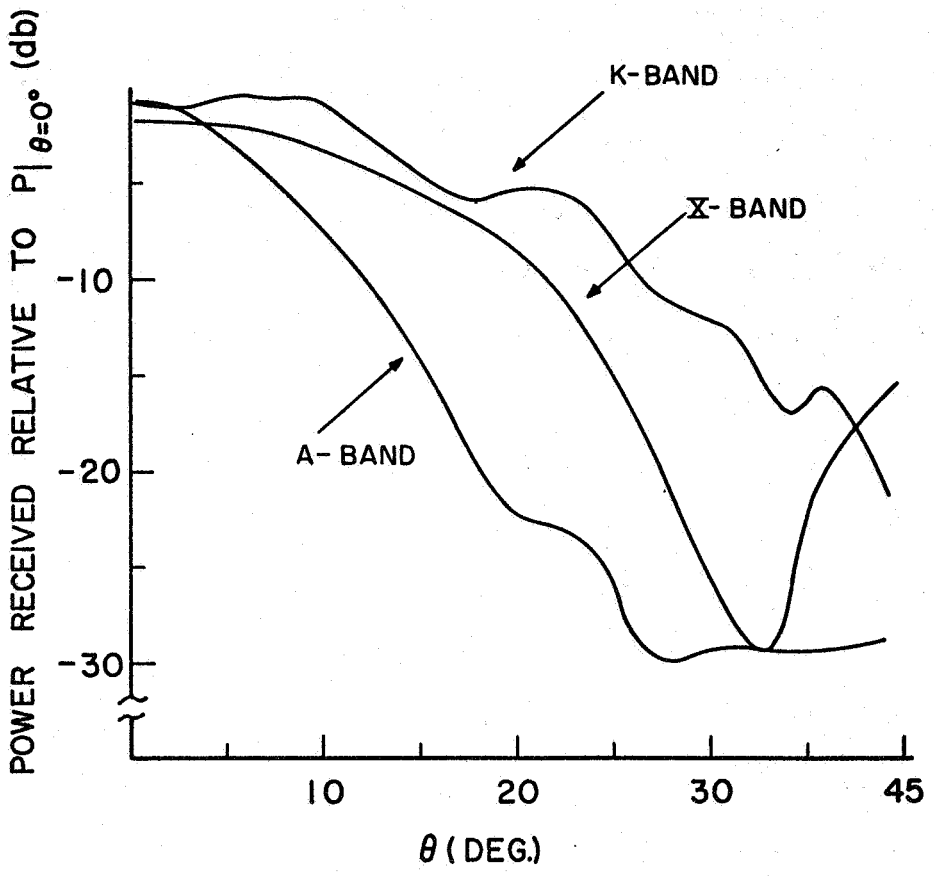

RECEIVED POWER WITH BELL JAR IN TRANSMISSION PATH

FIGURE 2.13

ratios obtained with the system configuration used throughout the experiment, i.e., the antennae are properly aligned, the bell jar is centered around the sphere and no modifications of the glass surface are made. The frequency of the incident field is 35 GHz and the current in the discharge is 30 ma for all the cases considered.

The first test performed included displacing the bell jar from its centered position approximately 2.2 cm perpendicular to the line defined by $\theta = 0^{o}$. Figure 2.14.a shows how the resultant power change curves agreed with the reference. For either displacement both curves agree, within measurement error, for the first 9^{o}. The first minimum value varies by +0.25 dB in one case and -0.45 dB in the other case. All three minima occur at 10.5^{o}. Beyond this value of θ the difference in dB is not as great as at 10.5^{o} but now the maxima and minima shift with respect to the reference.

Secondly, to permit the incident wave to enter the bell jar through approximately a plane glass slab, and to prohibit the side lobes of the transmitting antenna from interacting with the glass, an entrance aperture was surrounded by a heavy coating of absorber; the aluminum sheet covering the absorber described the aperture while the absorbing material reduced secondary reflections (12 dB) from the underside of the Al sheet. Figure 2.14.b shows the results of the aligned system when modified in this way and when the bell jar was displaced as shown. Both curves agree with the reference in the range $0 \leq \theta \leq 9^{o}$. The variation of the power ratios at the first minimum is -1.0 dB for the centered bell jar and 0.0 dB for the misaligned case.

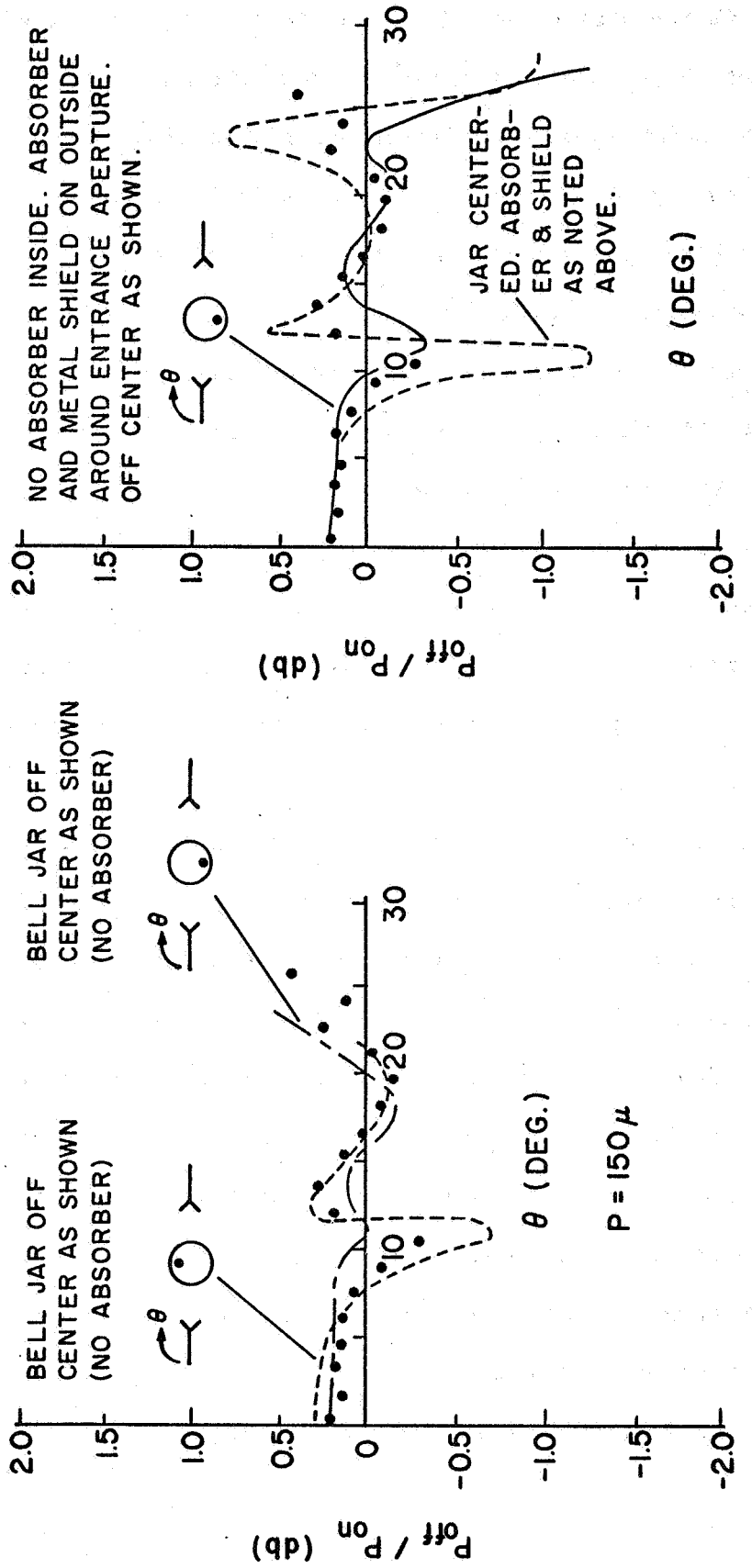

a. DISPLACING BELL JAR

b. ABSORBER EFFECTS

LIMITATIONS ON SCATTERING DATA : I

FIGURE 2.14

Thirdly, in an attempt to reduce internal reflections, the inner surface of the bell jar was coated with absorber everywhere except for a small entrance aperture and exit slit. Lastly, in trying to approach an ideal scattering situation by reducing internal reflections and side lobe-glass interaction, the bell jar with the interior coating of absorber had added to it the exterior absorber and the Al sheet described above. The effect on the power change data of these last two conditions are shown in Figure 2.15.a and 2.15.b. Reducing the internal reflections did not appreciably change the resultant power ratio curve. The "ideal" scattering geometry gave a change in the value of the first minimum of 0.2 dB and at the first maximum the change was 0.25 dB. Displacing the bell jar for this ideal case shifted the positions of the extrema and changed the value of the first minimum and maximum by 0.3 dB and 0.25 dB respectively.

For all these modifications of the bell jar surfaces and repositioning of the scattering geometry, the power changes agree with the reference points, within experimental accuracy, in the range $0 \lesssim \theta \lesssim 10^{o}$. For values of theta outside this range the shape of the curves are generally preserved but the depths of the minima and the heights of the maxima can be decreased or increased or shifted for misaligned geometries; this indicates that the internally reflected fields significantly alter the wave incident upon the receiving antenna in this range. Thus one can conclude that the presence of the bell jar can be neglected for forward scattering angles in the range $|\theta| \lesssim 10^{o}$, the experimental measurements are valid for the scattering geometry used throughout the laboratory investigation when θ is so limited and the error of each data point in this range is equal to the measurement error.

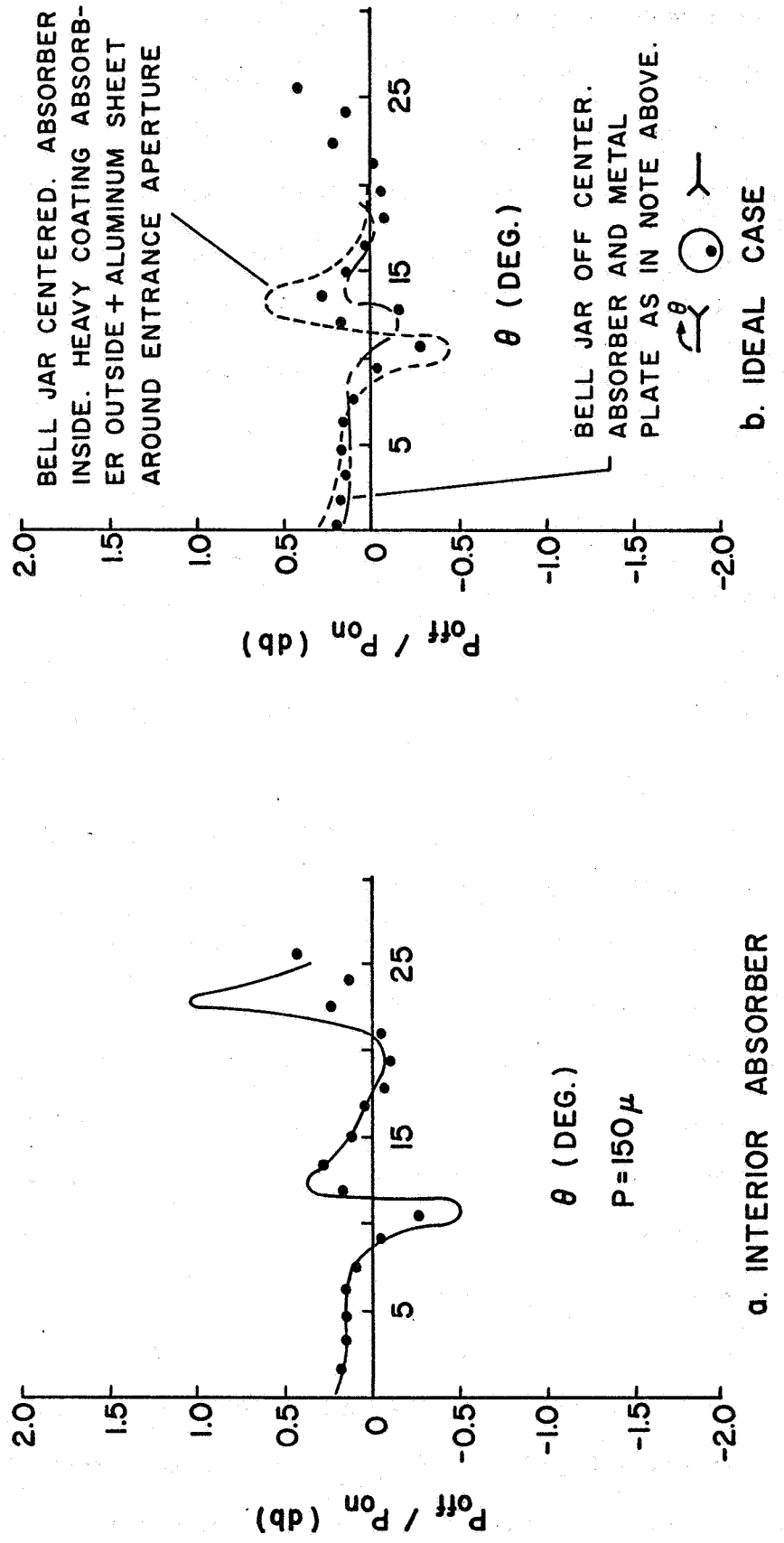

LIMITATIONS ON SCATTERING DATA: II

FIGURE 2.15

3. THEORETICAL EXPRESSIONS FOR LABORATORY OBSERVABLES

In this section the assumptions used in formulating a mathematical model of the experiment are stated and examined individually for validity. Consistent with these assumptions an idealized model is formulated and expressions for the scattering coefficients and scattered field quantities are given. Finally those quantities which describe the physical measurements are written in a form suitable for numerical analysis.

3.1 Assumptions of the Mathematical Model and the Scattering Geometry

From the description of the laboratory apparatus in Section 2, one realizes that the fields emitted by the transmitting antenna must pass through the glass bell jar, interact with the plasma-sphere scattering configuration and then be collected by the receiving antenna after passing through the glass jar a second time. To make the theory tractable, the presence of the bell jar is not included in the analysis. For all frequencies of interest the thickness of the vacuum vessel (0.635 cm) is an appreciable fraction of the wavelength. However, with a radius of curvature of 22.86 cm the above approximation is quite valid in forward scattering directions since in these directions the glass jar can be thought of as two plane parallel slabs of a lossless dielectric which would introduce a constant phase shift to the waves

passing through them. The validity of this assumption has been verified experimentally as discussed in Section 2.3.

The permanently magnetized sphere is assumed to be physically isolated in a free space region and thus the effect of its metal rod on the scattered field is neglected. In actuality the sphere is supported by a metal rod of 0.635 cm diameter; again the ratio of rod diameter to wavelength approaches unity near the highest frequency used. Verification of the validity of this assumption can be accomplished by at least two independent laboratory measurements. The first, which is quite difficult from a physical realization standpoint, would be to compare scattering patterns of the sphere supported by the 0.635 cm rod to similar measurements for a sphere supported by an infinitely thin rod. Secondly, the measured scattering pattern of the actual sphere-rod configuration can be compared to scattering patterns determined theoretically. This second method was used. Unfortunately, one detects not only the scattered field but the vector sum of the incident and scattered fields. Thus this question of validity could not be resolved by comparing the measured and calculated scattering patterns. Theoretically, however, the problem of scattering by a finite cylindrical rod terminated at one end with a spherical body would be very difficult to solve exactly; this theoretical difficulty prompts the use of the assumption given above.

The sphere is assumed to have infinite conductivity. Actually the sphere has a conductivity of approximately 2.1×10^6 (mhos/m); copper, which has a conductivity of approximately 5×10^7 (mhos/m), is usually assumed to be a perfect conductor. In making this assumption,

then, we are conforming to standard practice which has been proven to give good agreement in numerous other investigations.

The refractive index n of the plasma is related to the physical properties of the plasma by means of the Appleton-Hartree equation

$$n^2 = 1-X \Big/ \left[U - \frac{Y_T^2}{2(U-X)} \pm \left\{ \frac{Y_T^4}{4(U-X)^2} + Y_L^2 \right\}^{\frac{1}{2}} \right] \qquad (3.1)$$

where $X = \omega_p^2/\omega^2$, $U = 1+\nu/\omega$, $Y_T = \omega_B/\omega\sin\phi$, $Y_L = \omega_B/\omega\cos\phi$ and ϕ is the angle between the wave propagation vector and the magnetic induction vector. (Budden, 1961) To investigate the effect of the static magnetic field on the refractive index let us consider the worst possible case, i.e., points in the plasma where the magnitude of the static magnetic field is a maximum; also use the frequency of the incident wave which has the lowest value ($f = 10^{10}$ Hz). From the experimental values shown in Figure 3.1 we find the maximum value of the static B field to be 165 gauss. Further assuming $Y_L = 0$, the case of transverse propagation, and the magnitude of $i\nu/\omega$ can be neglected with respect to unity, then

$$n^2_{\substack{\text{ORD}\\\text{WAVE}}} = 1-X \quad \text{and} \quad n^2_{\substack{\text{XORD}\\\text{WAVE}}} = 1-X/\left(1 - \frac{Y_T^2}{1-X}\right) \qquad (3.2)$$

For the values of frequency and magnetic field strength given, $Y^2 = Y_T^2 = (eB/m\omega)^2 = 0.00212$. For an assumed density of 10^{11}, Figure 3.2 shows that $X = \omega_p^2/\omega^2 = 0.08$. Therefore

$$n_o^2 = 1-X \quad \text{and} \quad n_x^2 = 1-X/.998 \qquad (3.3)$$

or in this worst possible case the percent change between n_o^2 and n_x^2 is approximately 0.019. Thus the dipolar magnetic field of the sphere

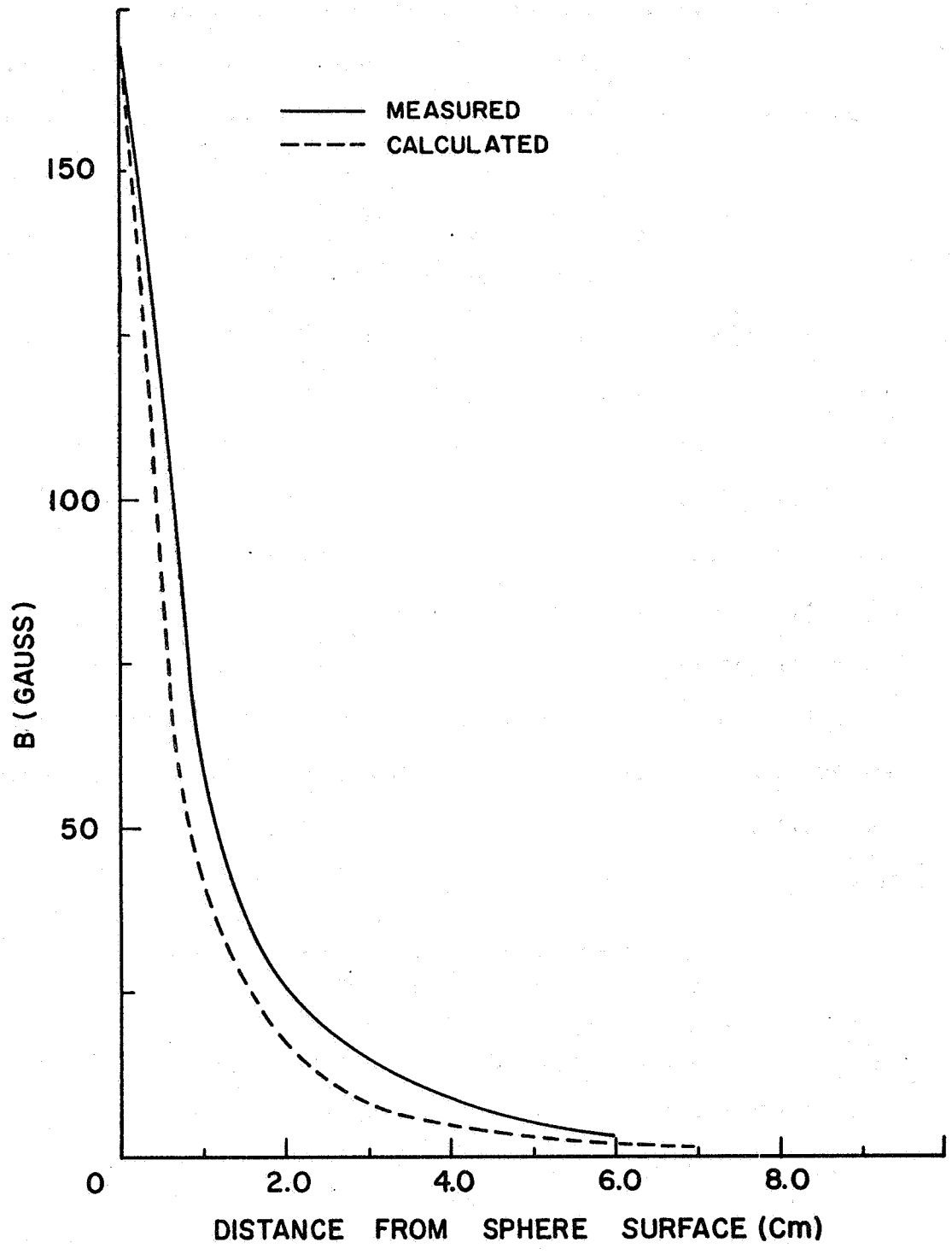

MAGNETIC FIELD STRENGTH IN EQUATORIAL PLANE

FIGURE 3.1

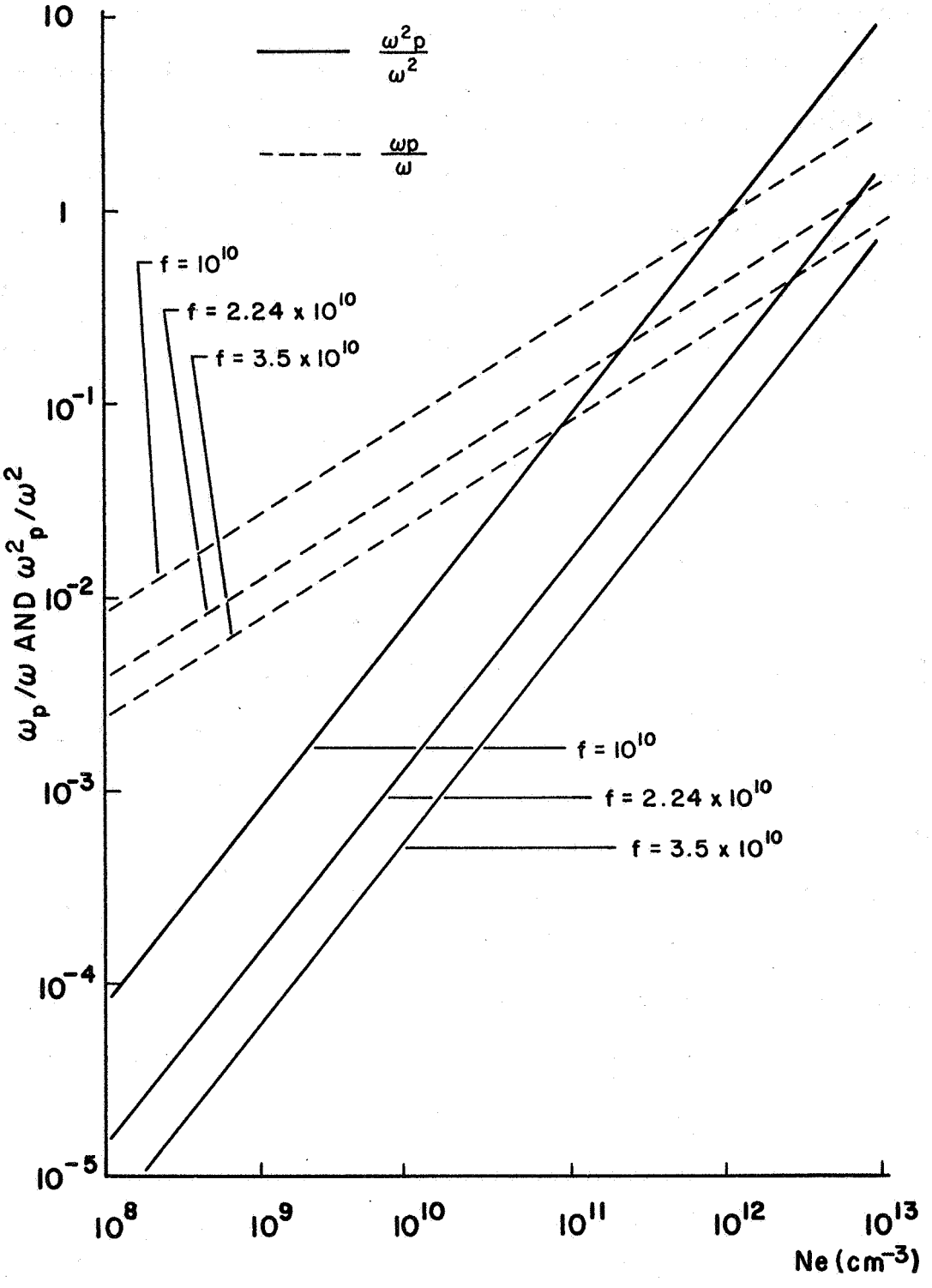

$\omega p/\omega$ AND $\omega^2 p/\omega^2$ VERSUS FREQUENCY

FIGURE 3.2

is regarded as a plasma confinement mechanism and is neglected in the complex refractive index which describes the plasma.

Figures 3.3 to 3.5 are graphs of the real and imaginary parts of the plasma refractive index for various operating frequencies, collision frequencies and electron densities as a function of radial distance. When drawing these curves it was assumed that the electron density has its maximum at the surface of the sphere while it decreases as $1/r^2$ in a radial direction away from the sphere. See Figure 3.6. Since for all cases the real part of n is so near unity and the imaginary part is so small, the plasma covering is assumed to be characterized by a constant complex refractive index. Only the regions of space above and below the magnetic poles of the sphere are not covered by a visible plasma; as a further approximation the plasma sheath is assumed to totally cover the sphere. In the simplified model then, the actual plasma, which has electrical properties that blend smoothly into those of free space, is replaced by a homogeneous plasma shell of constant refractive index n_o with an assumed radial extent b.

Although the work by Quinn and Fiorito (1967) shows that the ion number density exceeds the electron number density, we impose the simplifying assumption of charge neutrality existing at all points within the plasma region. Further, all nonthermal particle motions are neglected and thus the resultant model must be purely static in nature.

Finally, the electromagnetic field quantities are assumed to have a time variation of $e^{-i\omega t}$.

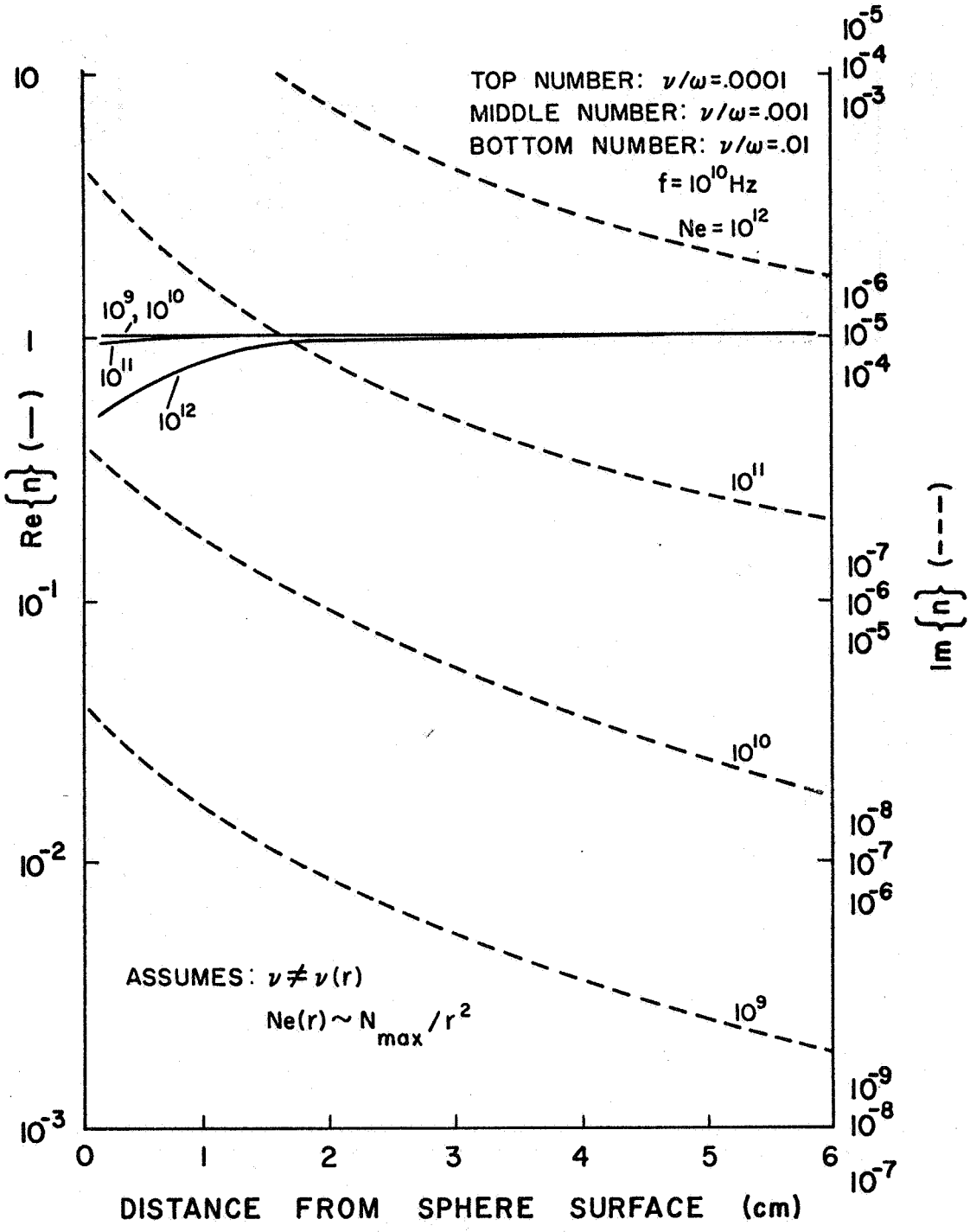

PLASMA REFRACTIVE INDEX : X-BAND

FIGURE 3.3

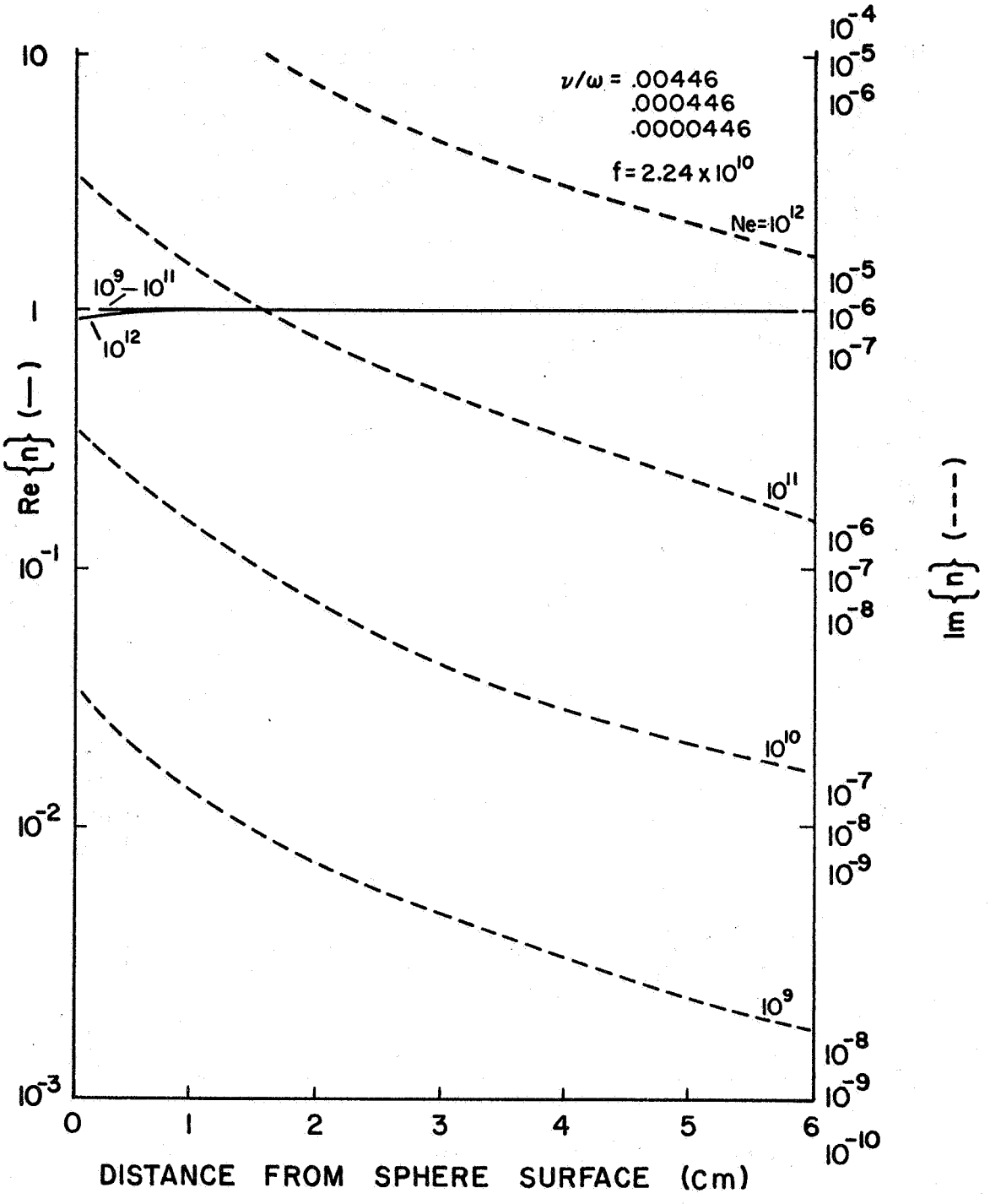

PLASMA REFRACTIVE INDEX : K-BAND

FIGURE 3.4

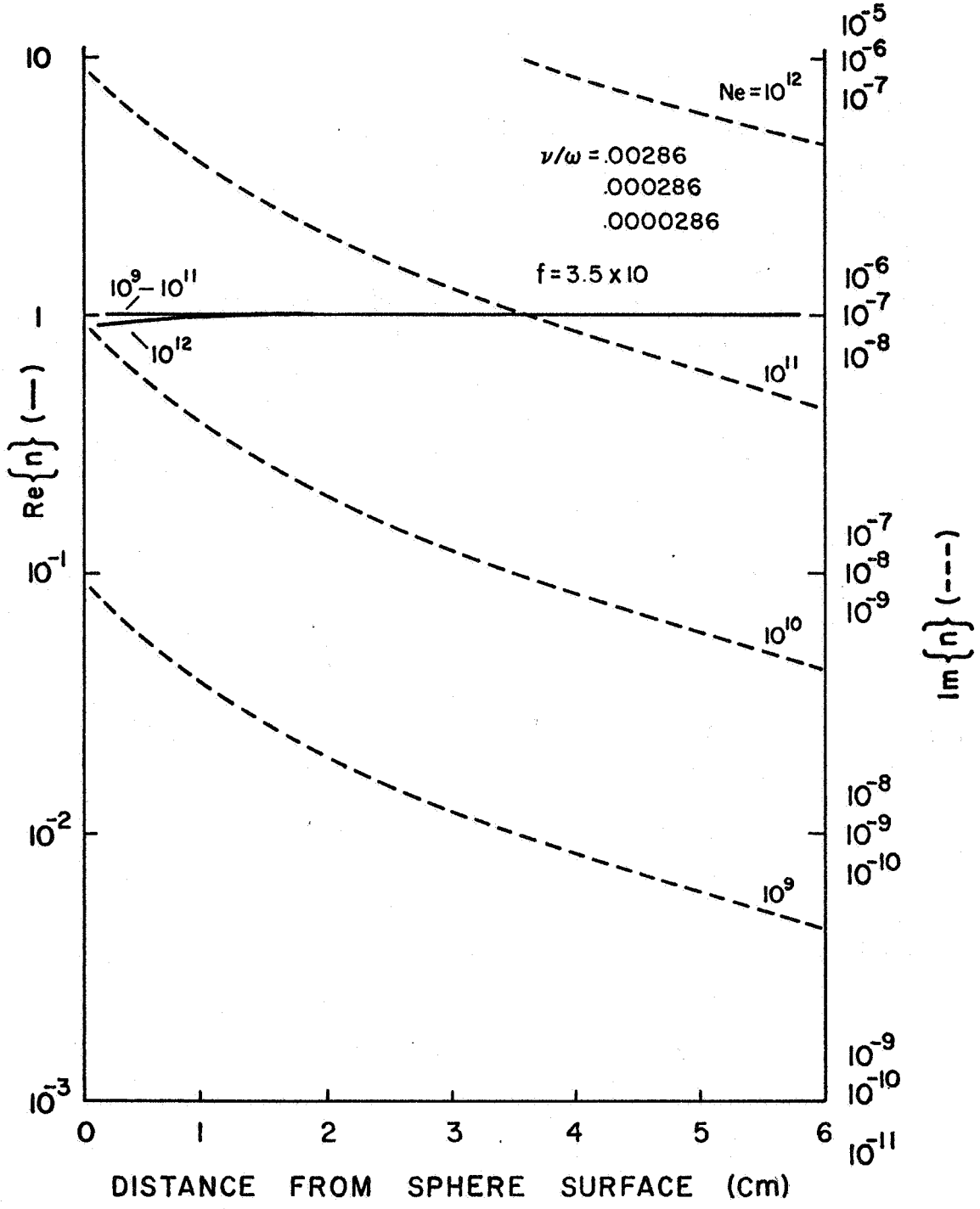

PLASMA REFRACTIVE INDEX: A-BAND

FIGURE 3.5

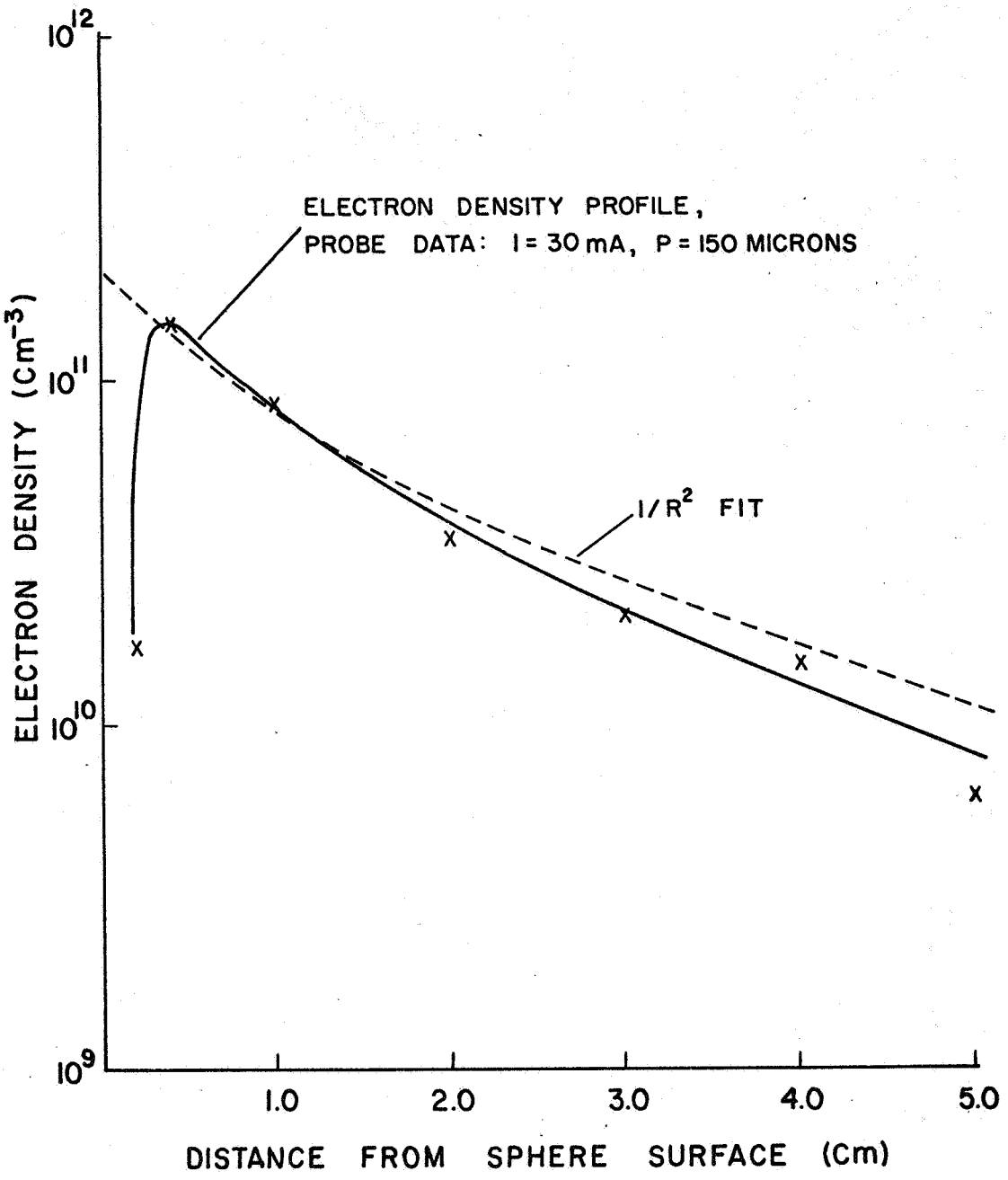

ELECTRON DENSITY DEPENDENCE ON R

FIGURE 3.6

Figure 3.7 shows the orientation of the incident plane wave and the scattering configuration with respect to a rectangular coordinate system having an origin at the center of the plasma coated sphere. The outer medium, the plasma sheath, and the metallic sphere are designated as Regions I, II and III respectively. The radius of the sphere is denoted by "a" while the outermost radial extent of the plasma is denoted by "b". The colatitude angle is measured from this z-axis in the spherical coordinate system referred to later in this section.

The incident plane wave is propagating in the positive z-direction. The electric vector is linearly polarized and lies along the positive x-direction.

3.2 The Scattering Coefficients and the Scattered Field

From the assumptions stated in the last section it is clear that the appropriate formulation of the problem should describe the scattering of plane electromagnetic waves from a plasma coated spherical conductor. The problem of scattering by a single spherical body has long existed in the tutorial literature. To solve the problem at hand one need only impose an identical set of boundary conditions on the electromagnetic fields at the plasma metal interface. This approach is well formulated and easily understandable in terms of classical electromagnetic theory; the solution to the problem is presented in its entirety in Appendix B. We will make use of the results of this appendix as needed.

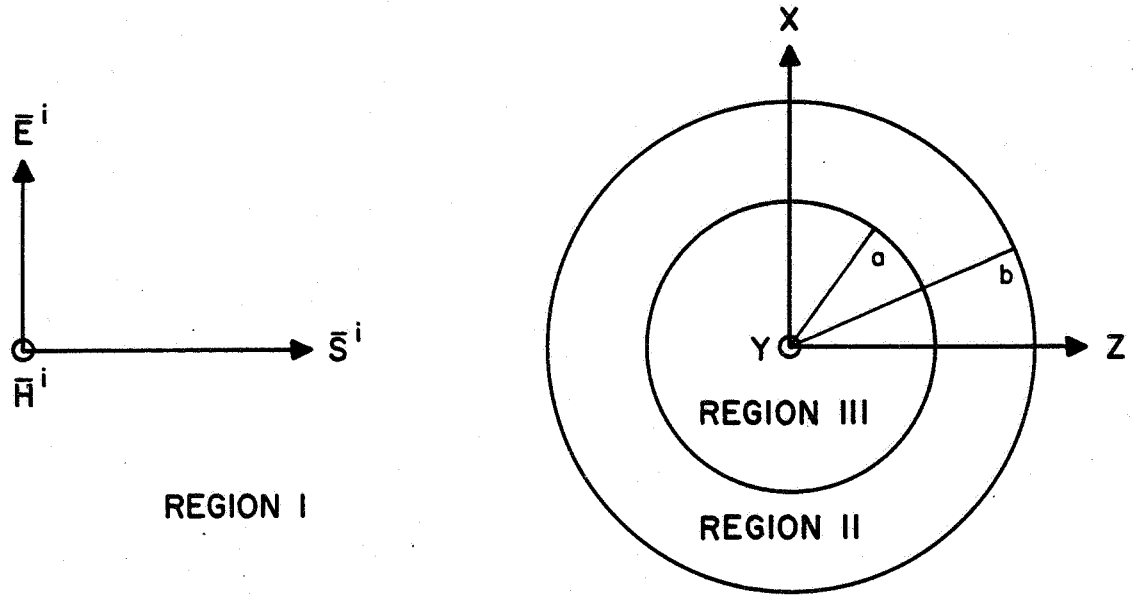

PLANE WAVE INCIDENT UPON PLASMA COATED SPHERE

FIGURE 3.7

We now wish to find expressions for the fields scattered by the plasma covered sphere and the fields scattered from the sphere alone.

For an assumed constant refractive index the quantities A, B, C, D, E, and F (see Equations B.112, B.114 and B.124 to B.127) reduce to

$$A = \psi_\ell'(n_2x)/n_2^2 \quad B = -\chi_\ell'(n_2x)/n_2^2 \quad C = \psi_\ell'(n_2y)/n_2^2$$
$$D = \chi_\ell'(n_2y)/n_2^2 \quad E = -\psi_\ell'(n_2x)/k_2^{II}n_2 \quad F = -\chi_\ell'(n_2x)/k_2^{II}n_2 \tag{3.4}$$

and the scattering coefficients become

$$e_{B_\ell}^{on} = \Big[-\psi_\ell(x)\Big\{-\psi_\ell'(n_2x)\,\chi_\ell'(n_2y) + \psi_\ell'(n_2y)\,\chi_\ell'(n_2x)\Big\} + \psi_\ell'(x)\Big\{-n_2^2\,\psi_\ell(n_2x)\,\chi_\ell'(n_2y) + n_2^2\,\psi_\ell'(n_2y)\,\chi_\ell(n_2x)\Big\}\Big] \Big/ \Big[\zeta_\ell^1(x)\Big\{\text{same as above}\Big\} - \zeta_\ell^{1'}(x)\Big\{\text{same as above}\Big\}\Big]$$
$$m_{B_\ell}^{on} = \Big[-\psi_\ell(x)\Big\{\psi_\ell'(n_2x)\,\chi_\ell(n_2y) - \chi_\ell'(n_2x)\,\psi_\ell(n_2y)\Big\} + \psi_\ell'(x)\Big\{\psi_\ell(n_2x)\,\chi_\ell(n_2y) - \chi_\ell(n_2x)\,\psi_\ell(n_2y)\Big\}\Big] \Big/ \Big[\zeta_\ell^1(x)\Big\{\text{same as above}\Big\} - \zeta_\ell^{1'}(x)\Big\{\text{same as above}\Big\}\Big] \tag{3.5}$$

To find the scattering coefficients for the sphere alone one need only set $n_2 = 1$ in these expressions and simplify. The results are

$$e_{B_\ell}^{off} = -\psi_\ell(y) \,/\, \zeta_\ell^{1'}(y)$$
$$m_{B_\ell}^{off} = -\psi_\ell(y) \,/\, \zeta_\ell^{1}(y) \tag{3.6}$$

The scattered fields are now completely defined and can be written in component form as:

$$E_r^s = E_o\cos\phi/(K^I r)^2 \sum_{\ell=1}^{\infty} {}^{e}B_\ell \, i^{\ell-1} \, (2\ell+1) \, P_\ell^1 \, (\cos\theta) \, \zeta_\ell^1(K^I r) \tag{3.7}$$

$$E_\theta^s = E_o\cos\phi/K^I r \sum_{\ell=1}^{\infty} i^{\ell-1} \frac{(2\ell+1)}{\ell(\ell+1)} \left\{ {}^{e}B_\ell \, \zeta_\ell^{1'}(K^I r) \, P_\ell^{1'}(\cos\theta) \sin\theta + i \, {}^{m}B_\ell \, \zeta_\ell^1(K^I r) \, P_\ell^1(\cos\theta)/\sin\theta \right\} \tag{3.8}$$

$$E_\phi^s = E_o\sin\phi/K^I r \sum_{\ell=1}^{\infty} i^{\ell-1} \frac{(2\ell+1)}{\ell(\ell+1)} \left\{ - {}^{e}B_\ell \, \zeta_\ell^{1'}(K^I r) \frac{P_\ell^1(\cos\theta)}{\sin\theta} + i \, {}^{m}B_\ell \, \zeta_\ell^1(K^I r) \, P_\ell^{1'}(\cos\theta) \sin\theta \right\} \tag{3.9}$$

$$H_r^s = i \, E_o\sin\phi/K^I k_2^I r^2 \sum_{\ell=1}^{\infty} i^{\ell-1} \, (2\ell+1) \, {}^{m}B_\ell \, \zeta_\ell^1(K^I r) \, P_\ell^1(\cos\theta) \tag{3.10}$$

$$H_\theta^s = E_o\sin\phi/k_2^I r \sum_{\ell=1}^{\infty} i^{\ell-1} \frac{(2\ell+1)}{\ell(\ell+1)} \left\{ - {}^{e}B_\ell \, \zeta_\ell^1(K^I r) \frac{P_\ell^1(\cos\theta)}{\sin\theta} - i \, {}^{m}B_\ell \, \zeta_\ell^{1'}(K^I r) \, P_\ell^{1'}(\cos\theta) \sin\theta \right\} \tag{3.11}$$

$$H_\phi^s = E_o\cos\phi/k_2^I r \sum_{\ell=1}^{\infty} i^{\ell-1} \frac{(2\ell+1)}{\ell(\ell+1)} \left\{ {}^{e}B_\ell \, \zeta_\ell^1(K^I r) \, P_\ell^{1'}(\cos\theta) \sin\theta + i \, {}^{m}B_\ell \, \zeta_\ell^{1'}(K^I r) \frac{P_\ell^1(\cos\theta)}{\sin\theta} \right\} \tag{3.12}$$

It is understood that the ${}^{e,m}B_\ell$ in these expressions become ${}^{e,m}B_\ell^{off}$ or ${}^{e,m}B_\ell^{on}$ for scattering by a sphere or plasma covered sphere respectively.

In this experiment the receiving horns moved only in the y-z plane so that $\phi = \pi/2$ and $\pi \leq \theta \leq 0$. Substituting $\phi = \pi/2$ in the above expressions yields

$$E_\phi^s = E_o/K^I r \sum_{\ell=1}^{\infty} i^{\ell-1} \frac{(2\ell+1)}{\ell(\ell+1)} \left\{ {}^{e}B_\ell \, \zeta_\ell^{1'} \, P_\ell^1/\sin\theta + i \, {}^{m}B_\ell \, \zeta_\ell^1 \, P_\ell^{1'} \sin\theta \right\} \quad (3.13)$$

$$H_r = i \, E_o/K^I k_2^I r^2 \sum_{\ell=1}^{\infty} i^{\ell-1} \, (2\ell+1) \, {}^{m}B_\ell \, \zeta_\ell^1 \, P_\ell^1 \quad (3.14)$$

$$H_\phi^s = E_o \cos\phi/k_2^I r \sum_{\ell=1}^{\infty} i^{\ell-1} \frac{(2\ell+1)}{\ell(\ell+1)} \left\{ - {}^{e}B_\ell \, \zeta_\ell^1 \, P_\ell^1 /\sin\theta - i \, {}^{m}B_\ell \, \zeta_\ell^{1'} \right.$$

$$\left. P_\ell^{1'} \sin\theta \right\} \quad (3.15)$$

The magnitude of the arguments of the spherical Hankel (Ricatti) functions are 154.27, 250.24 and 270.49 for X-Band, K-Band and A-Band respectively. For such large arguments it is valid to use the large argument expansion for these functions:

$$\zeta_\ell^1 (x) = (-i)^{\ell+1} \, e^{ix}$$

$$\zeta_\ell^{1'} (x) = (-i)^{\ell} \, e^{ix} \quad (3.16)$$

Introducing these approximations in Equations 3.13 to 3.15 one obtains the asymptotic expansions of the field components which are nonzero at the points of observation

$$E_\phi^s = i \, E_o/K^I r \sum_{\ell=1}^{\infty} e^{iK^I r} \frac{(2\ell+1)}{\ell(\ell+1)} \left\{ {}^{e}B_\ell \, P_\ell^1/\sin\theta - {}^{m}B_\ell \, P_\ell^{1'} \sin\theta \right\} \quad (3.17)$$

$$H_\theta^s = E_o/k_2^I r \sum_{\ell=1}^{\infty} e^{iK^I r} \frac{(2\ell+1)}{\ell(\ell+1)} \left\{ {}^eB_\ell \, P_\ell^1/\sin\theta - {}^mB_\ell \, P_\ell^{1\prime} \sin\theta \right\} \tag{3.18}$$

$$H_r^s = - i \, E_o/K^I k_2^I r^2 \sum_{\ell=1}^{\infty} e^{iK^I r} \, (2\ell+1) \, {}^mB_\ell \, P_\ell^1 \tag{3.19}$$

3.3 Expressions for the Power Ratio and Phase Change

To determine expressions for the power and phase change measured in the laboratory the total field must be used. The resultant field at any point outside the sphere is the sum of the incident and scattered fields.

$$\bar{E}^{TOT} = \bar{E}^s + \bar{E}^i \qquad \bar{H}^{TOT} = \bar{H}^s + \bar{H}^i \tag{3.20}$$

The radial component of the total complex Poynting vector is

$$S_R = \tfrac{1}{2} \, (\bar{E}^{TOT} \times \bar{H}^{TOT*})_R = - \tfrac{1}{2} \, (E_\phi^{TOT} \, H_\theta^{TOT*}) \tag{3.21}$$

Using this component, the power intercepted by the receiving antenna is

$$P = \int\int_S \text{Re} \, (\bar{S} \cdot \hat{r}) \, dS = - \tfrac{1}{2} \int\int_S \text{Re} \, (E_\phi^{TOT} \, H_\theta^{TOT*}) \, d\Omega \tag{3.22}$$

where S is the surface of the horn. Since the horns subtend such a small solid angle (at X-Band $|\theta| \leq 4^o$ and $|\phi| \leq 3^o$), Re $(E_\phi^{TOT} \, H_\theta^{TOT*})$ can be thought of as a constant over this integration and thus

$$P \cong - \tfrac{1}{2} \, \text{Re} \, (E_\phi^{TOT} \, H_\theta^{TOT*}) r^2 \int\int_S d\Omega \tag{3.23}$$

To eliminate this surface integral the ratio P^{off}/P^{on} is computed in terms of decibels as follows. First divide P by $\frac{1}{2}E_o^2/\eta_o$, the power in the incident wave, to cancel out the magnitude of the incident electric field. Changing this ratio to decibels one obtains

$$P \;/\; (E_o^2/2\eta_o)\;[dB] = 10\,\log_{10}\left[-\frac{1}{2P_o}\,\mathrm{Re}\;(E_\phi^{TOT}\,H_\theta^{TOT*})r^2\int_S\int d\Omega\right] \qquad (3.24)$$

Taking the difference of $P^{off}/\frac{1}{2}E_o/\eta_o$ and $P^{on}/\frac{1}{2}E_o/\eta_o$ gives

$$(P^{off}/P_o - P^{on}/P_o)\;[dB] = 10\,\log_{10}\left\{-\frac{1}{2P_o}\,\mathrm{Re}\;(E_\phi^{TOT}\,H_\theta^{TOT*})^{off}r^2\int_S\int d\Omega\right\} - 10\,\log_{10}\left\{-\frac{1}{2P_o}\,\mathrm{Re}\;(E_\phi^{TOT}\,H_\theta^{TOT*})^{on}r^2\int_S\int d\Omega\right\} \qquad (3.25)$$

Or

$$(P^{off}/P^{on})\;[dB] = 10\,\log_{10}\left\{\mathrm{Re}\;(E_\phi^{TOT}\,H_\theta^{TOT*})^{off}/\mathrm{Re}\,(E_\phi^{TOT}\,H_\theta^{TOT*})^{on}\right\} \qquad (3.26)$$

Since E_ϕ^{TOT} is a component of a complex vector, and is itself complex, its relative phase angle may be defined as

$$\Phi = \arctan\;(\mathrm{Im}\;(E_\phi^{TOT})/\mathrm{Re}\;(E_\phi^{TOT}))\;x\;57.3 \qquad (3.27)$$

Then, the change in phase observed in the laboratory is

$$\Delta\Phi = \Phi_{on} - \Phi_{off} = 57.3\;x\left[\arctan\;(\mathrm{Im}\;(E_\phi^{TOT})/\mathrm{Re}\;(E_\phi^{TOT}))^{on} - \arctan\;(\mathrm{Im}\;(E_\phi^{TOT})/\mathrm{Re}\;(E_\phi^{TOT}))^{off}\right] \qquad (3.28)$$

4. COMPARISON OF SIMPLIFIED THEORY WITH EXPERIMENT

The numerical analysis of the problem is in principle straight forward. One evaluates expressions (3.26) and (3.28) for a given value of θ by retaining enough terms in the various series which are used to define them to ensure proper convergence. The value of θ is then incremented and the summation process is repeated.

This section describes the digital computer techniques for evaluating these expressions, shows how each physical parameter influences the calculations and compares the simple theoretical model with experimental results.

4.1 Generation Techniques

The two equations mentioned above involve the three spherical Bessel-Ricatti functions and their derivatives which appear in the scattering coefficients (ψ_ℓ (x), χ_ℓ (x), ζ_ℓ^1 (x), ψ_ℓ' (x), χ_ℓ' (x) and $\zeta_\ell^{1'}$ (x)) for various real and complex arguments and the associated Legendre polynomials and their derivatives (P_ℓ^m (z) and $P_\ell^{m'}$ (z)) which appear in the scattered field expressions. For this problem ℓ is of integer value so that all these functions may be generated using recurrence relations. However, since generation is carried out with rounded values it is necessary to keep errors small in the recurrence process. Using Antosiewicz (1965) as a reference for generation

techniques it may be stated in general that ψ_ℓ (x) should be generated using a downward recurrence while P_ℓ^m (z) and χ_ℓ (x) may be generated using an upward recurrence. In so doing the round off errors do not grow relative to the size of the wanted functions. The remaining functions are easily generated for the derivatives of these functions are defined in terms of the functions themselves and ζ_ℓ^1 (x) is the complex sum of ψ_ℓ (x) and χ_ℓ (x).

The number of terms which must be retained in each series to adequately represent the scattering coefficients and thus the scattered field can be determined by considering the magnitude of the arguments appearing in the spherical Bessel-Ricatti functions. For example, $\text{Mod}(n_2 x) \simeq x = K^I b$ since $n_2 \simeq .9 + i10^{-8}$. The maximum value of b is approximately 9.0 cm. Thus at X-Band, $x = \omega b/c = 209(.09) = 18.81$. For values of ℓ less than Mod(arg) the Bessel-Ricatti functions are oscillatory. When ℓ is approximately 1.5 Mod(arg) they become monotonic. At A-Band $x_A = 3.5x_X$ which in this case is 65.8. In this instance nearly 100 terms should be retained to be certain the functions have approached their monotonic nature. However, attempts to generate such a large number of terms when the arguments were complex led to magnitudes of numbers which exceeded the capacity of the machine. Alternatively, the summation index was chosen so that $\text{Mod}(^{e,m}B_{\ell MAX})$ was always less than 10^{-6}. No less than 15 terms were used for any argument.

The programs used in this analysis were then restricted in the sense that limited, and not completely general, ranges of the arguments could be used. Fortunately these ranges were sufficiently large to permit analysis of the problem.

The accuracy of the generation methods and the validity of the total program were checked as follows. All the functions were computed for arguments and indices for which tabulated values exist in the literature; several H-plane bistatic scattering cross sections for conducting spherical scatterers were produced and compared to those published by King and Wu. (1959) In both checks nearly exact correspondence was accomplished.

4.2 Consideration of Basic Parameters and Comparison of Theory with Experiment

The important parameters in the model to be applied are a, the radius of the spherical magnet, b, the radial extent of the plasma, R, the distance from the scattering center to the receiving antenna, f, the frequency of the incident electromagnetic wave and n_o, the refractive index of the plasma which is defined in terms of ω_p/ω, the ratio of the plasma frequency to the radian frequency of the incident wave and ν/ω, the ratio of the electron-neutral collision frequency to the radian incident frequency.

The radius of the sphere used in all experiments was determined to be $1.651 \pm 5\text{x}10^{-2}$ cm. The value a = 1.651 cm was used in the calculations.

The frequencies used in the experiment, 10.0 GHz, 22.4 GHz, and 35.0 GHz, could be measured to an accuracy of ±0.005 GHz. To show how an incident frequency deviation of +1.0 GHz and -0.1 GHz can effect the power and phase changes obtained from Equations (3.26) and (3.28), Figure 4.1 is given. In this figure f_o = 10.0 GHz and R_o = 73.36 cm.

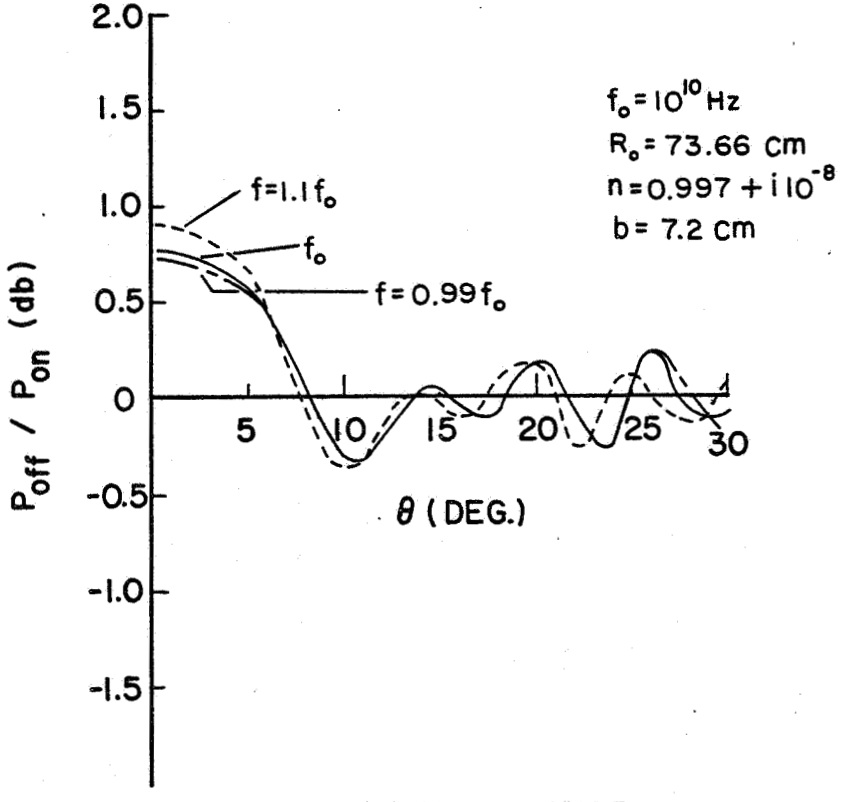

a. POWER CHANGE

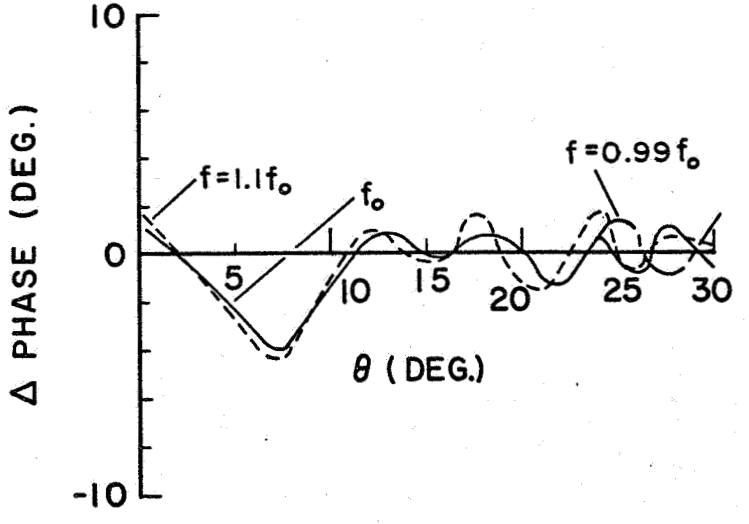

b. PHASE CHANGE

EFFECTS OF FREQUENCY CHANGES ON CALCULATIONS

FIGURE 4.1

The main effect of a frequency change is to shift the position of the extrema. The magnitudes of the maxima and minima are very nearly the same for all three frequencies given. In view of the measurement accuracy and the relatively small effect that extreme frequency changes have on the power and phase results, we conclude that the values quoted above may be assumed constant and introduce negligible error in the comparison.

Figure 4.2 shows how variations in R effect power and phase change results; f_o = 10 GHz and R_o = 73.36 cm. For variations in R of ±1.27 cm (± ½ inch) the power curves essentially agree everywhere but the position of the extrema of the phase change are shifted slightly. Again the measurement accuracy of this distance (± 0.2 cm) was well within the hypothetical changes shown on the figure. Thus R is given the value determined from physical measurements when evaluating the theoretical expressions.

Having shown that the values of f, R, and a are known from laboratory measurements, there remain b, the radial extent of the plasma, and n_o, the refractive index of the plasma, both the real and imaginary parts, as principal variables to which values must be assigned. These variables are now discussed jointly. The reason for doing so will become apparent.

To determine appropriate values of b and n_o the following procedure is adopted. A rough approximation of b and n_o is obtained from photographs and probe data. Using these approximate values as a first estimate we will fit the scattering data. Finally these values will be shown to fit the profile of electron density versus distance from the surface of the sphere.

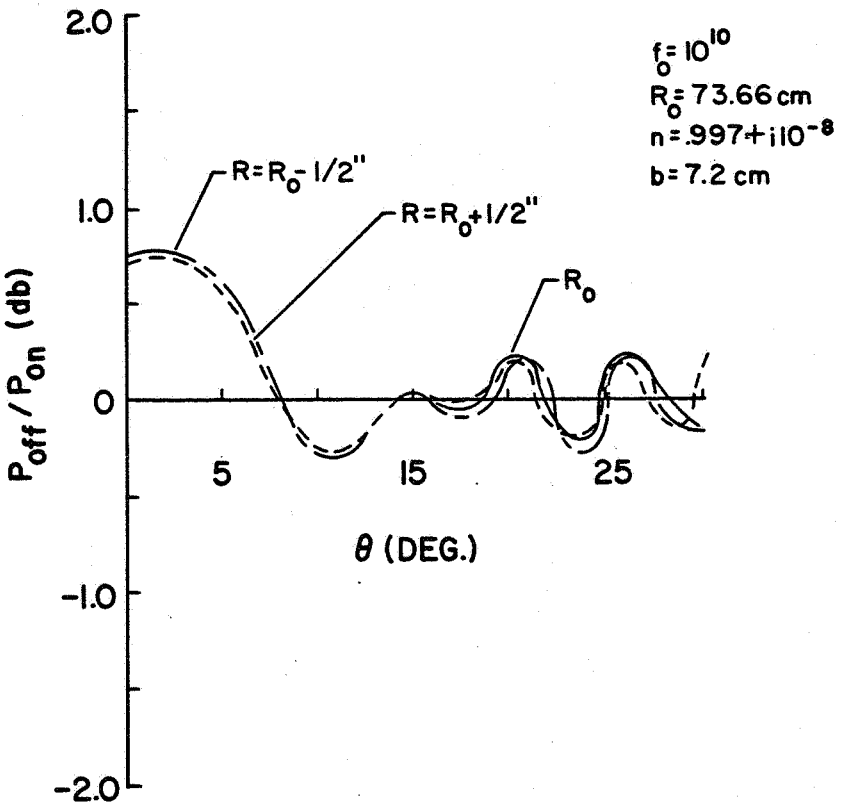

a. POWER CHANGE

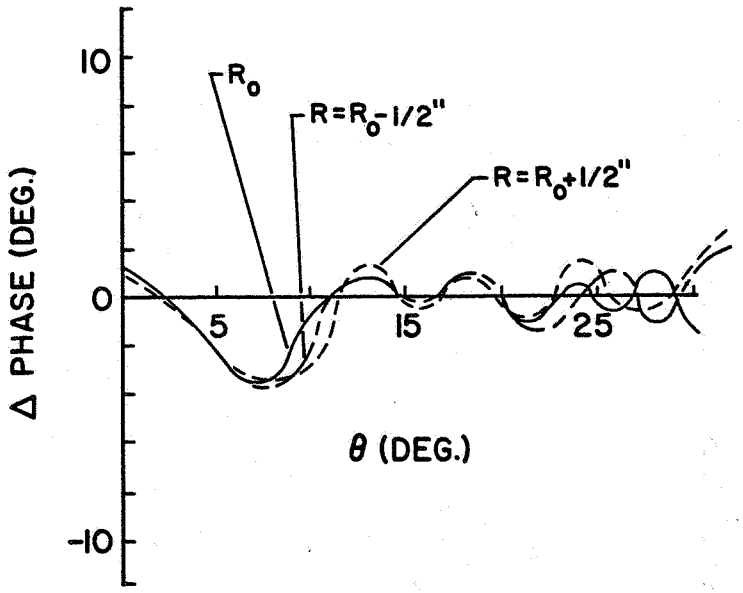

b. PHASE CHANGE

EFFECTS OF R CHANGES ON CALCULATIONS

FIGURE 4.2

4.2.1 Approximate Values of b and n_o from Photographs and Probe Data

To determine an approximate value of b consider Figure 4.3 which depicts the three regions of the plasma. The b_i are maximum radial extents of the various regions to be discussed. When b is in the range $a \leqslant b \leq b_1$ the uniform light intensity emitted by the plasma is most intense and corresponds to the region of maximum particle densities. The distance b_1, in terms of probe data, occurs at approximately the position of the density peak. In the region $b_1 \leqslant b \leqslant b_2$ this light intensity decreases from b_1 and is no longer visible when $b > b_2$. The value of b_2 is a function of discharge current and is approximately 9.0 cm at 70 ma. Somewhere in this range a suitable value of b must be chosen.

Magnitudes of the distances b_1 and b_2 can be approximated by scaling from photographs of the discharge for various currents. Strictly speaking they are not exact because of film sensitivity and exposure time considerations. Furthermore the extent of a trapped plasma of this nature is not definable in terms of an abrupt boundary. Keeping in mind these limitations the scaling was performed for the three discharge currents used in this experiment, 30, 50 and 70 ma; the three values of b_1 and b_2 obtained are respectively 5.5, 6.6 and 7.4 cm and 7.2, 8.3 and 9.1 cm.

The value of n_o to be used in the calculations must of course give power and phase changes consistent with experimental results. A starting value of n_o, however, may be determined from a simple calculation and the probe data. As stated previously n_o is defined in

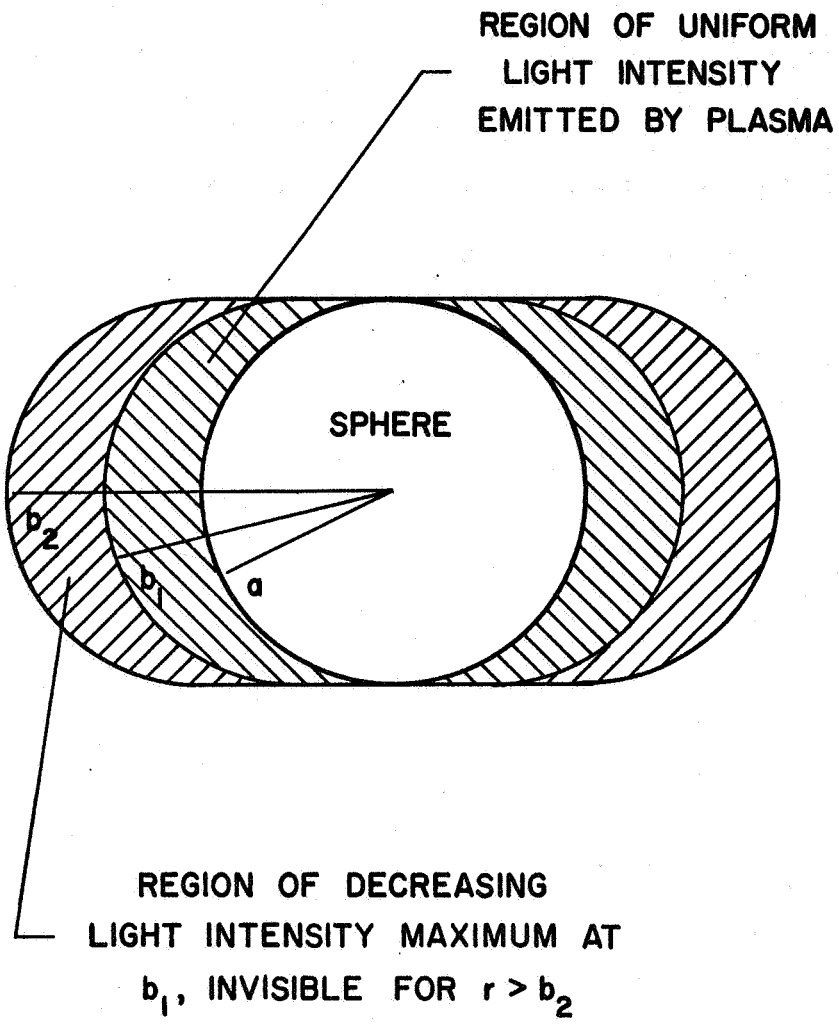

CROSS SECTION OF SPHERE AND PLASMA

FIGURE 4.3

terms of ω_p^2/ω^2 and ν_{en}/ω. Considering the latter term first it is necessary to determine an order of magnitude estimate of ν_{en}; doing so sets the value of Im(n). ν_{en} is defined to be $\langle\nu_e\rangle/\lambda_{en}$ where $\langle\nu_e\rangle$ is the velocity of an electron and λ_{en} is the mean free path between electron-neutral collisions; $\langle\nu_e\rangle$ is taken to be $1.224\ (2kT/m)^{\frac{1}{2}}$, the root mean square velocity obtained from a Maxwellian distribution and $\lambda_{en} = 1/N_n Q$ where N_n is the density of the neutrals and Q is the collision cross section. For neutral scatterers $Q = \pi r_n^2$ (r_n = radius of the molecule) $\cong 10^{-15}$ cm^2; at 150 microns of pressure $N_n \cong 10^{15}$ cm^3 and thus $\lambda_{en} \cong 1$ cm. The velocity $\langle\nu_e\rangle \cong 10^8$ for $T \cong 10^5$ ^oK. For X-Band frequencies this gives $\nu_{en}/\omega \cong 10^{-3}$. From Figure 3.4 one sees a ratio of this value for electron densities of approximately 10^{10} give $Im(n) \cong 10^{-7}$. Going to the higher frequencies (see Figures 3.5 and 3.6), Im(n) is approximately 10^{-8} and 10^{-9}. Substituting the range $.996 + i10^{-9} \lesssim n_o \lesssim .996 + i10^{-6}$ into the expressions gave deviations of power and phase changes that varied in the third decimal place. A value of 10^{-8} was assigned to Im(n) for all frequencies used.

Since $Im(n_o)$ is relatively small $Re(n_o) \cong (1 - \omega_p^2/\omega^2)^{\frac{1}{2}}$. From the electron densities determined from the probe data (see Figures 2.7 and 2.8) it is seen that the values of N_e which are typical of this experiment lie in the range $10^9 \lesssim N_e \lesssim 10^{11}$. Using the approximate expression for $Re(n_o)$ one can show that for electron densities in this range, $.999 \lesssim Re(n_o) \lesssim .93$ for all frequencies of interest.

4.2.2 Fitting the Scattering Data

Having now established a reasonable range of values for b and n_o, these values are used to fit the scattering data. Before doing so however, the manner in which b and n_o effect the power and phase results is investigated; from this investigation a systematic fitting procedure can be developed which sets limits on these variables.

Figure 4.4 displays curves with b as a parameter for constant n. In this discussion to follow f = 10 GHz and R = 73.36 cm. In part a of this figure $n = .996 + i10^{-8}$ and b varies from 3.3 cm to 9.08 cm. For increasing b and constant n the magnitude of the change in power increases in the range $0 \leqslant \theta \leqslant 15$ degrees. The first zero crossing of all the curves occur at $\theta = 8^o$ while the second crossings are confined in the range $13 \leqslant \theta \leqslant 14$ degrees. For values of $\theta \geq 14^o$ the position of the extrema depend on the particular value of b but all zero crossings occur at nearly the same places. In Figure 4.4.b, $3.3 \leqslant b \leqslant 5.5$ and $n = 0.95 + i10^{-8}$. Again the first two zero crossings occur for the same values of theta but now the shapes of the curves have changed and the power changes have greatly increased. From these curves one can also observe the effect n has on the power change results. For example, consider b = 5.5 cm in a and b of the figure. When Re(n) is near unity (0.996) then P^{off}/P^{on} = 0.75 dB; as Re(n) becomes smaller (0.95), P^{off}/P^{on} = 3.0 dB and $\theta = 0^o$. Substituting n = 1.0 + i0.0 into the programs gave power and phase changes of zero as would be expected.

One can now establish a systematic method to fit the scattering data from the knowledge of how b and n_o enter into the final results.

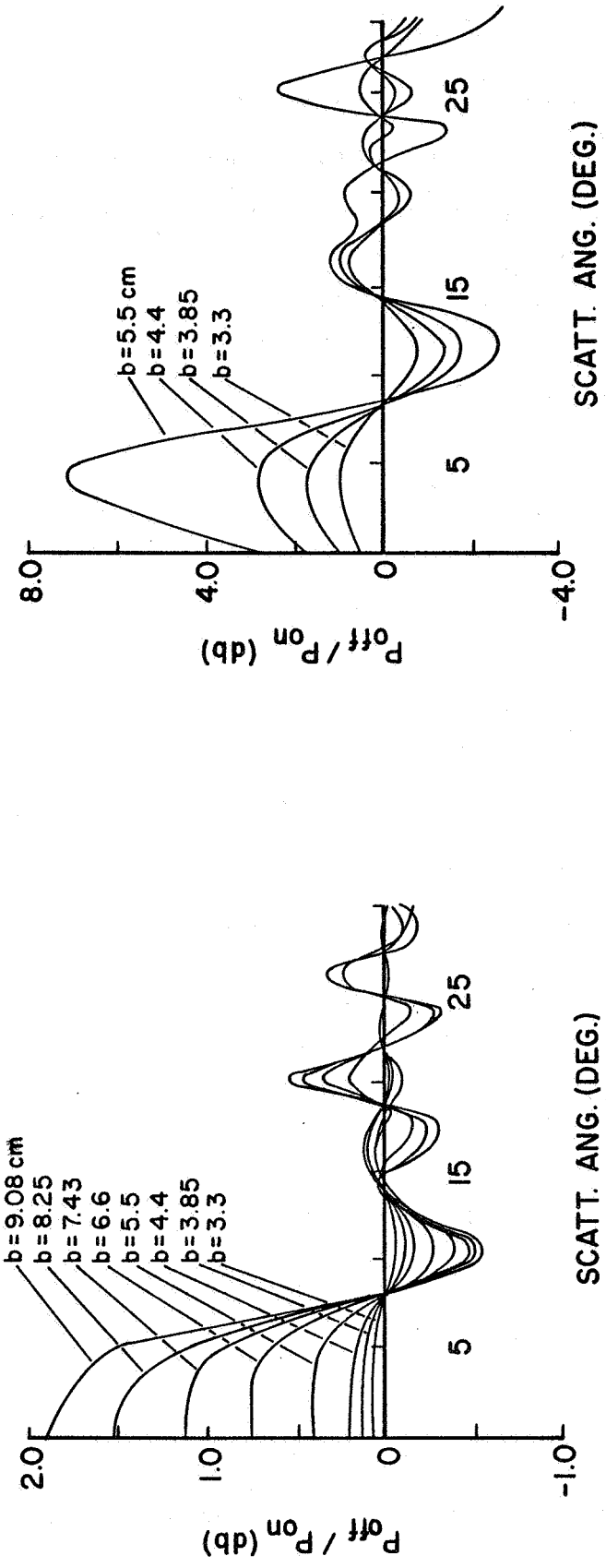

b. $n = 0.95 + i10^{-8}$

a. $n = .996 + i10^{-8}$

POWER CHANGES FOR VARIOUS b AND n

FIGURE 4.4

The range of theta in which the scattering data is valid is $|\theta| \lesssim 10^{o}$. Since all the curves for various b and n have the first zero crossings at $\theta = 8^{o}$, one merely has to match the measured P^{off}/P^{on} value at $\theta = 0^{o}$ with the calculated values; the appropriate values of n and b to be used are those which give the desired P^{off}/P^{on} values, phase changes and preserve the shape of the experimental curve.

A detailed example of this data fitting procedure for the particular case when f = 10 GHz, $P^{off}/P^{on}\,|_{\theta=0^{o}} = 1.75$ dB and I = 70 ma follows. To demonstrate the range of b and n_o values which will predict the data from the theoretical expressions we plot P^{off}/P^{on} as a function of b for various values of n_o; these curves are shown in Figure 4.5 (the scattering angle used is 0.01^{o}). It is immediately obvious that if one wishes to obtain a power change of 1.75 dB at this angle, then at least four pairs of b-n_o combinations can be used. Of course many more could be obtained by incrementing $Re(n_o)$ in smaller steps.

Consider now Figures 4.6 to 4.8 which show b-n_o combinations which match the power change data over the valid experimental range. For b = 9.1 cm, $n_o = .997 + i10^{-8}$ and b = 7.2 cm, $n_o = .994 + i10^{-8}$ (n given to three places) the P^{off}/P^{on} curves agree for $\theta \leq 8^{o}$, the shapes of the curves are preserved and in the latter case the magnitude of the phase change is nearly twice too large. In Figure 4.8 for b = 4.4 cm, $n_o = .97 + i10^{-8}$ the shape of the power ratio curve is no longer in agreement and the theoretical phase changes are too large. Using this method the b and n_o values which predicted theoretically magnitudes of power and phase changes and preserved the shape of the curves had uncertainties of (b, $Re(n_o)$) of approximately (± 1.5,

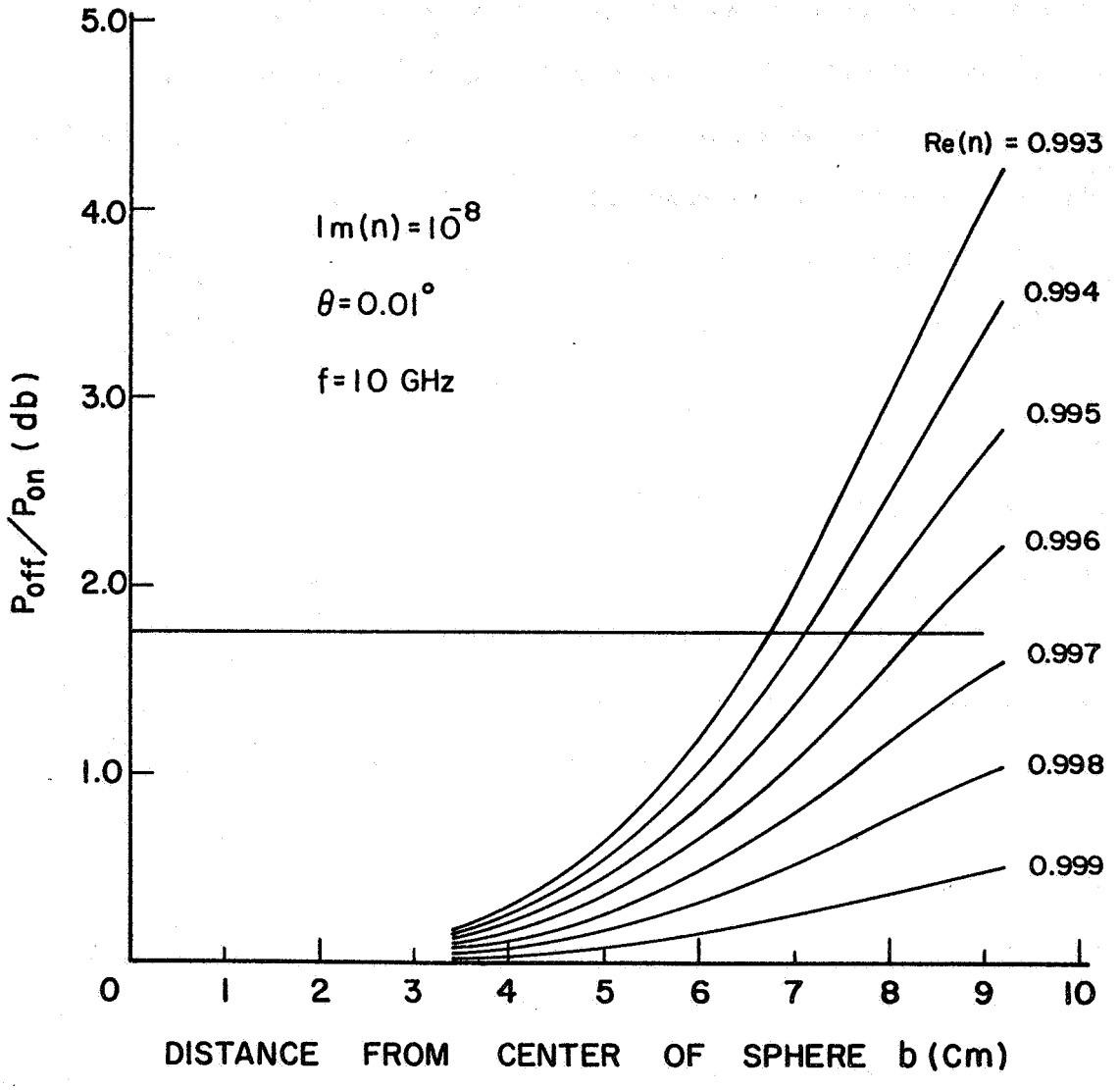

POWER CHANGE VERSUS b WITH n AS A PARAMETER

FIGURE 4.5

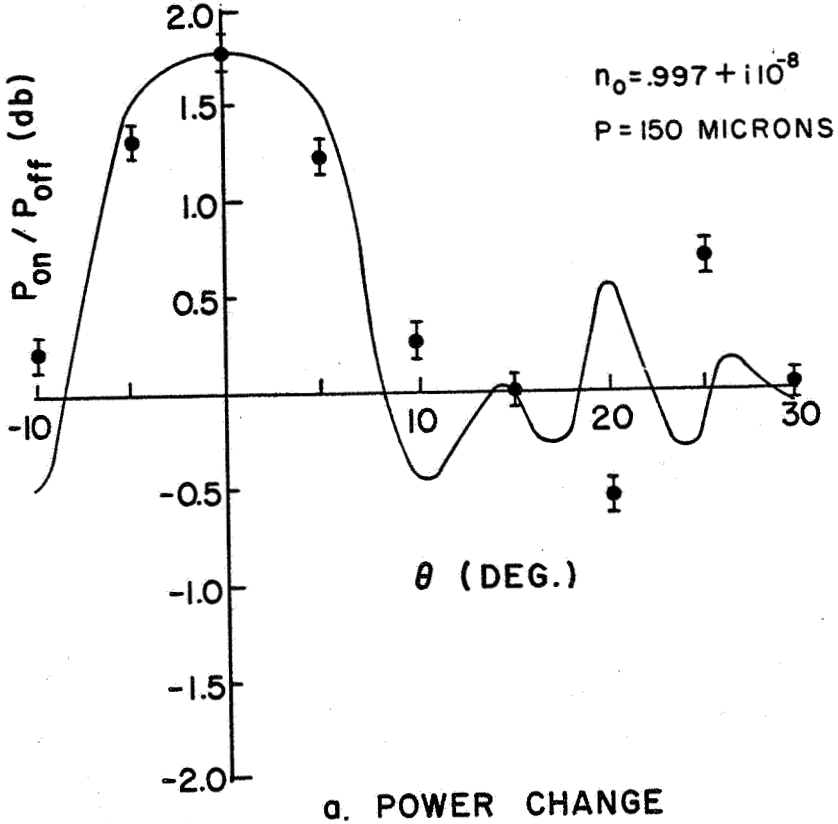

a. POWER CHANGE

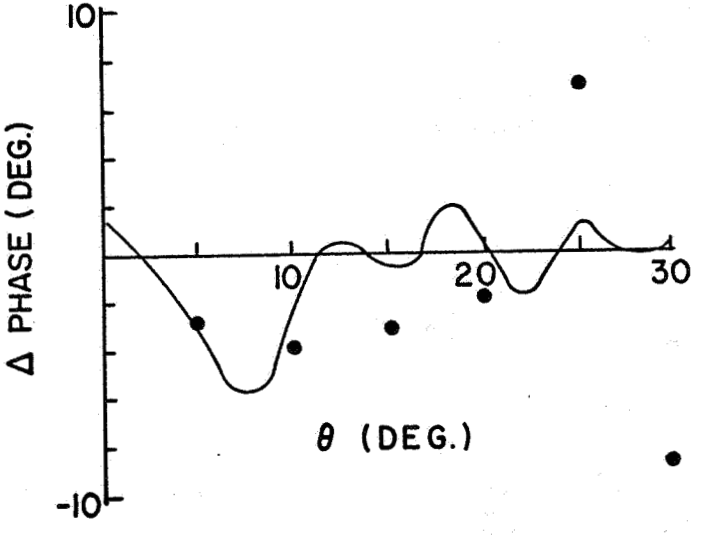

b. PHASE CHANGE

POWER AND PHASE CHANGES: X-BAND, b = 9.1cm

FIGURE 4.6

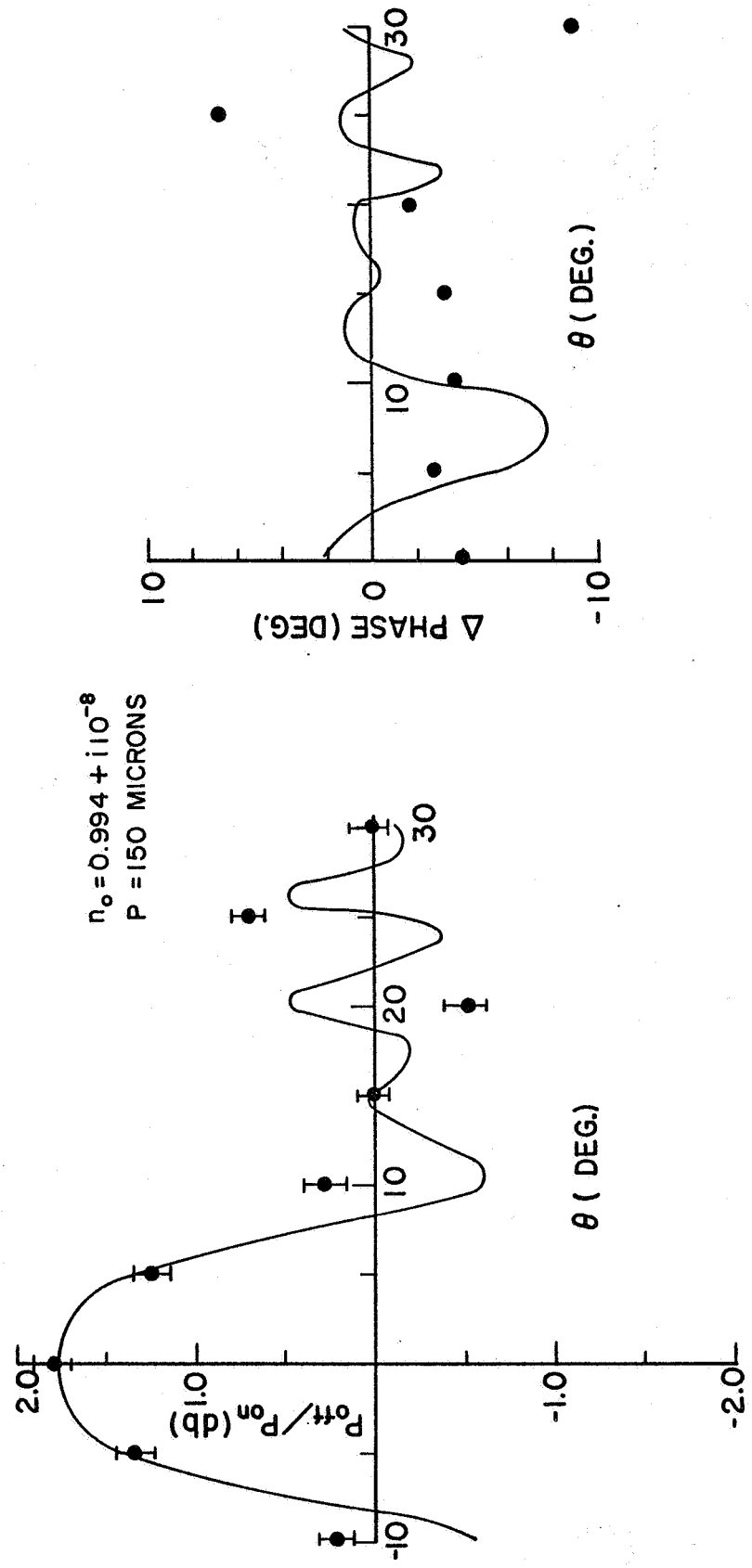

POWER AND PHASE CHANGES: X – BAND, b = 7.2 cm

FIGURE 4.7

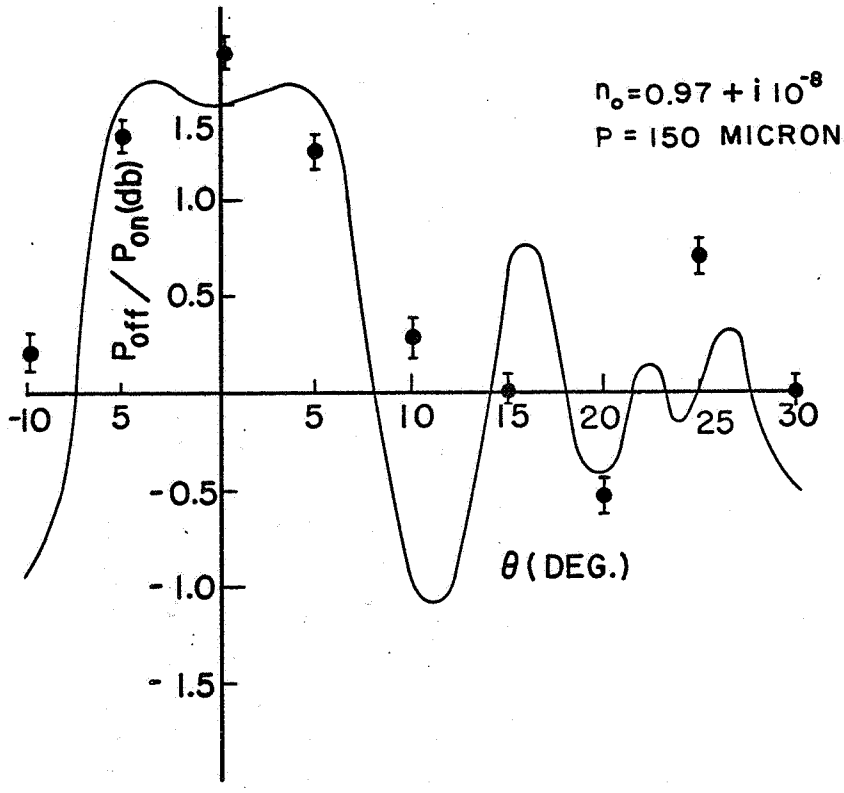

a. POWER CHANGE

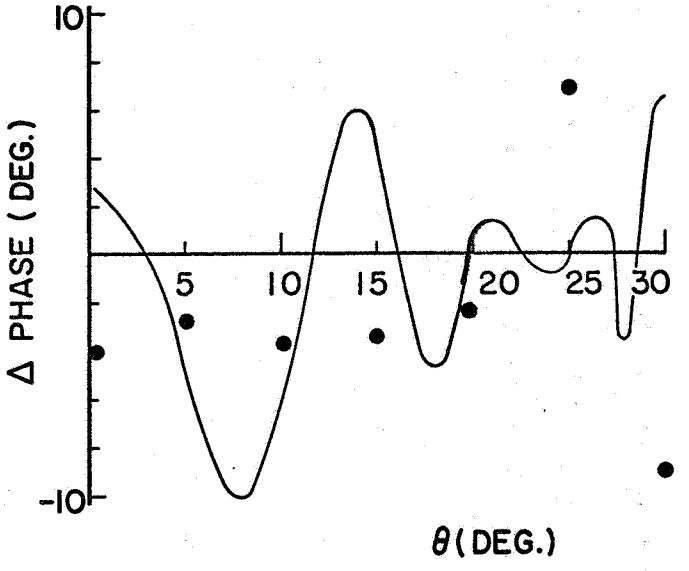

b. PHASE CHANGE

POWER AND PHASE CHANGES : X-BAND, b = 4.4 cm

FIGURE 4.8

± .002), (± 0.7, ± .002) and (± 0.3, ± .002) for X-, K- and A-Band respectively. For this example, the median value of n_o was determined to be .997 + 10^{-8} and the corresponding value of b was 9.0 cm.

The results of applying this procedure to the remaining data are shown in Figures 4.9 to 4.16. In all cases the values of b and n_o are median values of their respective ranges noted above. An explanation of why the values of b for the K- and A-Band data are smaller than those determined previously from experimental results is given later with the discussion of density profile determined from the microwave measurements.

The phase changes observed in the laboratory were so small that their usefulness is questionable. The phase shifters used in the microwave bridges had accuracies of ± $1\frac{1}{2}^{o}$. Failure to exactly locate the minimum on the null detector added another ± 1^{o} of uncertainty. Finally taking the difference of two successive readings gave the final results which were plotted a possible error of ± 5^{o}. For legibility, error bars are not indicated.

4.2.3 Comparison of Density Profiles

It is interesting to compare the electron number densities and the electron density profile using the values of b and n_o determined from microwave measurements to those obtained from probe data. For example, consider the case of 30 ma discharge current and a gas pressure of 150 microns. The electron densities can be deduced from the microwave data through the approximate expression $(\mathrm{Re}(n))^2 = 1 - \omega_p^2/\omega^2$

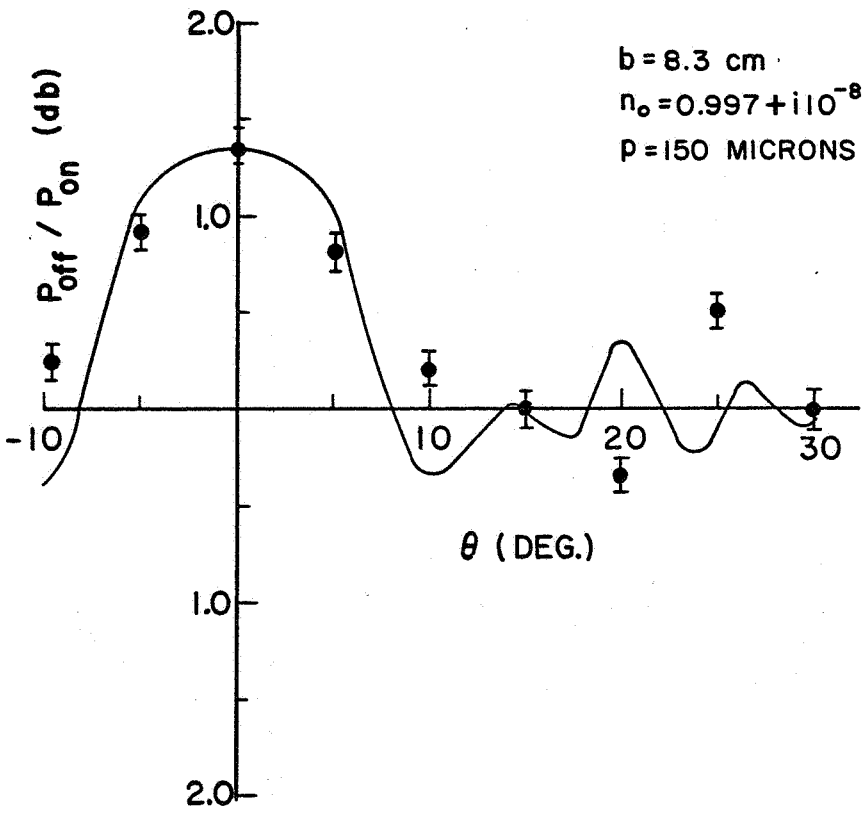

a. POWER CHANGE

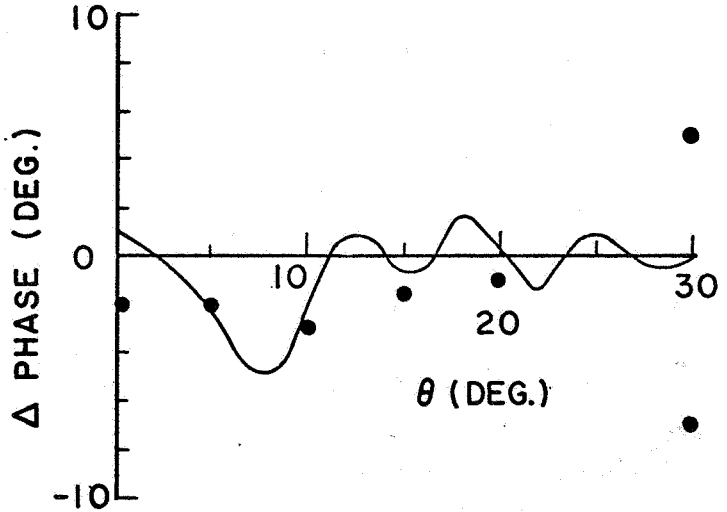

b. PHASE CHANGE

POWER AND PHASE CHANGES : X - BAND, 50 mA

FIGURE 4.9

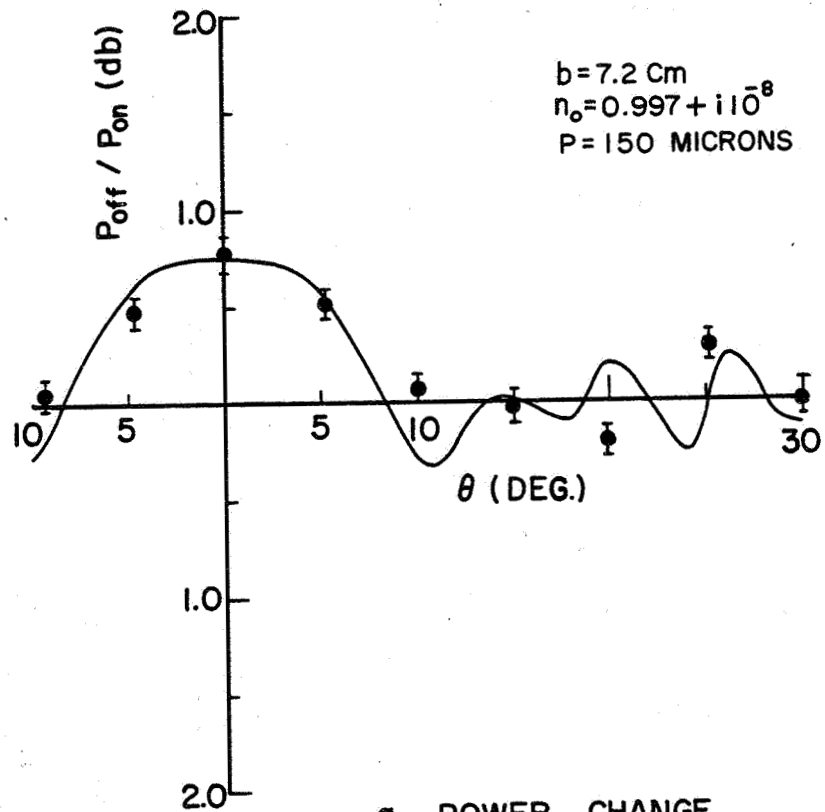

a. POWER CHANGE

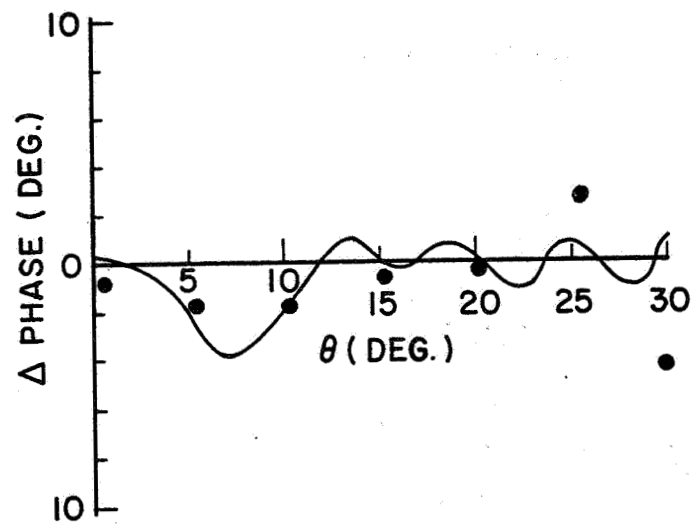

b. PHASE CHANGE

POWER AND PHASE CHANGES: X-BAND, 30 mA

FIGURE 4.10

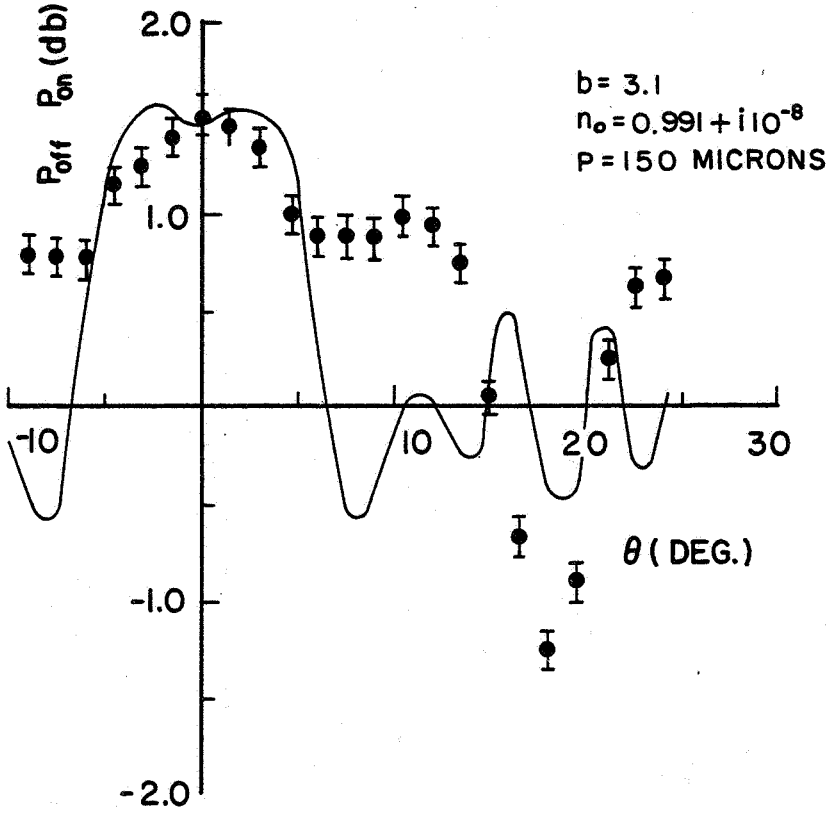

a. POWER CHANGE

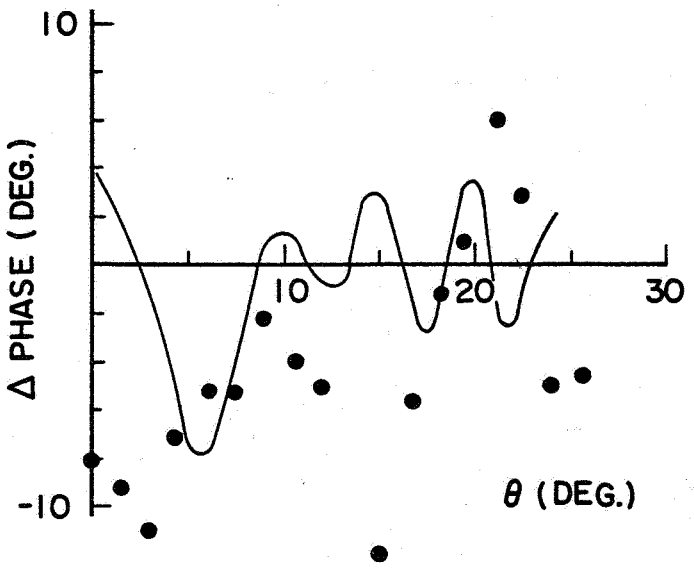

b. PHASE CHANGE

POWER AND PHASE CHANGES: K-BAND, 70 mA

FIGURE 4.11

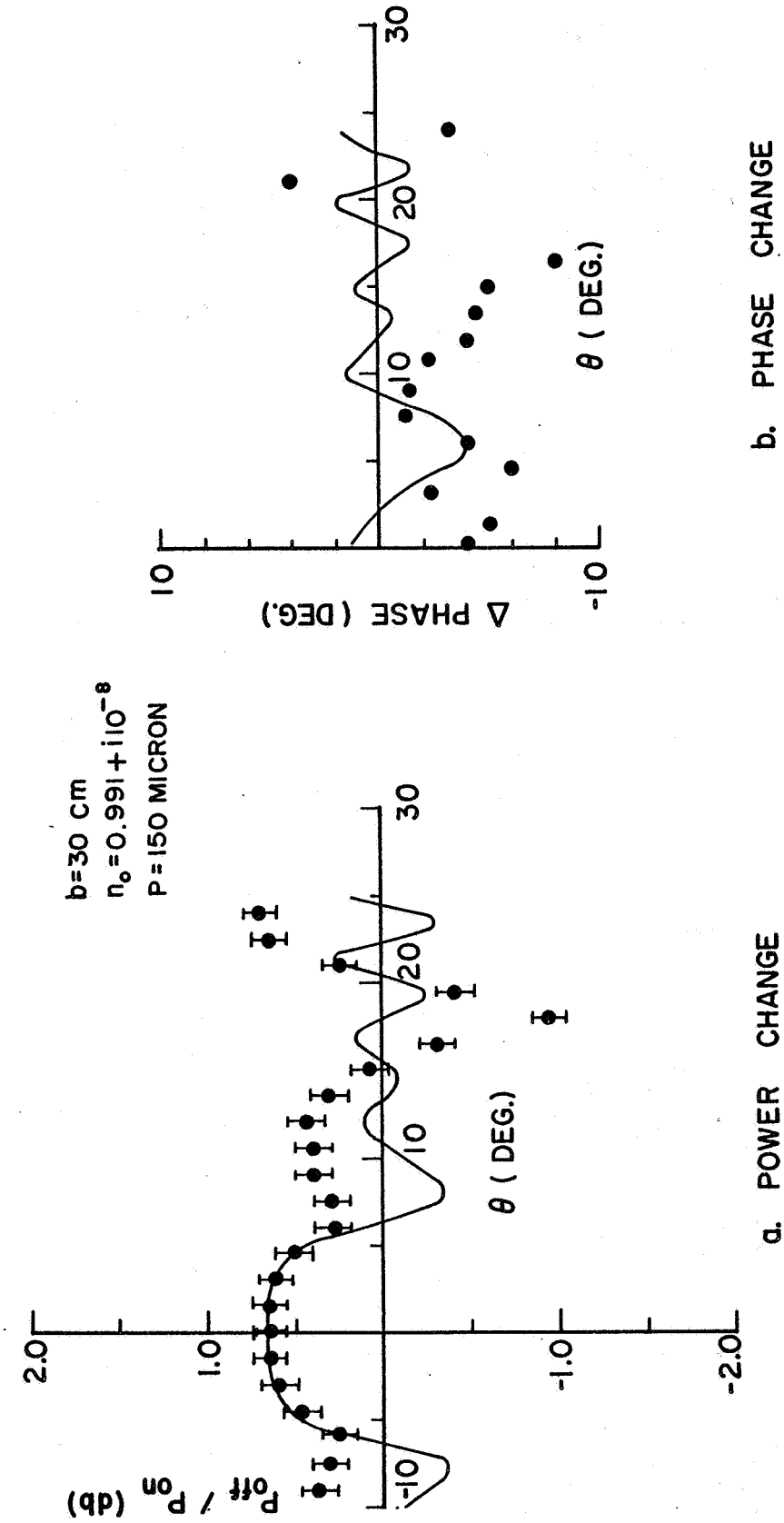

POWER AND PHASE CHANGES : K – BAND, 50 mA

FIGURE 4.12

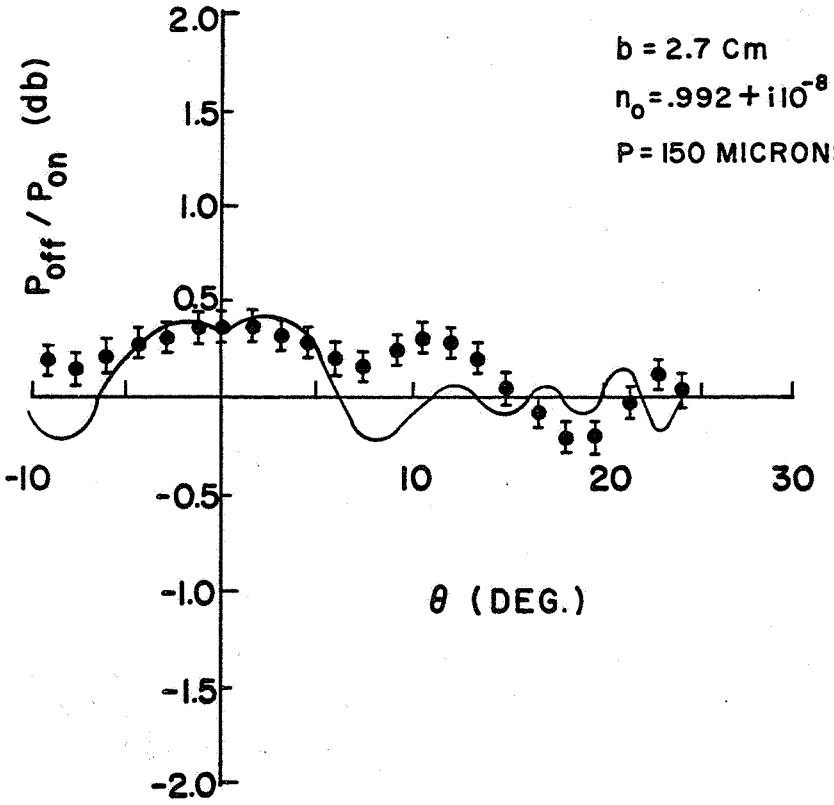

a. POWER CHANGE

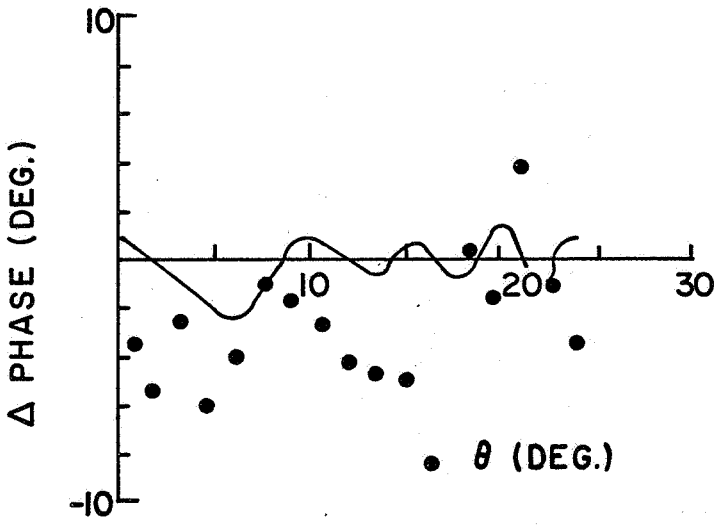

b. PHASE CHANGE

POWER AND PHASE CHANGES: K – BAND, 30 mA

FIGURE 4.13

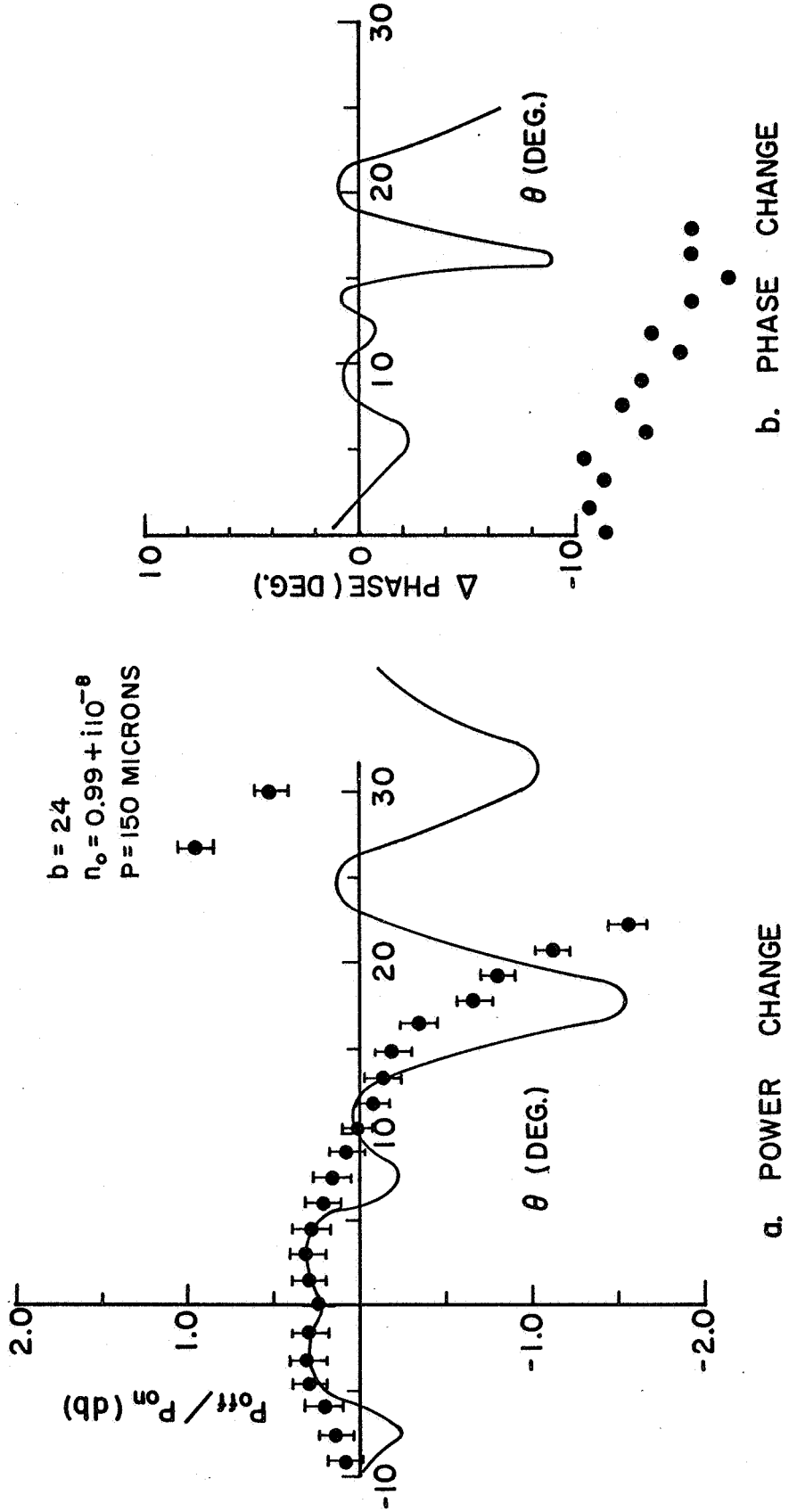

POWER AND PHASE CHANGES : A-BAND, 70 mA

FIGURE 4.14

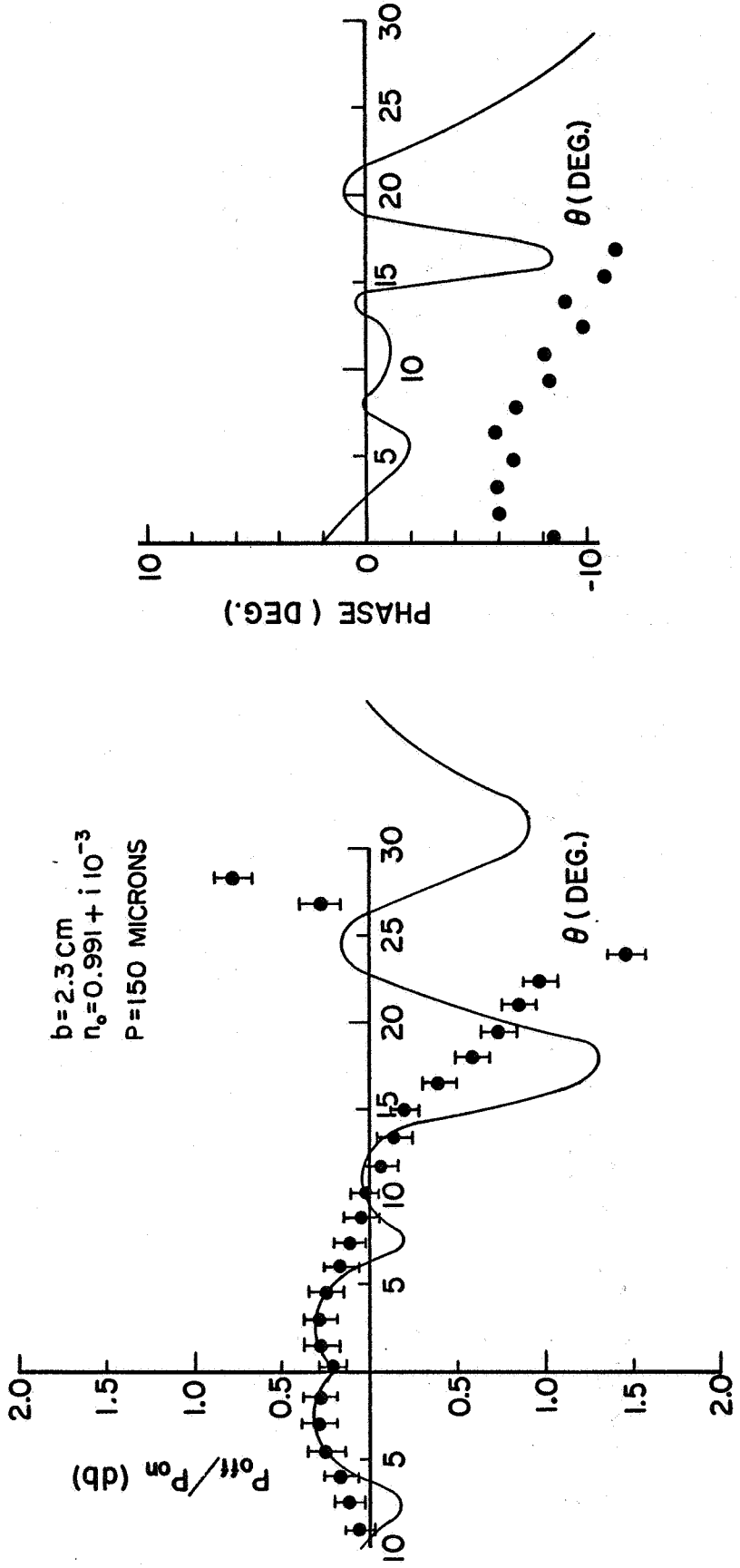

a. POWER CHANGE

b. PHASE CHANGE

POWER AND PHASE CHANGES: A-BAND, 50mA

FIGURE 4.15

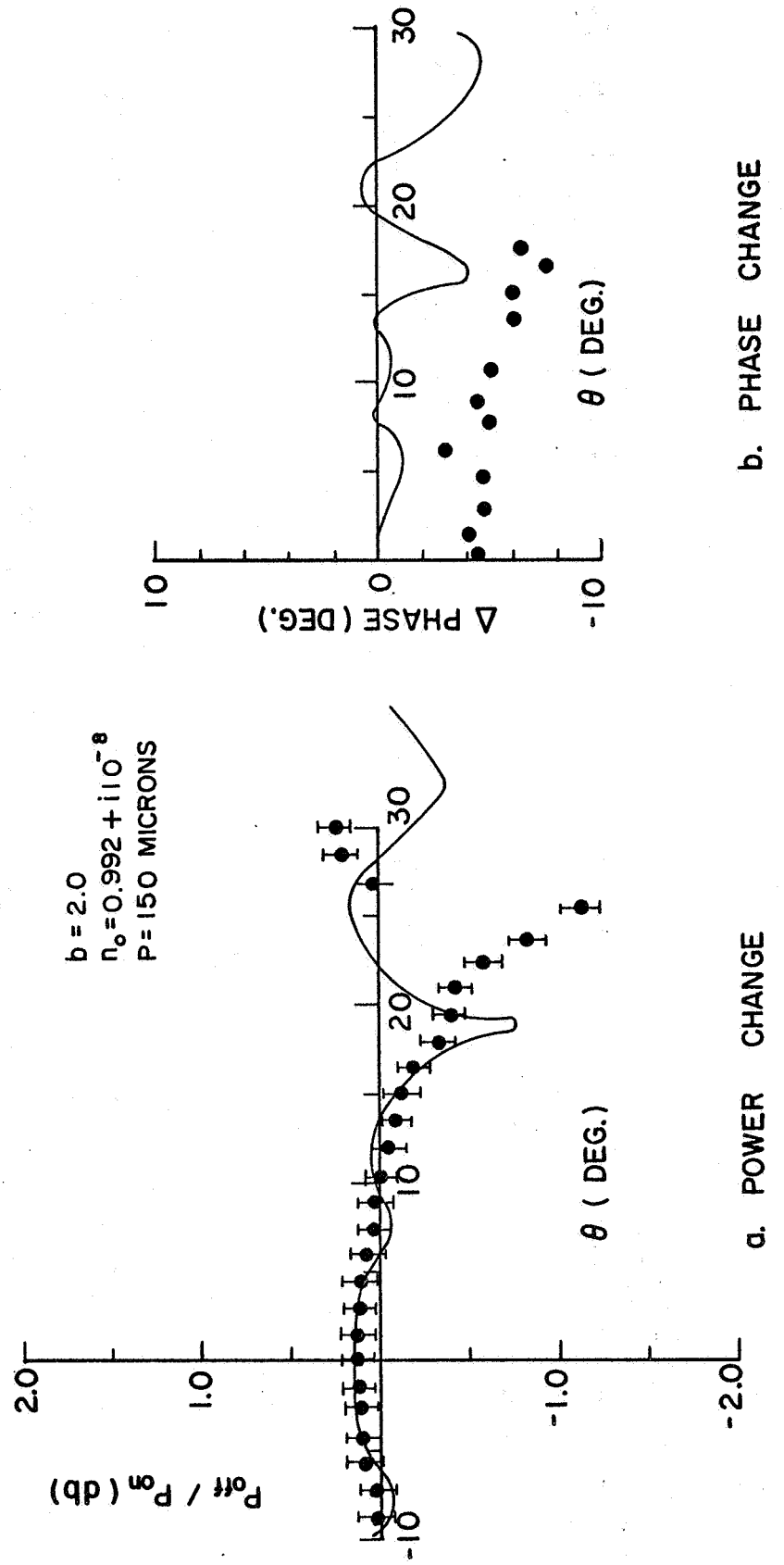

POWER AND PHASE CHANGES : A – BAND, 30 mA

FIGURE 4.16

where the Re(n) to be used is that value which agrees with scattering data. For this case the b and n_o for X-, K-, and A-Band are respectively (7.2, .997), (2.7, .992) and (2.05, .992). These Re(n) correspond to electron densities or 7.4×10^9, 9.5×10^{10} and 2.3×10^{11} cm^{-3}. The two methods agree quite well; the results are shown in Figure 4.17.

It must be remembered that the problem is formulated so that each microwave electron density profile is rectangular since constant values of n are used; thus each cross on the profile marks the beginning of a profile which a given frequency measurement predicts. Understandably as the frequency goes higher and higher the apparent thickness of the plasma decreases. The distance b_A, as can be seen from comparison to the probe profile in the figure included only the region of the plasma where the peak densities occurred; thus the A-Band measurements accurately predicted the peak densities of the plasma. The measurements at the two remaining frequencies can be thought of as predicting average densities where the averaging is carried out for that part of the real profile included between the surface of the sphere and b_K or b_X. The value of b for X-Band is nearly equal to the one obtained visually.

Finally it is possible to show that these values of b and n_o and the description of the plasma configuration are also consistent with another type of data measured during the experiement, i.e., power change as a function of pressure in the vacuum chamber for a fixed scattering angle. This data is shown in Figures 4.18 to 4.20. To fit this data one must know how the radial extent varies with pressure and appropriate values of b and n_o.

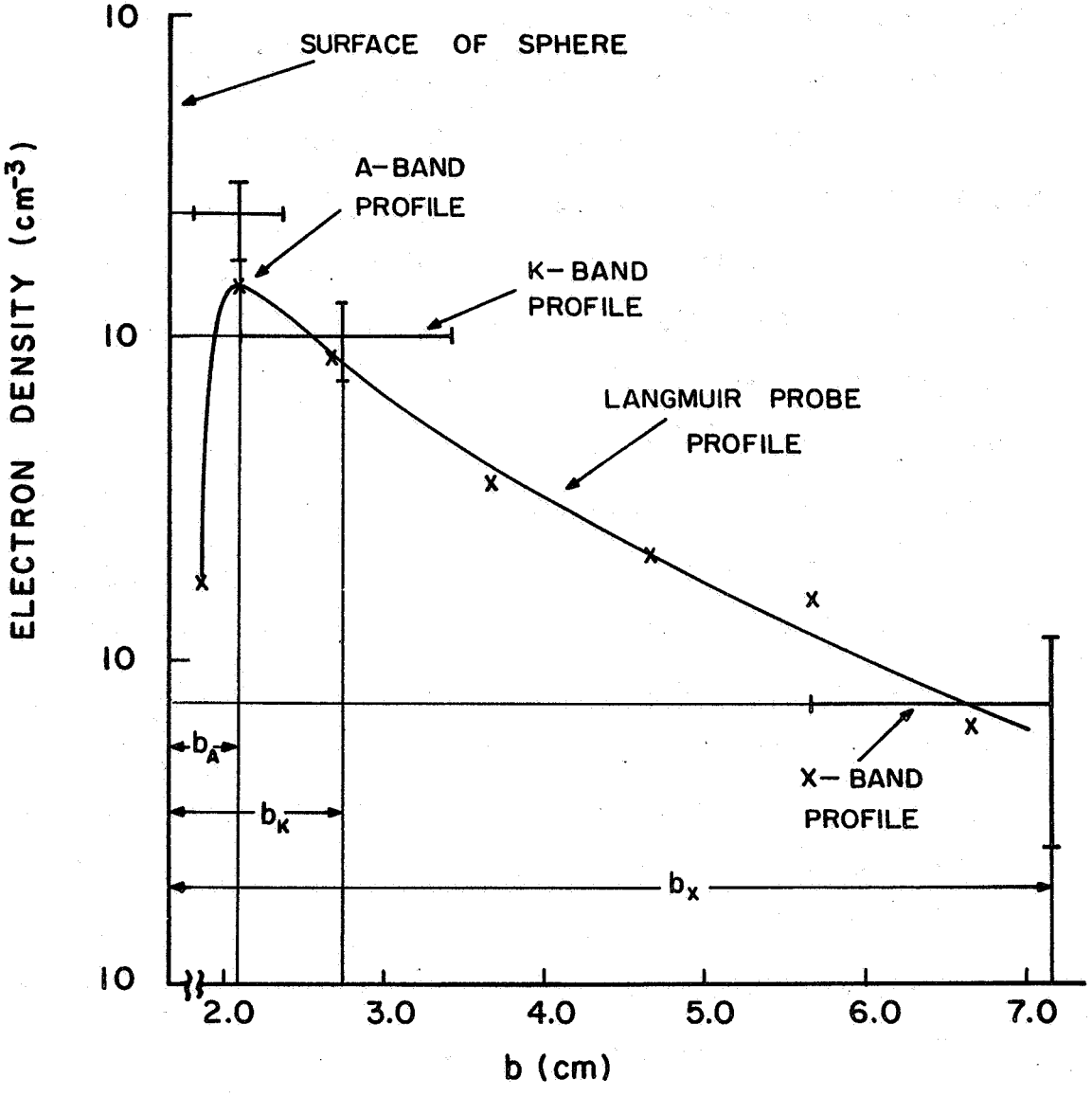

THE MICROWAVE DENSITY PROFILE

FIGURE 4.17

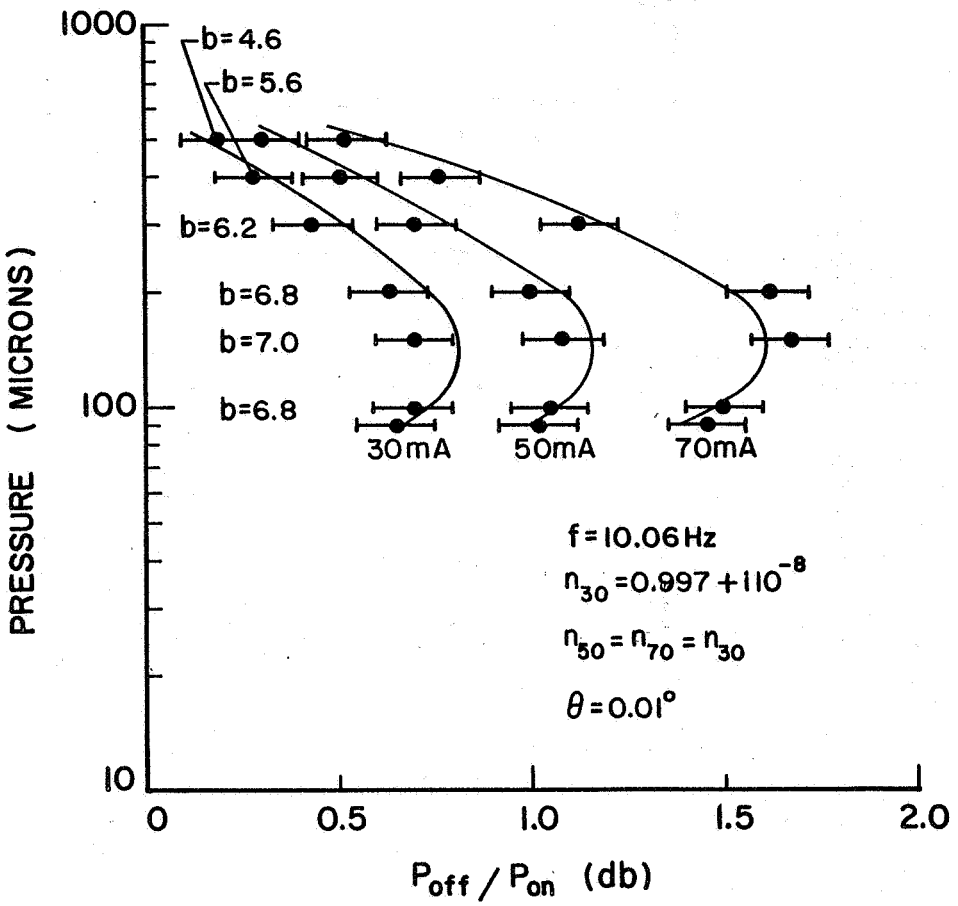

POWER CHANGES AS
A FUNCTION OF
PRESSURE : X-BAND

FIGURE 4.18

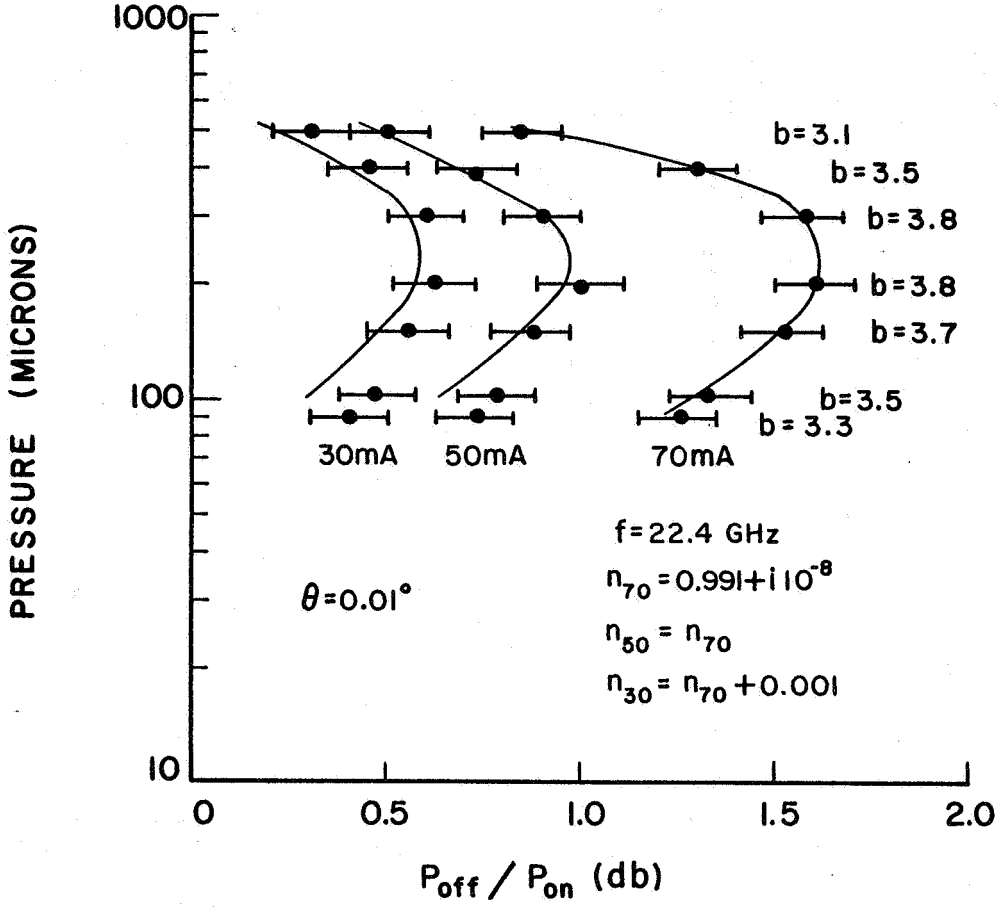

POWER CHANGES AS A FUNCTION OF PRESSURE: K-BAND

FIGURE 4.19

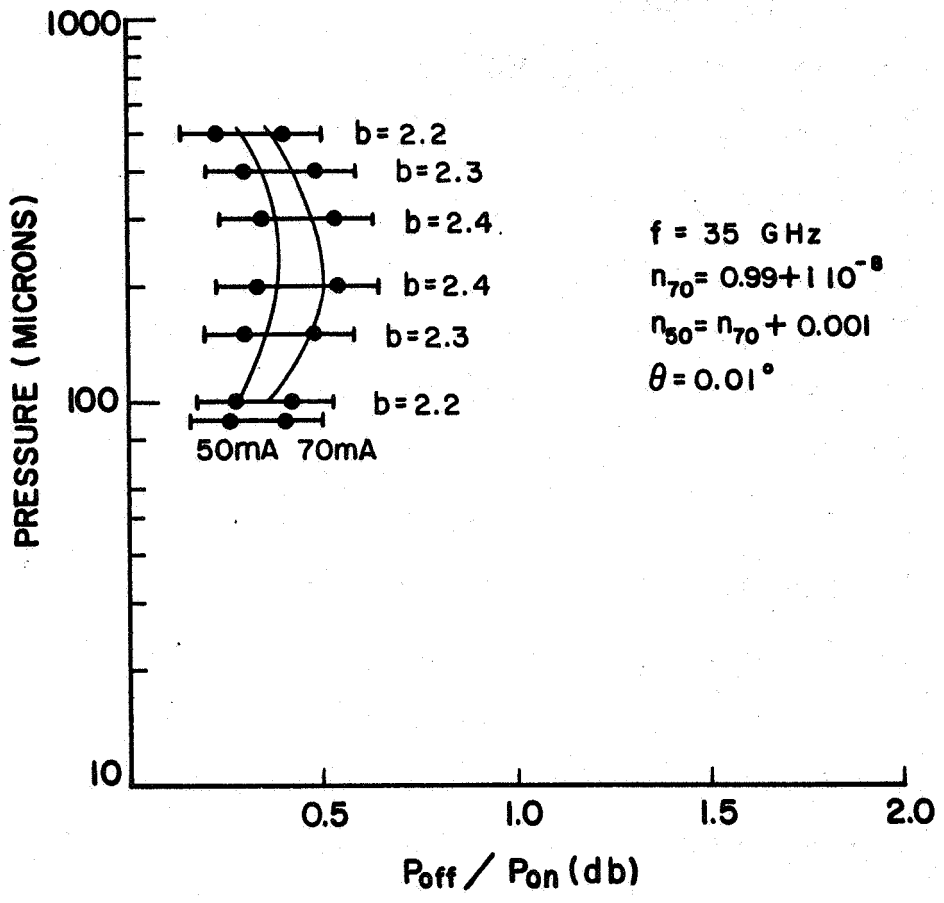

POWER CHANGE AS FUNCTION OF PRESSURE : A-BAND

FIGURE 4.20

From the discussion in Section 2 it was concluded that as the pressure in the vacuum chamber decreased from 500 to 150 microns, the radial extent of the plasma increased. Further, using the b and n_o values of the scattering data one can obtain a fixed value of these parameters for 150 microns.

As an example of how this data was fitted theoretically consider Figure 4.18. From the scattering data, b = 7.0 cm and n_{30} = .997 + $i10^{-8}$ for a discharge current of 30 ma. Using this b as a starting value all other data points for the 30 ma case was fitted by assuming smaller values of b as the pressure increased. To fit the curve for I = 50 ma we see from the scattering data that the increase in b from 150 microns, 30 ma to 150 microns, 50 ma at $\theta = 0^o$ is approximately 1.0 cm. Every value of b at various pressures for the 30 ma data was then incremented by 1.0 cm; the solid line through the 70 ma data was fitted by incrementing the values of b at 30 ma by 2.0 cm; this again is consistent with scattering data. For all these currents n_o was the same value. For the remaining frequencies when n_o changed with current, this exact change was taken into account.

5. DISCUSSIONS AND CONCLUSIONS

A discussion of the comparison of theory with experiment given in Section 4 is presented. Conclusions based on these comparisons are presented and methods to improve future investigations are suggested.

It should be noted that the microwave measurements are not presented in the usual manner. Normally, when one performs scattering measurements, the total scattering patterns are compared directly to the calculated patterns. Since it is not uncommon for scattering patterns to change by 20 to 30 dB from one angular range to another, a deviation of a few decibels between the measured and calculated patterns is accepted as good agreement. We have chosen, however, to measure this difference directly and compare it to the calculated differences. Thus small variations between theory and experiment are much more apparent.

It has been shown that the simple theory representing the plasma as a shell of constant density and radius predicts the experimental results quite well in the range $|\theta| \leq 8^{o}$.

If one considers regions outside this forward scattering range, theoretical and experimental results begin to deviate. Some assumptions used in formulating the simple model could limit agreement. For example, neglecting the support rod of the sphere could possibly introduce the limitations encountered here. Clearly at A-Band

frequencies, where the rod diameter is 3/4 λ the rod will definitely effect the scattering pattern. As the ratio D_R/λ becomes smaller, and the simple model is approached, the agreement between theory and experiment should hold for larger ranges of θ.

Effects of the incident field also introduce error. The incident field is not truly a plane wave as assumed in the theory. The magnitude by which it decreased as a function of distance and θ was taken into account by experimental measurements. However, information about the phase changes of the incident wave in the presence of a bell jar was not included in these measurements. This inadequate description of the incident field in the theoretical analysis produces perhaps the greatest effect in limiting the correlation of theory and experiment at large angles.

One could expect on the basis of physical reasoning that this particular model of the plasma should serve as a first approximation. The question arises as to whether it would be valid over a larger range of scattering angles, or would a more sophisticated model be necessary. In trying to resolve this problem the more refined approach of Bisbing (1966) could be utilized. He removes the assumption of finite plasma boundaries and treats the problem of scattering by media whose properties are analytic functions of r. The scattering coefficients are determined by asymptotic boundary conditions. Applying a similar solution to the plasma coated conductor problem would eliminate the variable b and thus one would have to treat the refractive index as a function of radial distance. (From an experimental standpoint this implies that instead of relying on measurements at many frequencies

which predict average values of densities for assumed radial extents, measurements at a single frequency could in principle predict the total profile.)

However, another difficulty is present for this problem; the plasma confined by a dipolar magnetic field does not totally cover the spherical magnet. The plasma properties have angular as well as radial dependencies. Thus the asymptotic model is again an approximation. Nevertheless, an independent investigation to formulate a more exact theoretical description of this plasma would be useful. Not only could one determine density profiles at a single frequency by appropriately adapting the asymptotic model but a model taking into account the changes in cyclic motions of the individual particles as a function of pressure in the bell jar for a given current could be correlated to power change as a function of pressure data to give information concerning the collisional processes in the plasma. In terms of the present model the collisional term of the refractive index was assumed constant for all pressures. Unfortunately the present experimental limitations mentioned herein preclude such further analysis.

The preceding suggests experimental improvements which should be considered for future work. To extend the range in theta over which the scattering data is valid, the horns should be placed inside a suitable vacuum chamber. Coating the walls of the vacuum vessel with a microwave absorber would essentially eliminate secondary reflections. In this situation one could measure only the scattered field at large scattering angles and would not need a description of phase and amplitude of the incident wave. Then using the changes of position

of the extrema and zero crossings of the power and phase data one could more accurately determine plasma properties. The phase and amplitude changes of the received wave were relatively small; as another laboratory modification, a method to increase the discharge current and the physical size of the plasma should be developed. To achieve the high currents, transient techniques, such as the discharging of capacitor banks, could be relied upon. The increase of physical size would follow as a consequence of the higher currents (see the photographs in Section 2). The associated transient microwave measurements would give scattering patterns for specific times throughout the duration of the transient. Thus a plasma decaying in a dipolar magnetic field could be investigated. Also, measurements for the case when $\omega_p > \omega$ could be taken. Finally, the magnitude of the static magnetic field could be made much larger so that ω_B/ω is not negligible. Then, as suggested by the work of Nagelberg (1964), measurements of the changes in the polarization of the received wave would also give information of the plasma properties. Such experiments will provide a broad spectrum of experimental results for verifying the many existing theories concerning the scattering properties of plasma clad bodies.

BIBLIOGRAPHY

Antosiewicz, H. A., Bessel Functions of Fractional Order, in Handbook of Mathematical Functions, edited by M. Abramowitz and I. A. Stegnun, Dover Publications, Inc., New York, 1965.

Baker, W. B., M. P. Bachynski, and A. I. Carswell, Electromagnetic Wave Scattering by Plasma Coated Re-entry Bodies, RCA Victor Research Report TM7-801-012, RCA Victor Company, Ltd., Montreal, Canada, Nov. 1964.

Bisbing, P. E., Electromagnetic Scattering by an Exponentially Inhomogeneous Plasma Sphere, IEEE Trans. AP-14, 219, 1966.

Born, M. and E. Wolf, Principles of Optics, Pergamon Press, London, 1959.

Budden, K. G., Radio Waves in the Ionosphere, Cambridge Univ. Press, London, 1961.

Chen, F. F., Electric Probes, in Plasma Diagnostic Techniques, edited by R. H. Huddelstone and S. L. Leonard, Academic Press, New York, 1965.

Easley, R. L., Diagnosis of Plasma Cylinders by Angular Scattering of Microwaves, Report No. RR-TR-63-14, U.S. Army Missile Command, Redstone Arsenal, Alabama, May 1963.

Erma, V. A., Radar Cross Sections of Inhomogeneous Plasma Spheres, Part I, Astrophysics Research Corp., Los Angeles, Calif., April 1965.

Erma, V. A., Radar Cross Sections of Inhomogeneous Plasma Spheres, Part II, TR-018, Astrophysics Research Corp., Los Angeles, Calif., Feb. 1967.

Heald, M. A. and C. B. Wharton, Plasma Diagnostics with Microwaves, John Wiley and Sons, Inc., New York, 1965.

Johnson, E. O. and L. Malter, A Floating Double Probe Method for Measurements in Gas Discharges, Phys. Rev., 80, 58, 1950.

Jones, A. R. and E. R. Wooding, Angular Distribution of Radiation Scattered Coherently by a Plasma Cylinder, J. Appl. Phys., 37, 4670, 1966.

King, W. P. and T. T. Wu, The Scattering and Diffraction of Waves, Harvard Univ. Press, Cambridge, 1959.

Midzuno, Y., Scattering of Microwaves from a Cylindrical Plasma in the Born Approximation. I, J. Phys. Soc. Japan, 16, 971, 1961.

Mikulski, J. J. and E. L. Murphy, The Computation of Electromagnetic Scattering from Concentric Spherical Structures, IEEE Trans. AP-11, 169, 1963.

Nagelberg, E. R., Microwave Interaction with Bounded Gyroelectric Plasmas, Technical Report 31, Antenna Lab., California Institute of Tech., April 1964.

Quinn, R. G., Laboratory Observations of Plasma Instabilities in a Dipole Magnetic Field, Nature, 208, 376, 1965.

Quinn, R. G. and C. C. Chang, Laboratory Observations of a Stable Plasma Trapped in a Permanent Dipolar Magnetic Field, J. Geophys. Res., 71, 253, 1966.

Quinn, R. G. and R. B. Fiorito, Investigation of Laboratory Plasma Instabilities in a Dipole Magnetic Field, J. Geophys. Res., 72, 1611, 1967.

Shmoys, J., Proposed Diagnostic Method for Cylindrical Plasma, J. Appl. Phys., 32, 689, 1961.

Wyatt, P. J., Scattering of Electromagnetic Plane Waves from Inhomogeneous Spherically Symmetric Objects, Phys. Rev., 127, 1837, 1962.

APPENDIX A

DETERMINATION OF ION DENSITIES AND ELECTRON TEMPERATURES

The procedure used to obtain ion densities from the probe data is presented in this appendix. The method to obtain these densities is given in a paper by Johnson and Malter. (1950) Their simple theory, assumed to be valid for this case, supposes that the energy distribution of the particles is Maxwellian, charge neutrality exists, the electron current is governed by the Boltzmann exponential law and no electric or magnetic fields are present. Using these assumptions the authors show the following relation to be true

$$N_+ = 1.34 \times 10^{27} \frac{i_+}{A_s} (M_+/T_+)^{\frac{1}{2}} \qquad (A.1)$$

where i_+ is the saturation current, A_s is the area of the probe sheath, M_+ is the mass of the ions and T_+ is the temperature of the ions.

In the following sample calculation we use the probe characteristics for a point in space 0.5 cm from the surface of the sphere when the discharge current is 30 ma and the pressure in the vacuum chamber is 150 microns (see Figure 2.4). For our case, with air as the gas in which the discharge was initiated, $M_+ \cong$ mass of the nitrogen molecule = 4.65×10^{-23} gms. Further, T_+ is expected to be slightly higher than the temperature of the neutral background and is taken to be $350^{\circ}K$ and A_s is approximated to be $2A_{probe}$. The value of i_+ is taken from the curves and is seen to be 94 ma. For these values N_+ from Equation (A.1) is 5.95×10^{11} cm^{-3}. The same calculations were carried out for each point in space and each current shown in Figures 2.5 and

2.6 by assuming that A_s, M_+ and T_+ remained constant for all these cases and thus

$$N_+(x) = N_+ (.5cm) \frac{i(x)}{i(.5cm)} \qquad (A.2)$$

where $N_+(x)$ and $i(x)$ are the density and saturation current respectively at the particular point in space where the expression is being evaluated.

Using the "equivalent resistance" method proposed by Johnson and Malter the electron temperature profile in the equitorial plane for the above example was determined. The basic equation for this method is

$$T_- = 11{,}600\ (G-G^2)\ R_o \sum i_p \qquad (A.3)$$

where $G = (i_{e_2}/i_p) \mid_{V_d = 0}$, $R_o = (dV_d/di_d) \mid_{V_d = 0}$ and $\sum i_p$ is the sum of the magnitudes of the saturation currents. Using the same saturation curve as above, $G-G^2 = 0.247$, $R_o = 0.228$, $\sum i_p = 160$ and thus $T_e = 10.5 \times 10^4$. Evaluating these constants at other points in space for this pressure and current led to Figure A.1.

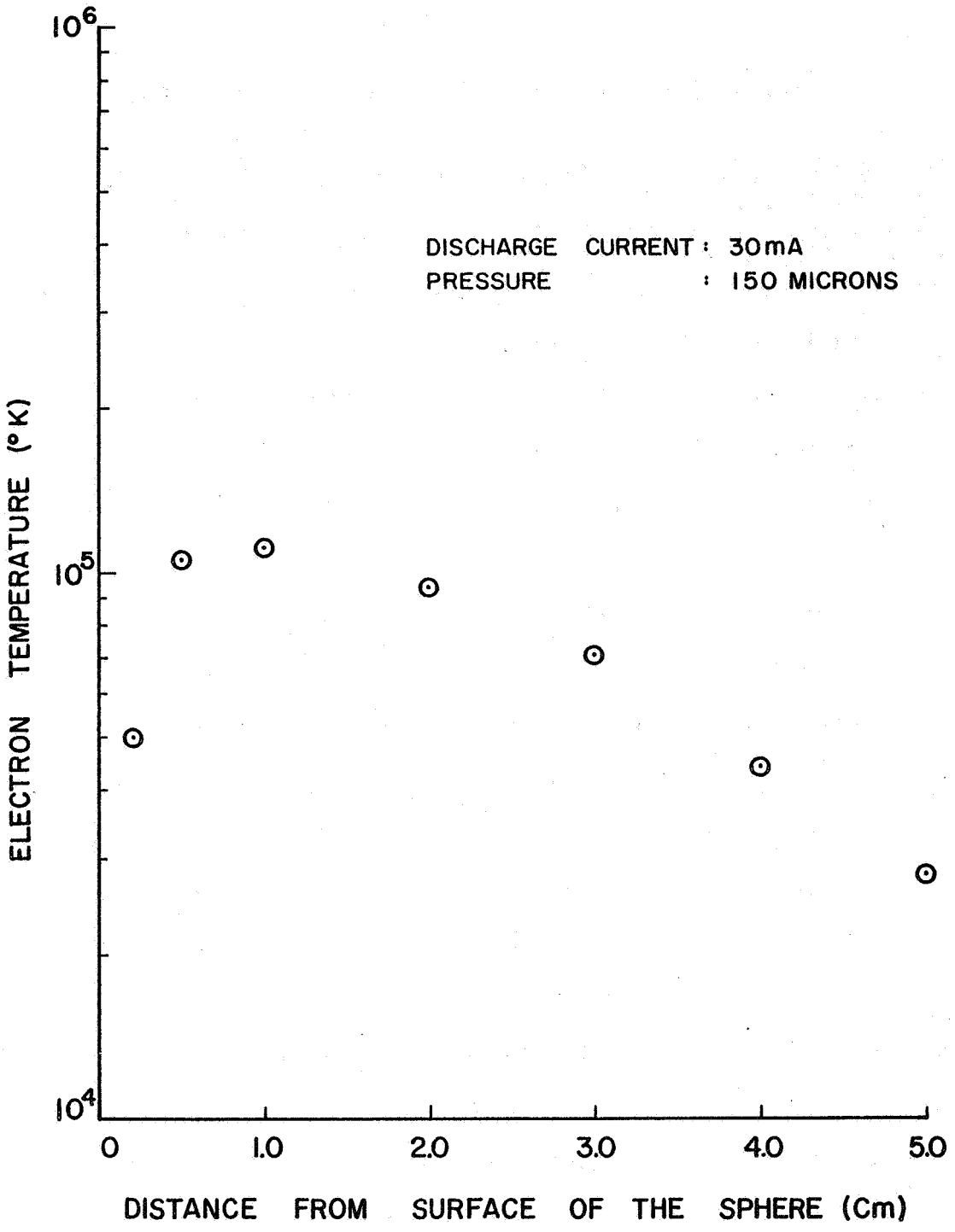

ELECTRON TEMPERATURE PROFILE

FIGURE A.1

APPENDIX B

ELECTROMAGNETIC SCATTERING BY A PLASMA COVERED SPHERE

In this appendix the theory of scattering of plane electromagnetic waves from a plasma coated spherical conductor is presented. The approach is general in the sense that the plasma properties are assumed to be radially symmetric. The geometry of the scattering problem is as described in Section 3. The analysis extends the combined works of Born and Wolf (1959), Wyatt (1962), and Erma (1965, 1967) through the introduction of a plasma-metal boundary. A discussion of the approach to the problem precedes the actual analysis.

To begin the problem, Maxwell's equations, the constitutive relations and the assumption of charge neutrality are discussed in terms of a spherically symmetric medium. To reduce the vector problem to one involving scalars, the two curl equations of Maxwell's equations are solved by the superposition of two linearly independent field solutions, namely; the transverse magnetic wave and the transverse electric wave. Each partial wave is expressable in terms of a scalar potential ${}^{e}\Pi$ or ${}^{m}\Pi$. It is shown that the equations ${}^{e,m}\Pi$ satisfy are separable in spherical coordinates; the θ and ϕ dependencies are in terms of standard orthogonal functions but the radial variable obeys quite complicated differential equations involving the plasma properties and only in special cases reduce to differential equations satisfied by analytic functions.

In a consistant manner scalar potentials for the incident field, scattered field and the field within the sphere are given. The incident

field potentials are completely defined but the potentials of the scattered field and the field within the sphere (as well as the potentials in the plasma region) contain unknown coefficients. Applying boundary conditions at the plasma-free space boundary and at the plasma-sphere boundary leads to eight simultaneous equations involving the unknown coefficients. This set is solved for the unknown constants appearing in the potentials of the scattered field, the so called "scattering coefficients." These coefficients are in terms of functions of the properties of the plasma, radial extent of the plasma and radius of the sphere. Allowing the conductivity of the sphere to grow large simplifies these expressions somewhat.

Specifying the plasma properties in terms of its refractive index completely defines the scattering coefficients and thus the scattered field. At the conclusion of the analysis the scattering coefficients are expressed for a special case of plasma refractive index.

B.1 Expressions for the Field Quantities in a Spherically Symmetric Medium

Using the MKS system of units Maxwell's equations may be written as

$$\nabla \times \bar{H} = \bar{J} + \partial\bar{D}/\partial t \tag{B.1}$$

$$\nabla \times \bar{E} = - \partial\bar{B}/\partial t \tag{B.2}$$

$$\nabla \cdot \bar{D} = \rho \tag{B.3}$$

$$\nabla \cdot \bar{B} = 0 \tag{B.4}$$

The field quantities are related by the following equations.

$$\bar{B} = \mu\bar{H} \tag{B.5}$$

$$\bar{D} = \varepsilon\bar{E} \tag{B.6}$$

$$\bar{J} = \sigma\bar{E} \tag{B.7}$$

We consider the case of constant magnetic permittivity in all regions while the dielectric constant ε and the conductivity σ may be functions of position. Using the assumed time convention of $e^{-i\omega t}$ equations (B.1) and (B.2) can be written in the form

$$\nabla \times \bar{H} = \sigma\bar{E} - i\omega\varepsilon\bar{E} = - k_1\bar{E} \tag{B.8}$$

$$\nabla \times \bar{E} = i\omega\mu\bar{H} \quad = \quad k_2\bar{H} \tag{B.9}$$

where

$$k_1 = i\omega\left(\varepsilon + \frac{i\sigma}{\omega}\right) = f(r) \tag{B.10}$$

$$k_2 = i\omega\mu = \text{constant} \tag{B.11}$$

and

$$K^2 = - k_1 k_2 \tag{B.12}$$

is the equation defining the propagation constant. Note that the problem is completely specified by (B.8) and (B.9) since (B.4) follows from the divergence of (B.9) and (B.3) follows from (B.7), (B.8), and (B.13), the assumption of charge neutrality

$$\nabla \cdot \bar{J} + \frac{\partial p}{\partial t} = 0 \ . \tag{B.13}$$

Having the two basic equations (B.8) and (B.9) we now concern ourselves with their solution when ε and σ are function of the radial

distance r from the origin. In a spherical coordinate system (r, θ, ϕ) equations (B.8) and (B.9) can be written (with the time dependence $e^{-i\omega t}$ suppressed)

$$- k_1 E_r = \frac{1}{r^2 \sin\theta} \left\{ \frac{\partial(r H_\phi \sin\theta)}{\partial\theta} - \frac{\partial(r H_\theta)}{\partial\phi} \right\} \qquad (B.14)$$

$$- k_1 E_\theta = \frac{1}{r \sin\theta} \left\{ \frac{\partial H_r}{\partial\phi} - \frac{\partial(r H_\phi \sin\theta)}{\partial r} \right\} \qquad (B.15)$$

$$- k_1 E_\phi = \frac{1}{r} \left\{ \frac{\partial(r H_\theta)}{\partial r} - \frac{\partial H_r}{\partial\theta} \right\} \qquad (B.16)$$

$$k_2 H_r = \frac{1}{r^2 \sin\theta} \left\{ \frac{\partial(r E_\phi \sin\theta)}{\partial\theta} - \frac{\partial(r E_\theta)}{\partial\phi} \right\} \qquad (B.17)$$

$$k_2 H_\theta = \frac{1}{r \sin\theta} \left\{ \frac{\partial E_r}{\partial\phi} - \frac{\partial(r E_\phi \sin\theta)}{\partial r} \right\} \qquad (B.18)$$

$$k_2 H_\phi = \frac{1}{r} \left\{ \frac{\partial(r E_\theta)}{\partial r} - \frac{\partial E_r}{\partial\theta} \right\} \qquad (B.19)$$

The general solution of this set of differential equations may be written as the superposition of two linearly independent field solutions: the "transverse magnetic wave" ($^{e}\bar{E}$, $^{e}\bar{H}$) for which $H_r = 0$, and the "transverse electric wave" ($^{m}\bar{E}$, $^{m}\bar{H}$) for which $E_r = 0$. Each wave will be derived from scalar potentials ($^{e}\Pi$, $^{m}\Pi$) which are known as Debye's potentials.

Considering first the ($^{e}\bar{E}$, $^{e}\bar{H}$) wave, Equations (B.14) to (B.19) take the form

$$- k_1 \, {}^{e}E_r = \frac{1}{r^2 \sin\theta} \left\{ \frac{\partial (r \, {}^{e}H_\phi \sin\theta)}{\partial \theta} - \frac{\partial (r \, {}^{e}H_\theta)}{\partial \phi} \right\} \tag{B.20}$$

$$- k_1 \, {}^{e}E_\theta = - \frac{1}{r} \left\{ \frac{\partial (r \, {}^{e}H_\phi)}{\partial r} \right\} \tag{B.21}$$

$$- k_1 \, {}^{e}E_\phi = \frac{1}{r} \left\{ \frac{\partial (r \, {}^{e}H_\theta)}{\partial r} \right\} \tag{B.22}$$

$$0 = \frac{1}{r^2 \sin\theta} \left\{ \frac{\partial (r \, {}^{e}E_\phi \sin\theta)}{\partial \theta} - \frac{\partial (r \, {}^{e}E_\theta)}{\partial \phi} \right\} \tag{B.23}$$

$$k_2 \, {}^{e}H_\theta = \frac{1}{r \sin\theta} \left\{ \frac{\partial \, {}^{e}E_r}{\partial \phi} - \frac{\partial (r \, {}^{e}E_\phi \sin\theta)}{\partial r} \right\} \tag{B.24}$$

$$k_2 \, {}^{e}H_\phi = \frac{1}{r} \left\{ \frac{\partial (r \, {}^{e}E_\theta)}{\partial r} - \frac{\partial \, {}^{e}E_r}{\partial \theta} \right\} \tag{B.25}$$

Two expressions which will be useful later can be obtained by substituting (B.21) into (B.25) and (B.22) into (B.24). Performing these substitutions one obtains

$$\left\{ K^2 + k_1 \frac{\partial}{\partial r} \left(\frac{1}{k_1} \frac{\partial}{\partial r} \right) \right\} r \, {}^{e}H_\theta = k_1 \frac{\partial \, {}^{e}E_r}{\partial \theta} \tag{B.26}$$

$$\left\{ K^2 + k_1 \frac{\partial}{\partial r} \left(\frac{1}{k_1} \frac{\partial}{\partial r} \right) \right\} r \, {}^{e}H_\theta = - \frac{k_1}{\sin\theta} \frac{\partial ({}^{e}E_r)}{\partial \phi} \tag{B.27}$$

Recalling that the gradient of a scalar function can be expressed in spherical coordinates as:

$$\nabla U = \frac{\partial U}{\partial r} \hat{r} + \frac{1}{r} \frac{\partial U}{\partial \theta} \hat{\theta} + \frac{1}{r \sin\theta} \frac{\partial U}{\partial \phi} \hat{\phi} \tag{B.28}$$

one sees that Equation (3.23) is satisfied by choosing ${}^{e}\bar{E} = \nabla U$. Or

$$ {}^{e}E_{\theta} = \frac{1}{r} \frac{\partial {}^{e}U}{\partial \theta} \tag{B.29} $$

$$ {}^{e}E_{\phi} = \frac{1}{r \sin\theta} \frac{\partial {}^{e}U}{\partial \phi} \tag{B.30} $$

Furthermore, if ${}^{e}U$ is defined in terms of another scalar ${}^{e}\Pi$ as

$$ {}^{e}U = \frac{\partial}{\partial r} (r {}^{e}\Pi) \tag{B.31} $$

then Equations (3.29) and (3.30) can be expressed in terms of ${}^{e}\Pi$:

$$ {}^{e}E_{\theta} = \frac{1}{r} \frac{\partial^2}{\partial r \partial \theta} (r {}^{e}\Pi) \tag{B.32} $$

$$ {}^{e}E_{\phi} = \frac{1}{r \sin\theta} \frac{\partial^2}{\partial r \partial \phi} (r {}^{e}\Pi) \tag{B.33} $$

Substitution Equation (B.32) into Equation (B.21) and Equation (B.33) into Equation (B.22) one obtains expressions for ${}^{e}H_{\phi}$ and ${}^{e}H_{\theta}$. Performing these substitutions one gets

$$ \frac{-k_1}{r} \frac{\partial^2}{\partial r \partial \theta} (r {}^{e}\Pi) = -\frac{1}{r} \frac{\partial}{\partial r} (r {}^{e}H_{\phi}) \tag{B.34} $$

and

$$ \frac{k_1}{r \sin\theta} \frac{\partial^2}{\partial r \partial \phi} (r {}^{e}\Pi) = \frac{1}{r} \frac{\partial}{\partial r} (r {}^{e}H_{\theta}) \tag{B.35} $$

These may be satisfied if ${}^{e}H_{\phi}$ and ${}^{e}H_{\theta}$ are defined as

$$ {}^{e}H_{\phi} = k_1 \frac{\partial}{\partial \theta} {}^{e}\Pi = \frac{k_1}{r} \frac{\partial}{\partial \theta} (r {}^{e}\Pi) \tag{B.36} $$

$$e_{H_\theta} = \frac{-k_1}{\sin\theta} \frac{\partial}{\partial\phi} e_\Pi = \frac{-k_1}{r \sin\theta} \frac{\partial(r\, e_\Pi)}{\partial\phi} \qquad \text{(B.37)}$$

Further, substitution of Equations (B.36) and (B.37) into (B.20) one obtains

$$e_{E_r} = \frac{-1}{r \sin\theta} \left\{ \frac{\partial}{\partial\theta} \left(\sin\theta \frac{\partial e_\Pi}{\partial\theta}\right) + \frac{1}{\sin\theta} \frac{\partial^2}{\partial\phi^2} e_\Pi \right\} \qquad \text{(B.38)}$$

Now substitute (B.38), (B.36) and (B.37) into (B.26) and (B.27) to obtain

$$\frac{\partial}{\partial\theta} \left\{ \left[K^2 + k_1 \frac{\partial}{\partial r} \left(\frac{1}{k_1} \frac{\partial}{\partial r}\right) \right] r\, e_\Pi + \frac{1}{r \sin\theta} \frac{\partial}{\partial\theta} \left(\sin\theta \frac{\partial e_\Pi}{\partial\theta}\right) + \frac{1}{r \sin^2\theta} \frac{\partial^2}{\partial\phi^2} e_\Pi \right\} = 0 \qquad \text{(B.39)}$$

$$\frac{\partial}{\partial\phi} \left\{ \left[K^2 + k_1 \frac{\partial}{\partial r} \left(\frac{1}{k_1} \frac{\partial}{\partial r}\right) \right] r\, e_\Pi + \frac{1}{r \sin\theta} \frac{\partial}{\partial\theta} \left(\sin\theta \frac{\partial e_\Pi}{\partial\theta}\right) + \frac{1}{r \sin^2\theta} \frac{\partial^2}{\partial\phi^2} e_\Pi \right\} = 0 \qquad \text{(B.40)}$$

A sufficient condition for both (B.39) and (B.40) to be satisfied is that the bracketed term in both equations vanish. Notice that setting the bracketed term equal to zero yields an equation which e_Π must satisfy, namely:

$$\left[k_1 \frac{\partial}{\partial r} \left(\frac{1}{k_2}\right) \frac{\partial}{\partial r} + \frac{\partial^2}{\partial r^2} + K^2 \right] r\, e_\Pi + \frac{1}{r \sin\theta} \frac{\partial}{\partial\theta} \left(\sin\theta \frac{\partial e_\Pi}{\partial\theta}\right) + \frac{1}{r \sin^2\theta} \frac{\partial^2 e_\Pi}{\partial\phi^2} = 0 \qquad \text{(B.41)}$$

$$\frac{1}{r}\left(-\frac{1}{k_1}\frac{\partial k_1}{\partial r}\frac{\partial}{\partial r}\right) r\,{}^{e}\Pi + \frac{2}{r}\frac{\partial {}^{e}\Pi}{\partial r} + \frac{\partial^2 {}^{e}\Pi}{\partial r^2} + K^2\,{}^{e}\Pi + \frac{1}{r^2\sin\theta}$$

$$\frac{\partial}{\partial\theta}\left(\sin\theta\frac{\partial {}^{e}\Pi}{\partial\theta}\right) + \frac{1}{r^2\sin^2\theta}\frac{\partial^2 {}^{e}\Pi}{\partial\phi^2} = 0 \qquad \text{(B.41)}$$

which can be written in a more concise form as

$$\nabla^2\,{}^{e}\Pi - \frac{1}{k_1 r}\frac{\partial k_1}{\partial r}\frac{\partial}{\partial r}(r\,{}^{e}\Pi) + K^2\,{}^{e}\Pi = 0 \qquad \text{(B.42)}$$

Combining Equations (B.41) and (B.38) leads to an expression for ${}^{e}E_r$ in terms of ${}^{e}\Pi$. The result is

$${}^{e}E_r = \left[\frac{\partial^2}{\partial r^2} + K^2 - \frac{1}{k_1}\frac{\partial k_1}{\partial r}\frac{\partial}{\partial r}\right](r\,{}^{e}\Pi) \qquad \text{(B.43)}$$

We have succeeded in satisfying the original Equations (B.20) to (B.25) in terms of the potential ${}^{e}\Pi$ which satisfies Equation (B.42).

We now turn our attention to the magnetic wave (${}^{m}\bar{E}$, ${}^{m}\bar{H}$) with ${}^{m}E_r = 0$. Equations (B.14) to (B.19) then take the form

$$0 = \frac{1}{r^2\sin\theta}\left\{\frac{\partial(r\,{}^{m}H_\phi\sin\theta)}{\partial\theta} - \frac{\partial(r\,{}^{m}H_\theta)}{\partial\phi}\right\} \qquad \text{(B.44)}$$

$$-k_1\,{}^{m}E_\theta = \frac{1}{r\sin\theta}\left\{\frac{\partial {}^{m}H_r}{\partial\phi} - \frac{\partial(r\,{}^{m}H_\phi\sin\theta)}{\partial r}\right\} \qquad \text{(B.45)}$$

$$-k_1\,{}^{m}E_\phi = \frac{1}{r}\left\{\frac{\partial(r\,{}^{m}H_\theta)}{\partial r} - \frac{\partial {}^{m}H_r}{\partial\theta}\right\} \qquad \text{(B.46)}$$

$$k_2\,{}^{m}H_r = \frac{1}{r^2\sin\theta}\left\{\frac{\partial}{\partial\theta}(r\,{}^{m}E_\phi\sin\theta) - \frac{\partial}{\partial\phi}(r\,{}^{m}E_\theta)\right\} \qquad \text{(B.47)}$$

$$k_2\ {}^{m}H_\theta = \frac{-1}{r\sin\theta}\left\{\frac{\partial(r\ {}^{m}E_\phi\ \sin\theta)}{\partial r}\right\} \tag{B.48}$$

$$k_2\ {}^{m}H_\phi = \frac{1}{r}\left\{\frac{\partial}{\partial r}\ (r\ {}^{m}E_\theta)\right\} \tag{B.49}$$

However, this last system of equations can be obtained from Equations (B.20) to (B.25) under the transformations:

$${}^{e}\bar{E} \rightarrow {}^{m}\bar{H};\quad {}^{e}\bar{H} \rightarrow -{}^{m}\bar{E};\quad k_1 \rightarrow k_2;\quad k_2 \rightarrow k_1 \tag{B.50}$$

Since those transformations convert the electric equations (Equations B.20 to B.25) identically to the magnetic wave case (Equations B.44 to B.49), all components of the magnetic wave vectors can be expressed in terms of a scalar potential ${}^{m}\Pi$ transforming equations (B.32), (B.33), (B.36), (B.37), (B.42) and (B.43) according to (B.50), and letting ${}^{e}\Pi \rightarrow {}^{m}\Pi$. The result is (keeping in mind that $K_2 \neq K_2(r)$ so that $\partial K_2/\partial r = 0$):

$${}^{m}H_r = \frac{1}{k_2}\left[\frac{\partial^2}{\partial r^2} + K^2\right](r\ {}^{m}\Pi)$$

$${}^{m}H_\theta = \frac{1}{k_2 r}\ \frac{\partial^2}{\partial r \partial\theta}\ (r\ {}^{m}\Pi)$$

$${}^{m}H_\phi = \frac{1}{k_2 r\ \sin\theta}\ \frac{\partial^2}{\partial r \partial\phi}\ (r\ {}^{m}\Pi)$$

$${}^{m}E_r = 0 \tag{B.51}$$

$$ {}^{m}E_{\theta} = \frac{1}{\sin\theta} \frac{\partial}{\partial\phi} {}^{m}\Pi $$

$$ {}^{m}E_{\phi} = -\frac{\partial}{\partial\theta} {}^{m}\Pi \qquad \text{(B.51)} $$

where ${}^{m}\Pi$ must satisfy

$$ \nabla^2 {}^{m}\Pi + K^2 {}^{m}\Pi = 0 \qquad \text{(B.52)} $$

Finally assuming that the most general solutions of the electromagnetic vectors are $\bar{E} = {}^{e}\bar{E}({}^{e}\Pi, {}^{m}\Pi) + {}^{m}\bar{E}({}^{e}\Pi, {}^{m}\Pi)$ and $\bar{H} = {}^{e}\bar{H}({}^{e}\Pi, {}^{m}\Pi) + {}^{m}\bar{H}({}^{e}\Pi, {}^{m}\Pi)$ the total field may be expressed as

$$ E_r = \left[\frac{\partial^2}{\partial r^2} - \frac{1}{k_1} \frac{\partial k_1}{\partial r} \frac{\partial}{\partial r} + K^2 \right] r \, {}^{e}\Pi \qquad \text{(B.53)} $$

$$ E_{\theta} = \frac{1}{r} \frac{\partial^2}{\partial r \partial\theta} (r \, {}^{e}\Pi) + \frac{k_2}{r \sin\theta} \frac{\partial}{\partial\phi} (r \, {}^{m}\Pi) \qquad \text{(B.54)} $$

$$ E_{\phi} = \frac{1}{r \sin\theta} \frac{\partial^2}{\partial r \partial\phi} (r \, {}^{e}\Pi) - \frac{k_2}{r} \frac{\partial}{\partial\theta} (r \, {}^{m}\Pi) \qquad \text{(B.55)} $$

$$ H_r = \left[\frac{\partial^2}{\partial r^2} + K^2 \right] (r \, {}^{m}\Pi) \qquad \text{(B.56)} $$

$$ H_{\theta} = \frac{-k_1}{r \sin\theta} \frac{\partial}{\partial\phi} (r \, {}^{e}\Pi) + \frac{1}{r} \frac{\partial^2}{\partial r \partial\theta} (r \, {}^{m}\Pi) \qquad \text{(B.57)} $$

$$ H_{\phi} = \frac{k_1}{r} \frac{\partial}{\partial\theta} (r \, {}^{e}\Pi) + \frac{1}{r \sin\theta} \frac{\partial^2}{\partial r \partial\theta} (r \, {}^{m}\Pi) \qquad \text{(B.58)} $$

The scalar functions ${}^{e}\Pi$ and ${}^{m}\Pi$ appearing in Equations (B.53) to (B.58) are obtained by solving Equations (B.42) and (B.52). Equations (B.42)

and (B.52) may be separated in spherical coordinates according to standard methods and the general solutions written in the forms:

$$r\,{}^{e}\Pi = \sum_{\ell=0}^{\infty} \sum_{m=0}^{\ell} W_\ell(r) \left[a_m \cos m\phi + b_m \sin m\phi \right] P_\ell^m(\cos\theta) \qquad \text{(B.59)}$$

$$r\,{}^{m}\Pi = \sum_{\ell=0}^{\infty} \sum_{m=0}^{\ell} G_\ell(r) \left[c_m \cos m\phi + d_m \sin m\phi \right] P_\ell^m(\cos\theta) \qquad \text{(B.60)}$$

where ${}^{a}m$, ${}^{b}m$, ${}^{c}m$, and ${}^{d}m$ are arbitrary constants, $P_\ell^m(\cos\theta)$ is the associated Lengendre Polynomial, and W_ℓ and G_ℓ are general solutions of the differential equations

$$\frac{d^2}{dr^2} W_\ell - \frac{2}{K} \frac{dK}{dr} \frac{d}{dr} W_\ell + \left[K^2 - \frac{\ell(\ell+1)}{r^2} \right] W_\ell = 0 \qquad \text{(B.61)}$$

$$\frac{d^2}{dr^2} G_\ell = \left[K^2 - \frac{\ell(\ell+1)}{r^2} \right] G_\ell = 0 \qquad \text{(B.62)}$$

This completes the description of Maxwell's Equations in a radially inhomogeneous medium. Thus given a specific K(r), one may find the general solutions W_ℓ and G_ℓ and then determine the arbitrary constants by imposing suitable boundary conditions.

B.2 Incident Field Expressed in Terms of ${}^{e,m}\Pi$

To impose boundary conditions at the spherical surfaces the incident plane wave is expressed in terms of scalar potentials. The polarization of the incident wave and the reference coordinate system

is shown in Figure 3.7. With this scattering configuration the incident wave is characterized by the following field components.

$$
\begin{aligned}
E_x^i &= E_o\, e^{\,i(K^I z - \omega t)} \\
E_y^i &= E_z^i = 0 \\
H_y^i &= \frac{K^I}{\mu_o \omega}\, E_o\, e^{\,i(K^I z - \omega t)} \\
H_x^i &= H_z^i = 0
\end{aligned}
\tag{B.63}
$$

The spherical coordinates (r, θ, ϕ) appropriate to the problem are defined by

$$
\begin{aligned}
x &= r \sin\theta \cos\phi \\
y &= r \sin\theta \sin\phi \\
z &= r \cos\theta \ ;
\end{aligned}
\tag{B.64}
$$

and

further one may transform the components of any Cartesian vector $(\bar{A})$ to a spherical system according to the rule

$$
\begin{aligned}
A_r &= A_x \sin\theta \cos\phi + A_y \sin\theta \sin\phi + A_z \cos\theta \\
A_\theta &= A_x \cos\theta \cos\phi + A_y \cos\theta \sin\phi - A_z \sin\theta \\
A_\phi &= A_x \sin\phi + A_y \cos\phi
\end{aligned}
\tag{B.65}
$$

Using this rule one can express the r-components of the incident field as:

$$E_r^i = E_o\, e^{iK^I r \cos\theta} \sin\theta \cos\phi \tag{B.66}$$

$$H_r^i = \frac{iK^I E_o}{K_2^I}\, e^{iK^I r \cos\theta} \cos\theta \sin\phi \tag{B.67}$$

To find the potential functions ${}^{e}\Pi^{i}$, ${}^{m}\Pi^{i}$ from which the above fields can be derived we proceed with the well-known formula

$$e^{iK^I r \cos\theta} = \sum_{\ell=0}^{\infty} i^{\ell} (2\ell+1)\, j_{\ell}(K^I r)\, P_{\ell}(\cos\theta) \tag{B.68}$$

where $$j_{\ell}(K^I r) = \left\{ \frac{\Pi}{2K^I r} \right\}^{\frac{1}{2}} J_{\ell+\frac{1}{2}}(K^I r) \tag{B.69}$$

defines the so-called "spherical-Bessel function." Using the identities

$$e^{iK^I r \cos\theta} = \frac{1}{iK^I r} \frac{\partial e^{iK^I r \cos\theta}}{\partial(\cos\theta)} \tag{B.70}$$

$$\sin\theta \frac{dP_{\ell}(\cos\theta)}{d(\cos\theta)} = P_{\ell}^{1}(\cos\theta) \tag{B.71}$$

and

$$P_o^1(\cos\theta) = 0 \tag{B.72}$$

Equation (3.68) can be written as:

$$e^{iK^I r \cos\theta} = \frac{1}{K^I r \sin\theta} \sum_{\ell=1}^{\infty} i^{\ell-1} (2\ell+1) j_\ell (K^I r) P_\ell^1 (\cos\theta); \quad (B.73)$$

further, if we introduce the Ricatti-Bessel function defined by

$$\psi_\ell (K^I r) = K^I r \, j_\ell (K^I r) = \left[\frac{\pi K^I r}{2}\right]^{\frac{1}{2}} J_{\ell+\frac{1}{2}} (K^I r) \quad (B.74)$$

into (B.73) the Equations (B.66) and (B.67) can be written in the form

$$E_r^i = \frac{E_o \cos\phi}{(K^I r)^2} \sum_{\ell=1}^{\infty} i^{\ell-1} (2\ell+1) \psi_\ell (K^I r) P_\ell^1 (\cos\theta) \quad (B.75)$$

$$H_r^i = \frac{i E_o \sin\phi \, K^I}{K_2^I (rK^I)^2} \sum_{\ell}^{\infty} i^{\ell-1} (2\ell+1) \psi_\ell (K^I r) P_\ell^1 (\cos\theta) \quad (B.76)$$

In terms of ($^e\Pi^i$, and $^m\Pi^i$) Equations (B.75) and (B.76) can be written as

$$E_r^i = \left[\frac{\partial^2}{\partial r^2} + K^{I\,2}\right] r \, {}^e\Pi^i \quad (B.77)$$

$$H_r^i = \left[\frac{\partial^2}{\partial r^2} + K^{I\,2}\right] r \, {}^m\Pi^i \quad (B.78)$$

Equations (B.77) and (B.78) were derived from (B.53) and (B.56) by noting that in Region I, $K_1^I \neq K_1^I(r)$. But when $K_1^I \neq K_1^I(r)$ then W_ℓ and G_ℓ satisfy the same differential equation, namely:

$$\frac{d^2}{dr^2} G_\ell + \left[K^{I\,2} - \frac{\ell(\ell+1)}{r^2}\right] G_\ell = 0 \quad (B.79)$$

However, this equation is satisfied by $\psi_\ell(K^I r)$ so that in Region I

$$W_\ell \ , \ G_\ell \ \rightarrow \ \psi_\ell(K^I r) \tag{B.80}$$

Consequently one may write the trial solution of the general expressions for potentials of the incident wave as

$$r\ {}^{e}\Pi^{i} = \frac{E_o \cos\phi}{(K^I)^2} \sum_{\ell=1}^{\infty} a_\ell \ \psi_\ell(K^I r)\ P_\ell^1(\cos\theta) \tag{B.81}$$

$$r\ {}^{m}\Pi^{i} = \left[\frac{i\ E_o \sin\phi}{(K^I)^2}\right] \frac{K^I}{k_2^I} \sum_{\ell=1}^{\infty} b_\ell \ \psi_\ell(K^I r)\ P_\ell^1(\cos\theta) \tag{B.82}$$

Substituting Equations (B.81) and (B.84) into Equations (B.77) and (B.78) one obtains the following expressions

$$E_r^i = \frac{E_o \cos\phi}{(K^I)^2} \sum_{\ell=1}^{\infty} a_\ell \ P_\ell^1(\cos\theta) \left[\frac{\partial^2}{\partial r^2} \psi_\ell + (K^I)^2 \ \psi_\ell\right] \tag{B.83}$$

$$H_r^i = \frac{i\ E_o \sin\phi}{(K^I)^2} \sum_{\ell=1}^{\infty} b_\ell \ P_\ell^1(\cos\theta) \left[\frac{\partial^2}{\partial r^2} \psi_\ell + (K^I)^2 \ \psi_\ell\right] \frac{K^I}{k_2^I} \tag{B.84}$$

Equating Equation (B.83) to Equation (B.75) and Equation (B.84) to Equation (B.76) one can write

$$\frac{E_o \cos\phi}{(K^I)^2} \sum_{\ell=1}^{\infty} a_\ell \ P_\ell^1 \frac{\ell(\ell+1)}{r^2} = \frac{E_o \cos\phi}{(K^I r)^2} \sum_{\ell=1}^{\infty} i^{\ell-1} \ (2\ell+1) \ \psi_\ell \ P_\ell^1 \tag{B.85}$$

and

$$\frac{i\,E_o\,\sin\phi}{(K^I)^2}\,\frac{K^I}{k_2^I}\sum_{\ell=1}^{\infty} b_\ell\,P_\ell^1\,\frac{\ell(\ell+1)}{r^2}\,\psi_\ell = \frac{i\,E_o\,\sin\phi\,K^I}{k_2^I\,r^2\,(K^I)^2}\sum_{\ell=1}^{\infty} i^{\ell-1}\,(2\ell+1)$$

$$\psi_\ell\,P_\ell^1 \tag{B.86}$$

where the bracketed terms in Equations (B.83) and (B.84) were eliminated through the use of Equation (B.79). By comparing coefficients in Equation (B.85) and (B.86) one obtains the following relations for the coefficients a_ℓ and b_ℓ.

$$a_\ell = i^{\ell-1}\,\frac{(2\ell+1)}{\ell(\ell+1)} \tag{B.87}$$

$$b_\ell = i^{\ell-1}\,\frac{(2\ell+1)}{\ell(\ell+1)} \tag{B.88}$$

Using these expressions for the coefficients the scalar potentials for the incident can be written as:

$$r\,{}^{e}\Pi^{i} = \frac{E_o\,\cos\phi}{(K^I)^2}\sum_{\ell=1}^{\infty} i^{\ell-1}\,\frac{(2\ell+1)}{\ell(\ell+1)}\,\psi_\ell(K^I r)\;\;P_\ell^1(\cos\theta) \tag{B.89}$$

$$r\,{}^{m}\Pi^{i} = \frac{i\,K^I\,\sin\phi\,E_o}{k_2^I\,(K^I)^2}\sum_{\ell=1}^{\infty} i^{\ell+1}\,\frac{(2\ell+1)}{\ell(\ell+1)}\,\psi_\ell(K^I r)\;P_\ell^1(\cos\theta) \tag{B.90}$$

B.3 Expressions for the Scattered Fields

We now turn to the problem of determining the total fields in the presence of a plasma covered spherical body. This general field, at all points outside the scattering configuration, is assumed to be composed of the incident plane wave and a scattered wave. The scalar

potentials of the plane wave were derived in the last section and are given by Equations (B.89) and (B.90). The potentials of the scattered field (superscripted with s) and the field within the sphere (superscripted with III) can be obtained from the general expressions (B.59) and (B.60) where $W_\ell(r)$ and $G_\ell(r)$ must satisfy

$$\frac{d^2 U_\ell}{dr^2} + \left[K^2 - \frac{\ell(\ell+1)}{r^2} \right] U_\ell = 0 \qquad \text{(B.91)}$$

To integrate this equation, set $Kr = \rho$ and $U_\ell = (\rho)^{-\frac{1}{2}} Z(\rho)$ (remembering that $U_\ell = rR$) and obtain Bessel's equation:

$$\frac{d^2 Z}{d\rho^2} + \frac{1}{\rho} \frac{dZ}{d\rho} + \left\{ K^2 - \frac{(\ell+\frac{1}{2})^2}{\rho} \right\} Z = 0 \qquad \text{(B.92)}$$

The solutions to this equation can be written as

$$\psi_\ell(\rho) = \left(\frac{\pi\rho}{2}\right)^{\frac{1}{2}} J_{\ell+\frac{1}{2}}(\rho) \qquad \text{(B.93)}$$

$$\chi_\ell(\rho) = -\left(\frac{\pi\rho}{2}\right)^{\frac{1}{2}} N_{\ell+\frac{1}{2}}(\rho) \qquad \text{(B.94)}$$

The general solution to (B.91) may be written

$$rR = M_\ell \psi_\ell(Kr) + N_\ell \chi_\ell(Kr) \qquad \text{(B.95)}$$

with $M_\ell = 1$ and $N_\ell = -i$ we have the "Hankel function" $(\zeta_\ell^1 (K^I r))$ which vanishes at infinity. The radial functions in the expression for the scattered wave is assumed to be of the form

$$^{e,m}B_\ell \, \zeta_\ell^1 (K^I r) \qquad \text{(B.96)}$$

since this wave must vanish at infinity, while the radial function in the potentials from which the field within the sphere is derivable takes the form

$$c_\ell \psi_\ell, \; d_\ell \psi_\ell \tag{B.97}$$

so that this field is finite at the origin. In Equations (B.96) and (B.97) ${}^{e,m}B_\ell$, c_ℓ and d_ℓ are constants chosen to satisfy boundary conditions.

Moreover, since the boundary conditions at r = a and r = b must hold for all values of θ and ϕ it is assumed that all potentials have the functional dependence on θ and ϕ as does ${}^{e,m}\Pi^i$. Using this assumption, the potentials of the scattered field and the field transmitted into the sphere can be written as

$$r\,{}^{e}\Pi^{s} = \frac{E_o \cos\phi}{(K^I)^2} \sum_{\ell=1}^{\infty} {}^{e}B_\ell \, i^{\ell-1} \frac{(2\ell+1)}{\ell(\ell+1)} \zeta_\ell^1(\rho) \, P_\ell^1(\cos\theta) \tag{B.98}$$

$$r\,{}^{m}\Pi^{s} = \frac{i\,E_o \sin\phi}{K^I \, k_2^I} \sum_{\ell=1}^{\infty} {}^{m}B_\ell \, i^{\ell-1} \frac{(2\ell+1)}{\ell(\ell+1)} \zeta_\ell^1(\rho) \, P_\ell^1(\cos\theta) \tag{B.99}$$

$$r\,{}^{e}\Pi^{III} = \frac{E_o \cos\phi}{(K^{III})^2} \sum_{\ell=1}^{\infty} c_\ell \, i^{\ell-1} \frac{(2\ell+1)}{\ell(\ell+1)} \psi_\ell(n_3\rho) \, P_\ell^1(\cos\theta) \tag{B.100}$$

$$r\,{}^{m}\Pi^{III} = \frac{i\,E_o \sin\phi}{K^{III} \, k_2^{III}} \sum_{\ell=1}^{\infty} d_\ell \, i^{\ell-1} \frac{(2\ell+1)}{\ell(\ell+1)} \psi_\ell(n_3\rho) \, P_\ell^1(\cos\theta) \tag{B.101}$$

Introduced into these equations is the "relative dielectric constant" of the plasma and the Greek letter rho defined by

$$n_i = \frac{K^i}{K^I} \; ; \quad \rho = K^I r \; ; \quad i = II, III \tag{B.102}$$

Similarly the potentials in Region II may be written in the form

$$r\ {}^{e}\Pi^{II} = \frac{E_o \cos\phi}{(K^{II})^2} \sum_{\ell=1}^{\infty} i^{\ell-1} \frac{(2\ell+1)}{\ell(\ell+1)} P_\ell^1(\cos\theta)\left[\alpha_\ell\ X_\ell(\rho) + \beta_\ell\ Y_\ell(\rho)\right] \quad \text{(B.103)}$$

$$r\ {}^{m}\Pi^{II} = \frac{i\ E_o \sin\phi}{K^{II}\ k_2^{II}} \sum_{\ell=1}^{\infty} i^{\ell-1} \frac{(2\ell+1)}{\ell(\ell+1)} P_\ell^1(\cos\theta)\left[\gamma_\ell\ U_\ell(\rho) + \delta_\ell\ V_\ell(\rho)\right] \quad \text{(B.104)}$$

where $X_\ell(\rho)$, $Y_\ell(\rho)$, $U_\ell(\rho)$, and $V_\ell(\rho)$ are defined through the relations

$$W_\ell(\rho) = \alpha_\ell\ X_\ell(\rho) + \beta_\ell\ Y_\ell(\rho) \quad \text{(B.105)}$$

$$G_\ell(\rho) = \gamma_\ell\ U_\ell(\rho) + \delta_\ell\ V_\ell(\rho) \quad \text{(B.106)}$$

and α_ℓ, β_ℓ, γ_ℓ and δ_ℓ are arbitrary constants. Note that Region II does not contain the origin so that the four solutions of the two radial equations

$$\frac{d^2W_\ell(\rho)}{d^2\rho} - \frac{2}{n_2}\frac{dn_2}{d\rho}\frac{dW_\ell(\rho)}{d\rho} + \left[n_2^2 - \frac{\ell(\ell+1)}{\rho^2}\right] W_\ell(\rho) = 0 \quad \text{(B.107)}$$

$$\frac{d^2G_\ell(\rho)}{d\rho^2} + \left[n_2^2 - \frac{\ell(\ell+1)}{\rho^2}\right] G_\ell(\rho) = 0 \quad \text{(B.108)}$$

must be retained in the ${}^{e,m}\Pi^{II}$ expressions.

Requiring the tangential components of the $\bar{E}$ and $\bar{H}$ vectors to be continuous at the boundaries defined by r = a and r = b leads to the following boundary conditions in terms of the scalar potentials,

$$k_1^{I,II}\ (r\ {}^{e}\Pi^{I,II}) = k_1^{II,III}\ (r\ {}^{e}\Pi^{II,III}) \quad \text{(B.109)}$$

$$\partial/\partial r\ (r\ {}^{e}\Pi^{I,II}) = \partial/\partial r\ (r\ {}^{e}\Pi^{II,III})$$

$$k_2^{I,II}\ (r\ {}^{m}\Pi^{I,II}) = k_2^{II,III}\ (r\ {}^{m}\Pi^{II,III}) \qquad \text{(B.109)}$$

$$\partial/\partial r\ (r\ {}^{m}\Pi^{I,II}) = \partial/\partial r\ (r\ {}^{m}\Pi^{II,III})$$

In these expressions ${}^{e,m}\Pi^{I} = {}^{e,m}\Pi^{i} + {}^{e,m}\Pi^{s}$ etc. By satisfying these boundary conditions at r = a (ρ = y) and r = b (ρ = x) one obtains:

$${}^{e}B_\ell \left[\zeta_\ell^1(x)/k_2^I\right] - \alpha_\ell \left[X_\ell(x)/k_2^{II}\right] - \beta_\ell \left[Y_\ell(x)/k_2^{II}\right] = -\psi_\ell(x)/k_2^I$$

$${}^{e}B_\ell \left[\zeta_\ell^{1'}(x)\right] - \frac{\alpha_\ell}{n_2^2}\left[-\frac{2}{n^2}\frac{dn_2}{d\rho}X(x) + X'(x)\right] - \frac{\beta_\ell}{n_2^2}\left[-\frac{2}{n_2}\frac{dn_2}{d\rho}Y(x) - Y'(x)\right] = -\psi_\ell'(x)$$

$${}^{m}B_\ell \left[\zeta_\ell^1(x)\right] - \frac{\gamma_\ell}{n_2}U_\ell(x) - \frac{\delta_\ell}{n_2}V_\ell(x) = -\psi_\ell(x)$$

$${}^{m}B_\ell\ \zeta_\ell^{1'}(x)/k_2^I - \frac{\gamma_\ell}{k_2^{II}n_2}\left[U'(x) - \frac{1}{n_2}\frac{dn_2}{d\rho}U(x)\right] - \frac{\delta_\ell}{k_2^{II}n_2}\left[V'(x) - \frac{1}{n_2}\frac{dn_2}{d\rho}V(x)\right] = -\frac{\psi_\ell'(x)}{k_2^I}$$

$$\alpha_\ell\ X(y)/k_2^{II} + \beta_\ell\ Y(y)/k_2^{II} - c_\ell\ \psi_\ell\ (n_3 y)/k_2^{III} = 0$$

$$\frac{\alpha_\ell}{n_2^2(y)}\left[-\frac{2X(y)}{n_2(y)}\frac{dn_2(y)}{d\rho} + X'(y)\right] + \frac{\beta_\ell}{n_2^2(y)}\left[-\frac{2Y(y)}{n_2}\frac{dn_2(y)}{d\rho} + Y'(y)\right]$$

$$-\frac{c_\ell}{n_3(y)}\ \psi_\ell'(n_3 y) = 0 \qquad \text{(B.110)}$$

$$\frac{\gamma_\ell}{n_2(y)}\, U_\ell(y) + \delta_\ell\, V_\ell(y)/n_2(y) - d_\ell\, \psi_\ell(n_3 y)/n_3(y) = 0$$

$$\frac{\gamma_\ell}{k_2^{II}}\,\frac{1}{n_2(y)}\left[-\frac{1}{n_2(y)}\,\frac{dn_2(y)}{d\rho}\,U_\ell(y) + U_\ell'(y)\right] + \frac{\delta_\ell}{k_2^{II}}\,\frac{1}{n_2(y)}\left[-\frac{1}{n_2(y)}\,\frac{dn_2(y)}{d\rho}\right.$$

$$\left. V_\ell(y) + V'(y)\right] - \frac{d_\ell}{k_2^{III}}\,\psi_\ell'(n_3 y) \equiv 0 \qquad \text{(B.110)}$$

These eight equations can be solved for the scattering coefficients $^{e,m}B_\ell$. The results are

$$^{e}B_\ell \simeq \frac{\dfrac{-\psi_\ell(x)}{k_2^I}\left\{AD - BC\right\} + \psi_\ell'(x)\left\{-D\,\dfrac{X_\ell(x)}{k_2^{II}} + C\,\dfrac{Y_\ell(x)}{k_2^{II}}\right\}}{\zeta_\ell^1(x)\left\{AD - BC\right\}/k_2^I - \zeta_\ell^{1\prime}(x)\left\{-D\,\dfrac{X_\ell(x)}{k_2^{II}} + C\,\dfrac{Y_\ell(x)}{k_2^{II}}\right\}} \qquad \text{(B.111)}$$

where

$$A = \left[\frac{2}{n_2^3(x)}\,\frac{dn_2(x)}{d\rho}\,X(x) - \frac{X'(x)}{n_2^2(x)}\right];\quad B = \left[\frac{2}{n_2^3(x)}\,\frac{dn_2(x)}{d\rho}\,Y(x) - \frac{Y'(x)}{n_2^2(x)}\right]; \qquad \text{(B.112)}$$

$$C = \left[-\frac{2}{n_2^3(y)}\,\frac{dn_2(y)}{d\rho}\,X(y) + \frac{X'(y)}{n_2^2(y)}\right] \text{and } D = \left[-\frac{2}{n_2^3(y)}\,\frac{dn_2(y)}{d\rho}\,Y(y) + \frac{Y'(y)}{n_2^2(y)}\right]$$

$$^{m}B_\ell = \frac{-\psi_\ell(x)\{-n_2(x)\,E\,V_\ell(y) + n_2(x)\,F\,U_\ell(y)\}}{\zeta_\ell^1(x)\{\quad \text{same as above} \quad\}}$$

$$+ \frac{\dfrac{\psi_\ell'(x)}{k_2^I}\{U_\ell(x)\,V_\ell(y) - V_\ell(x)\,U_\ell(y)\}}{-\dfrac{\zeta_\ell^{1\prime}(x)}{k_2^I}\{\quad \text{same as above} \quad\}} \qquad \text{(B.113)}$$

$$E = \left[- \frac{U'(x)}{k_2^{II} n_2(x)} + \frac{1}{k_2^{II} n_2^2(x)} \frac{dn_2(x)}{d\rho} U(x) \right];$$

$$F = \left[- \frac{V'(x)}{k_2^{II} n_2(x)} + \frac{1}{k_2^{II} n_2^2(x)} \frac{dn_2(x)}{d\rho} V(x) \right] \qquad \text{(B.114)}$$

The limit of $n_3 \to \infty$ has been used in the derivation of these equations.

Having now the scattering coefficients, one may substitute ${}^{e,m}\Pi$ into Equations (B.53) to (B.58) to find general expressions for the components of the scattered fields.

$$E_r^s = E_o \cos\phi/(K^I r)^2 \sum_{\ell=1}^{\infty} {}^{e}B_\ell \, i^{\ell-1} (2\ell+1) P_\ell^1(\cos\ ) \zeta_\ell^1(K^I r) \qquad \text{(B.115)}$$

$$E_\theta^s = E_o \cos\phi/(K^I r) \sum_{\ell=1}^{\infty} i^{\ell-1} \frac{(2\ell+1)}{\ell(\ell+1)} \left\{ - {}^{e}B_\ell \, \zeta_\ell^{1'}(K^I r) P_\ell^{1'}(\cos\theta)\sin\theta \right.$$

$$\left. + i \, {}^{m}B_\ell \, \zeta_\ell^1(K^I r) P_\ell^1(\cos\theta)/\sin\theta \right\} \qquad \text{(B.116)}$$

$$E_\phi^s = E_o \sin\phi/K^I r \sum_{\ell=1}^{\infty} i^{\ell-1} \frac{(2\ell+1)}{\ell(\ell+1)} \left\{ - {}^{e}B_\ell \, \zeta_\ell^{1'}(K^I r) \frac{P_\ell^1(\cos\theta)}{\sin\theta} \right.$$

$$\left. + i \, {}^{m}B_\ell \, \zeta_\ell^1(K^I r) P_\ell^{1'}(\cos\theta) \sin\theta \right\} \qquad \text{(B.117)}$$

$$H_r = i E_o \sin\phi/K^I k_2^I r^2 \sum_{\ell=1}^{\infty} i^{\ell-1} (2\ell+1) \, {}^{m}B_\ell \, \zeta_\ell^1(K^I r) P_\ell^1(\cos\theta) \qquad \text{(B.118)}$$

$$H_\theta = E_o \sin\phi/k_2^I r \sum_{\ell=1}^{\infty} i^{\ell-1} \frac{(2\ell+1)}{\ell(\ell+1)} \left\{ - {}^{e}B_\ell \, \zeta_\ell^1(K^I r) \frac{P_\ell^1(\cos\theta)}{\sin\theta} \right.$$

$$\left. + i \, {}^{m}B_\ell \, \zeta_\ell^{1'}(K^I r) P_\ell^{1'}(\cos\theta) \sin\theta \right\} \qquad \text{(B.119)}$$

$$H_\phi = E_o \cos\phi/k_2^I r \sum_{\ell=1}^{\infty} i^{\ell-1} \frac{(2\ell+1)}{\ell(\ell+1)} \left\{ e_{B_\ell} \zeta_\ell^1(K^I r) P_\ell^{1'}(\cos\theta) \sin\theta \right.$$

$$\left. + i\, {}^{m}B_\ell \zeta_\ell^{1'}(K^I r) \frac{P_\ell^1(\cos\theta)}{\sin\theta} \right\} \qquad \text{(B.120)}$$

B.4 The Refractive Index of a Plasma Medium: The Scattering Coefficients for Constant n

The refractive index n is related to the physical parameters of the plasma by means of the Appleton-Hartree (Budden, 1961) equation:

$$n^2 = 1 - \frac{X}{U - \frac{Y_T^2}{2(U-X)} \pm \left[\frac{Y_T^4}{4(U-X)^2} + Y_L^2 \right]^{\frac{1}{2}}} \qquad \text{(B.121)}$$

With the assumption of no externally applied magnetic field present in the plasma region, this expression reduces to

$$n^2(\rho) = 1 - \frac{\omega^2(\rho)}{\omega^2} \frac{1}{U} \qquad \text{(B.122)}$$

We consider the special case of a plasma coating which is characterized by a constant refractive index. When the refractive index of the plasma is a constant value, $dn_2/d\rho = 0$. Consequently, the differential equations which $W_\ell(\rho)$ and $G_\ell(\rho)$ satisfy become identical and have the two solutions

$$\psi_\ell(n_2\rho) = \left(\frac{\pi n_2 \rho}{2}\right)^{\frac{1}{2}} J_{\ell+\frac{1}{2}}(n_2\rho) \qquad \text{(B.123)}$$

$$\chi_\ell(n_2\rho) = \left(\frac{\pi n_2\rho}{2}\right)^{\frac{1}{2}} N_{\ell+\frac{1}{2}}(n_2\rho) \tag{B.124}$$

Letting

$$X_\ell(\rho) = U_\ell(\rho) = \psi_\ell(n_2\rho) \tag{B.125}$$

$$Y_\ell(\rho) = V_\ell(\rho) = \chi_\ell(n_2\rho) \tag{B.126}$$

the scattering coefficients may be written as

$$\begin{aligned} {}^{e}B_\ell = \Big[& - \psi_\ell(x) \left\{ - \psi_\ell'(n_2x)\, \chi_\ell'(n_2y) + \psi_\ell'(n_2y)\, \chi_\ell(n_2x) \right\} + \psi_\ell'(x) \\ & \left\{ - n_2^2\, \psi_\ell(n_2x)\, \chi_\ell'(n_2y) + n_2^2\, \psi_\ell'(n_2y)\, \chi_\ell(n_2x) \right\} \Big] \Big/ \Big[\zeta_\ell^1(x) \\ & \left\{ \text{same as above} \right\} - \zeta_\ell^{1\prime}(x) \left\{ \text{same as above} \right\} \Big] \end{aligned} \tag{B.127}$$

$$\begin{aligned} {}^{m}B_\ell = \Big[& - \psi_\ell(x) \left\{ \psi_\ell'(n_2x)\, \chi_\ell(n_2y) - \chi_\ell'(n_2x)\, \psi_\ell(n_2y) \right\} + \psi_\ell'(x) \\ & \left\{ \psi_\ell(n_2x)\, \chi_\ell(n_2y) - \chi_\ell(n_2x)\, \psi_\ell(n_2y) \right\} \Big] \Big/ \Big[\zeta_\ell^1(x) \\ & \left\{ \text{same as above} \right\} - \zeta_\ell^{1\prime}(x) \left\{ \text{same as above} \right\} \Big] \end{aligned} \tag{B.128}$$